NOTE TO USERS

This reproduction is the best copy available.

UNIVERSITÉ DE MONTRÉAL

ANNULAR-FLOW-INDUCED VIBRATIONS OF A SIMPLY-SUPPORTED CYLINDER IN A FINITE-LENGTH NARROW-GAP SUPPORT

HEUNG SEOK KANG
DÉPARTEMENT DE GÉNIE MÉCANIQUE
ÉCOLE POLYTECHNIQUE DE MONTRÉAL

THÈSE PRÉSENTÉE EN VUE DE L'OBTENTION
DU DIPLÔME DE PHILOSOPHIAE DOCTOR (Ph.D.)
(GÉNIE MÉCANIQUE)
JUIN 2009

Your file Votre référence
ISBN: 978-0-494-53798-5
Our file Notre référence
ISBN: 978-0-494-53798-5

UNIVERSITÉ DE MONTRÉAL

ÉCOLE POLYTECHNIQUE DE MONTRÉAL

Cette thèse intitulée:

ANNULAR-FLOW-INDUCED VIBRATIONS OF A SIMPLY-SUPPORTED CYLINDER IN A FINITE-LENGTH NARROW-GAP SUPPORT

présentée par: KANG, Heung Seok

en vue de l'obtention du diplôme de: Philosophiae Doctor

a été dûment acceptée par le jury d'examen constitué de:

M. HÉBERT Alain, D.Ing., président

M. MUREITHI Njuki W., Ph.D., membre et directeur de recherche

M. PETTIGREW Michel J., Post grad. dipl., membre et codirecteur de recherche

M. LAKIS Aouni A., Ph.D., membre

M. PAIDOUSSIS Michael P., Ph.D., membre

ACKNOWLEDGMENTS

I would like to express my most sincere gratitude to my dear advisor Professor Njuki W. Mureithi and co-advisor Professor Michel J. Pettigrew for their insightful guidance, unending encouragement, financial support and even personal help. They have been a constant source of inspiration and creativity. I am indebted to their continuous, generous and diligent efforts for the publications and dissertation.

I would like to acknowledge and thank Professor Alain Hébert, Professor Aouni A, Lakis and Professor Michael P. Paidoussis for honouring me by serving on my committee. I would like to thank professor Woo Gun Sim for valuable discussions whenever I asked him for advice on fluids.

I would like to acknowledge and thank Mr. Thierry Lafrance for his technical support and for the fabrication and modification of my gap supports, Mr. Bénedict Besner for teaching me and helping me to operate the data acquisition system. I would also like to thank them for purchasing and installing the flow meter and the pressure gages.

Thanks to Cedric Bèguin, my brilliant colleague, for teaching me French and for his judicious translation of the "Résumé" and the "Condensé en français".

I am grateful to Bobcock&Wilcox Canada for their financial support and for supplying the tubes and supports for the experiment.

I would like to express my deepest sense of gratitude to my wife, Jeong Hyun, lovely daughter, Jin and son, Jin Wook for their support, patience and sacrifice throughout those years in the pursuit of my study.

RÉSUMÉ

Dans de très nombreuses applications industrielles particulièrement dans le domaine de l'énergie, de nombreuses structures sont soumises a des vibrations induites par des écoulements annulaires ou de fuite. On peut citer par exemple, les tubes de générateur de vapeur au niveau de leur support avec jeu, les faisceaux d'éléments de matière fissible (UO_2) au niveau des grilles d'espacement ou entre les attaches de combustible dans les réacteurs refroidis au gaz lors des opérations de remplissage, etc. Pourtant, la recherchè dans ce domaine se limite qu'à quelques articles. Dans cette étude, nous étudierons à la fois expérimentalement et analytiquement les vibrations induites par un écoulement annulaire sur un cylindre de 2.5m de long simplement supporté aux deux extrémités. Les expériences ont été réalisées avec ou sans la présence d'un "diffuseur a faible jeu" de quelque dizaine de millimètres de long situé à la mi-longueur du cylindre.

Le modèle analytique pour modéliser les vibrations du cylindre induite par un écoulement annulaire est fondé sur les hypothèses suivantes : (1) La vibration induit que de petites perturbations dans l'écoulement principal. (2) L'écoulement reste 2D; on néglige la composante radiale de l'écoulement. (3) La force de friction due à la perturbation ne dépend que de la variation dans l'espace et le temps de la composante axiale de l'écoulement. Cette étude a permis d'aboutir aux conclusions suivantes : (1) La différence entre un modèle 1D et 2D dépend essentiellement du rapport du rayon sur la longueur du cylindre. (2) Le modèle 1D n'est valide que pour les problèmes à un degré de liberté ou pour des cylindres présentant un rapport rayon sur longueur très faible. (3) La méthode des petites perturbations n'a que peu d'influence sur la dynamique du système mais permet une bien meilleure évaluation de la vitesse critique, qui est considérablement diminuée.

Le modèle analytique a été confronté à des expériences sur un tube simplement supporté soumis à un écoulement annulaire dans un "diffuseur a faible jeu" situé à mi-longueur

du tube. La longueur du banc d'essai est de 2.5m. Plusieurs diffuseurs ont été utilisés avec différents jeux, longueurs et angle d'entrée et sortie du diffuseur. Nous avons observé une instabilité par flottement du tube. La vitesse critique d'instabilité est fortement dépendante du jeu entre le tube et le diffuseur, ainsi que de l'angle d'entrée du diffuseur. Les perturbations de pression sur le tube ont été obtenues analytiquement considérant la perte par friction, la contraction à l'entrée du diffuseur et le rétablissement de la pression en sortie. La solution analytique démontre le rôle prédominant de la condition limite de sortie pour matérialiser le rétablissement de la pression. Cependant nous ne trouvons pas d'instabilité par flottement pour des conditions idéales comme aucune perte de pression à l'entrée et la conversion du débit en pression à la sortie. Un modèle semi-analytique a été proposé pour prédire la vitesse d'instabilité. La prédiction semi-analytique s'accorde raisonnablement bien avec les résultats expérimentaux. Cependant, le rétablissement de la pression à la sortie du diffuseur devrait être mesuré plus précisément afin d'améliorer la précision du modèle.

ABSTRACT

Many engineering applications with annular- or leakage-flow over a finite length can be encountered especially in the power generation plants. For instance, heat exchanger tubes with gap supports in steam generator, UO_2 fuel rods with spacer grids in fuel bundles and fuel assemblies in gas-cooled reactors during refueling, etc. Nonetheless, few articles can be found on this subject. In this study, therefore, the annular-flow-induced vibrations of a pinned-pinned cylinder with and without a finite-length narrow-gap diffuser are studied by analytical and experimental methods.

For the annular-flow-induced vibrations of a pinned-pinned cylinder, an analytical model is proposed based on three main assumptions; (1) small perturbations in flow components, (2) negligible radial flow to reduce the annular flow to two-dimensional flow, and axial flow only for reduction to one-dimensional flow, and (3) perturbation frictional loss depending on the variation of axial perturbation velocity in terms of space and time. In this study, it is concluded that (1) the difference in fluidelastic forces between two- and one-dimensional flow models depends mostly on cylinder radius, and on whether perturbation flow is mainly allowed in the axial or circumferential direction, (2) the one-dimensional flow model should be limited to 1-d.o.f vibration analysis or the case of a cylinder having a large radius-to-length ratio, and (3) perturbation assumption makes little change to the dynamics of annular-flow-induced vibrations, however, the critical flow velocity is diminished considerably.

The stability of a simply-supported tube subjected to narrow annular flow in a finite-length gap support is experimentally and analytically investigated. For the experiment, a 2.5 m test section and several finite-length gap supports have been made considering different gap size and diffuser angles of the support. The tube was observed to lose stability by flutter. The critical flow velocity was strongly dependent on the annular gap size and the diffuser angle at the downstream end of the support. A solution for the

perturbation pressure on the tube is analytically obtained considering the friction loss, the contraction loss at the entrance, and the pressure recovery at the exit of the support. In the analytical solution, the exit boundary condition for pressure recovery is found to be predominant for flutter instability. However, flutter instability does not materialize for lossless boundaries such as short-lossless inlet and free-discharge outlet. Based on the solution, a simple semi-analytical model to predict the critical flow velocity is proposed for the first mode instability. The prediction of the semi-analytical model agrees reasonably well with the experimental results. However, it is judged that the pressure recovery at the diffuser should be experimentally measured more accurately to have better prediction.

CONDENSÉ EN FRANÇAIS

Introduction

Les problèmes de vibrations induites par les écoulements sont classés selon leur type : i) écoulement transversal ii) écoulement interne axial iii) écoulement externe axial iv) écoulement annulaire ou de fuite sur une distance finie, parfois nommé configuration avec diffuseur. La taille du confinement permet de distinguer les écoulements annulaires (confinement normal) et de fuite (confinement extrême). L'écoulement annulaire peut aussi bien faire référence à un écoulement autour d'un cylindre qu'autour d'une barre plate ou d'un élément rectangulaire. On retrouve des écoulements annulaires et/ou de fuite en particulier :

- dans les réacteurs nucléaires refroidis à gaz
- dans les générateurs de vapeur ou les fluides (primaire et secondaire) s'écoulent dans des passages très étroits
- autour des boucliers thermiques dans les conduits des réacteurs à eau pressurisée
- autour des éléments de contrôles, entre les barres d'uranium et les conduits des réacteurs refroidis au gaz de deuxième génération
- entre les tubes et leurs supports dans les échangeurs de chaleur.

Une raison fondamentale de l'intérêt pour cette configuration d'écoulement c'est qu'elle est observée dans des systèmes très flexibles.

L'équation du mouvement pour un cylindre dans un écoulement axial, développée par Paidoussis (1966, 1973 et 1974), est bien connue et citée par de nombreux chercheurs. Le confinement ne change pas le mécanisme de base de l'instabilité mais la vitesse critique est beaucoup plus faible.

Dans les systèmes conservatifs (simplement supportés ou encastrés), il est bien admis que les cylindres en écoulement axial deviennent instables par divergence. Paidoussis et Pettigrew (1979) ont montré expérimentalement qu'un cylindre flexible en écoulement axial peut être significativement déstabilisé par le confinement.

Un modèle non visqueux pour un corps interne dans un écoulement annulaire a été développé par Mateescu et Paidoussis (1985). Dans cette étude, on considère un corps axisymétrique rigide simplement supporté en un point et coaxialement monté dans un canal avec un petit jeu de forme annulaire. L'écoulement est modélisé par un écoulement potentiel afin de déterminer les forces instationnaires créées par le fluide. Dans les articles suivants, les auteurs ont proposé une correction visqueuse (1988), ainsi qu'un modèle analytique pour un corps flexible. Sim (1987) a prouvé que les forces visqueuses ainsi que le confinement d'un jeu de forme annulaire contribuent à stabiliser le système.

Inada et Hayama (1988, 1990 et 2000) ont étudié le cas d'un écoulement de fuite sur une plaque supportée par des ressorts en translation et en rotation dans un passage étroit délimité par deux plaques planes. Dans leur travail, les forces instationnaires sont modélisées comme une masse, un amortissement et une raideur ajoutée. Ils démontrent qu'une instabilité de flottement ou par divergence est possible pour un conduit divergeant. Leurs études ont contribué à stimuler la recherche japonaise dans ce domaine.

Le modèle mathématique développé par Li, Kaneko et Hayama a été amélioré par Langthjem, Morita, Nakamura and Nakano (2006). Ils ont étudié le cas d'un cylindre flexible avec un déséquilibre (excentricité) avec des écoulements de fuite laminaire ou turbulent. Selon eux, un cylindre simplement supporté peut devenir instable par flottement ou par divergence. En considérant, le travail des forces, ils ont prouvé que la force centrifuge est la seule responsable de l'instabilité par divergence d'un cylindre simplement supporté ou encastré. Autrement dit, l'instabilité par divergence est indépendante de la force de friction fluide. Cependant, des ondes progressives sont la seule solution pour obtenir une instabilité par flottement.

Hobson (1982) est responsable de la première tentative pour développer un modèle analytique pour les écoulements de fuite. Son étude considère le mouvement unidimensionnel d'un cylindre central, positionné dans un passage annulaire étroit. Négligeant les perturbations de la vitesse radiale du fluide, la dynamique du cylindre a été étudiée dans le but de comprendre le rôle des conditions limites du fluide sur l'amortissement aérodynamique. Même si l'étude ne décrit pas complètement la dynamique de l'ensemble, elle démontre l'existence d'une instabilité par flottement pour des écoulements divergents en aval. Spur et Hobson (1984) ont prouvé expérimentalement la présence d'une instabilité par amortissement négatif pour des angles de diffuseur de 4° ou plus.

La théorie de Hobson a été validée par les expériences de Fujita (1922) et Ito et al. (1994). Leur banc d'essai permettait d'obtenir un mouvement a un degré de liberté dans un conduit avec diffuseur et permettait de mesurer la force dynamique due au fluide (air ou eau). Ils ont vérifié que le système peut devenir instable pour une configuration divergente en amont.

Parkin et Watson (1984) ont rapporté des problèmes de vibration des éléments de combustible dans un réacteur refroidit au gaz. Ils ont mis en évidence expérimentalement que le mécanisme d'instabilité dans un diffuseur à 30° est dû à la formation de tourbillons alternés. En revanche dans un diffuseur à 6°, l'origine des vibrations provient des caractéristiques de récupération de pression. Cette découverte fondamentale nous propose des directions de recherches pour les instabilités par amortissement négatif.

Mulcahy (1984) a rapporté des problèmes de vibration induite par un écoulement de fuite à travers un joint de glissement pour un tube en porte à faux. Il a découvert qu'à un débit inférieur à celui où le tube frappe la paroi, un cycle limite est atteint. A haut débit, le mouvement d'instabilité passe du premier mode au second mode. Plusieurs années

après l'étude avec mode à un degré de liberté de Hobson, Mulcahy (1988) étudia à son tour les amortissements dynamiques dus aux écoulements.

Gorman, Godin et Planchard (1987) ont rapporté une vibration fluide-élastique d'un tube à gobelet dans un réacteur à eau pressurisée. Dans cette étude, une buse divergente, droite et de section carré avec quatre rayons verticaux différents ont été utilisées. Ils ont découvert que de grandes vibrations apparaissent avec une buse divergente.

Yasuo et Paidoussis (1989) considéré le problème d'instabilité induite par un écoulement des tubes d'échangeur de chaleur soumis a un écoulement axial dans des supports de type divergent, qui sont similaires à ceux utilisés dans notre étude. Dans leur étude, une approximation à un mode pour le tube intérieur a été utilisée de même qu'un diffuseur de petite longueur et la théorie des écoulements potentiels. Ils ont abouti à une équation de la vitesse critique pour l'instabilité par divergence et par flottement.

Objectifs

Aujourd'hui, les simulations numériques comme FEM ou BEM sont très populaires. Elles sont parfois très utiles, cependant dans certaines situations une solution analytique est plus utile, en particulier pour expliquer les phénomènes inconnus et déchiffrer la physique de ces phénomènes. Une solution analytique permet de donner un aperçu des applications et d'avancer par la suite sur l'ingénierie pratique.

Premièrement, la raison de cette étude est d'obtenir une solution analytique pour les perturbations de pression à l'intérieur de l'espace annulaire lorsque le tube interne est soumis a un écoulement annulaire 2D. Cette étude a la prétention d'étendre les travaux de Hobson en considérant un système continu ainsi que les pertes par friction au sein du liquide.

Deuxièmement, nous allons étudier analytiquement et expérimentalement les vibrations d'un cylindre entouré d'un écoulement de fuite axial autour d'un diffuseur de petite longueur. Le but de ces travaux est l'étude en détail des instabilités et la prédiction de la vitesse critique d'instabilité pour un cylindre simplement supporté en fonction du jeu annulaire et de la longueur du support.

Résultats

Dans cette étude, le travail de Hobson est étendu afin d'être utilisable pour les vibrations d'un cylindre simplement supporté induites par des écoulements annulaires, grâce à une modélisation 2D de l'écoulement avec perte visqueuse. Afin de modéliser la friction, un nouveau facteur de perturbation de la friction est introduit sous la forme d'un nombre complexe. L'utilisation de ce modèle de friction permet d'analyser les effets de la friction sur tous les modes de vibrations. Il est démontré que non seulement le facteur de friction mais aussi les perturbations de pression sont fortement couplés avec les modes du cylindre simplement supporté.

Avec ce facteur de friction, les solutions théoriques pour des pressions et des vitesses d'écoulement instationnaires sont facilement trouvées. De plus, les perturbations de pression peuvent être raisonnablement formulées avec trois termes : le terme en ω^2, celui en ω et enfin celui indépendant de ω. Le terme indépendant de ω (la force de raideur fluide-élastique) est le terme prédominant et une instabilité statique est attendue.

Le modèle d'écoulement 2D montre que les forces fluides prédites sont significativement différentes que celles prévues par un modèle 1D pour un cylindre simplement supporté soumis a un écoulement annulaire. La grande différence entre les modèles est probablement due au ratio rayon sur longueur du cylindre et sur la différence entre un écoulement plan et circonférentiel. Le modèle 1D ne permet pas à l'écoulement de se déplacer dans la direction circonférentielle, donc le modèle 1D est limité au ratio rayon sur longueur plus grand que 0.8 ou à des vibrations à un degré de

liberté comme une translation pure ou une rotation pure (Hobson ,1982, Fujita and Ito, 1992 and 1994, Porcher and de Langre, 1997).

La théorie des petites perturbations conduit à des changements dans la dynamique des vibrations du cylindre induites par les écoulements annulaires comparativement à la théorie ne considérant que l'écoulement moyen. La théorie des petites perturbations diminue la vitesse adimensionnelle critique d'instabilité à 2.4. comparativement à 3.14 pour la théorie avec écoulement moyen.

Le modèle incluant les pertes par friction est supposé donner des solutions dépendant des différents supports ou conditions limites du cylindre (porte à faux, encastré-encastré...). Ce modèle peut être développé davantage pou donner des solutions analytiques au problème de support avec jeu annulaire de longueur limitée.

La stabilité d'un cylindre flexible simplement supporté soumis à un écoulement annulaire sur la longueur limitée du support a été explorée analytiquement et expérimentalement. Les expériences ont permis de mesurer des vitesses critiques d'instabilité pour des supports de longueur limitée ayant différents jeux et angles de diffuseurs. L'approche analytique a permis d'obtenir les perturbations de pression agissant sur le cylindre simplement supporté soumis à un écoulement annulaire de fuite sur la longueur du support. La solution analytique considère un écoulement 2D avec deux conditions limites du fluide. Les deux types de conditions sont :

- le cas idéal, une entrée sans perte et à la sortie une conversion complète
- le cas plus réel considérant une perte due à la contraction à l'entrée et à la detente en sortie.

Dans les expériences avec un tube intérieur en acier de 2.2 m de long et un support 3.8 cm de long, on observe une instabilité par flottement avec des débits d'air assez faibles et cela pour tous les supports indépendamment du jeu et de l'angle du diffuseur. Pour

des écoulements annulaires, un cylindre simplement supporté perd sa stabilité par divergence pour des vitesses bien plus grandes que celles rencontrées habituellement dans les problèmes d'ingénierie. Un petit support joue un rôle essentiel dans le changement de comportement de la dynamique du cylindre en diminuant significativement la vitesse critique d'instabilité. La vitesse critique d'instabilité obtenue expérimentalement est très en dessous de celle rencontrée habituellement dans les générateurs de vapeur. En général, plus le jeu et l'angle du diffuseur sont petits la vitesse critique diminue ou un amortissement négatif apparait. D'un autre côté, pour le jeu le plus grand (2.2 mm), la vitesse critique d'instabilité pour un grand angle de diffuseur (20^{o}) est plus petite que celle rencontrée pour le plus petit angle de diffuseur (10^{o}).

Dans la théorie, les forces d'amortissement négatif sont très dépendantes de la performance adimensionnel le du diffuseur ($\boldsymbol{\delta}$) qui est le ratio de l'efficacité du diffuseur sur le jeu résiduel lors de la vibration. L'autre résultat important est que les forces d'amortissement négatif sont essentiellement créées en sortie. À partir de ces deux résultats, on peut conclure que l'expansion du canal en aval est la cause de l'instabilité par flottement. Cela est en accord avec les recherches précédentes.

Un modèle semi-analytique pour la force d'amortissement est proposé en s'appuyant sur la solution analytique de la pression. Dans l'hypothèse où il n'y a aucune perte, l'amortissement fluide-élastique est toujours positif. Pour les cas expérimentaux, les calculs numériques par le modèle semi-empirique conduit à des résultats en accord avec les expériences. Un jeu et un angle de diffuseur plus faible sont plus déstabilisants. Cependant, le jeu le plus grand (2.2 mm) et un grand angle de diffuseur (20^{o}) génèrent une vitesse critique d'instabilité assez basse.

Pour un cylindre simplement supporté soumis à un écoulement de fuite sur un support de petite longueur placé à mi-longueur, la vitesse critique d'instabilité pour de l'air comprimé est plus faible que 3 m/s, ce qui est une vitesse que l'on peut rencontrer dans les problèmes d'ingénierie.

TABLE OF CONTENTS

ACKNOWLEDGMENTS IV

RÉSUMÉ V

ABSTRACT VII

CONDENSÉ EN FRANÇAIS IX

TABLE OF CONTENTS XVII

LIST OF TABLES XX

LIST OF FIGURES XXI

LIST OF SYMBOLS XXVII

LIST OF APPENDICES XXXII

CHAPTER 1 INTRODUCTION AND LITERATURE REVIEW 1

1.1 REVIEW OF PREVIOUS STUDIES 1

1.2 MOTIVATION 7

1.3 OBJECTIVES 8

1.4 THESIS OUTLINE 9

CHAPTER 2 ANALYTICAL SOLUTION FOR A VIBRATING SIMPLY-SUPPORTED CYLINDER SUBJECTED TO 2-D CONCENTRIC ANNULAR FLOW CONSIDERING FRICTION 11

2.1 ABSTRACT 15

2.2 INTRODUCTION 15

2.3 FLUID AND STRUCTURE EQUATIONS 17

2.3.1 Equation of motion of a flexible inner cylinder in annular flow 17

2.3.2 Fluid equations and boundary conditions 18

2.3.3 Two-dimensional flow 19
2.3.4 One-dimensional flow 26
2.4 COMPARISON OF 1-D WITH 2-D FLOW EQUATIONS 28
2.4.1 Simplified Comparison 29
2.4.2 Full Comparison 30
2.5 FRICTION 35
2.5.1 Perturbation pressure and axial flow velocity 35
2.5.2 Perturbation friction factor 38
2.6 CONCLUSIONS 45

APPENDIX 2A: PRESSURE FUNCTIONS FOR 2-D FLOWS FOR SEVERAL FLOW BOUNDARY CONDITIONS WITHOUT FRICTION TERM 60
APPENDIX 2B: PRESSURE FUNCTIONS FOR 1-D FLOWS FOR SEVERAL FLOW BOUNDARY CONDITIONS 65

2.7 REFERENCES 67

CHAPTER 3 ANNULAR-FLOW-INDUCED VIBRATIONS OF A SIMPLY-SUPPORTED TUBE IN A FINITE-LENGTH NARROW-GAP SUPPORT 70

3.1 ABSTRACT 74
3.2 INTRODUCTION 74
3.3 EXPERIMENTS 76
3.3.1 Description of apparatus 76
3.3.2 Experimental results 77
3.4 ANALYTICAL MODEL 79
3.4.1 Assumptions 79
3.4.2 Equation of motion of a flexible inner-cylinder 79
3.4.3 Fluid equations and boundary conditions 82
3.4.5 Friction coefficient and friction loss 85
3.4.6 Analytical solution for pressure perturbation 86

3.5 NUMERICAL CALCULATIONS 99
3.5.1 Parametric study 100
3.5.2 Experimental cases 102
3.6 CONCLUSIONS 106
3.7 REFERENCES 129

CHAPTER 4 GENERAL DISCUSSION 131

4.1 REVIEW OF OBJECTIVES 131
4.2 CONTRIBUTIONS 131

CHAPTER 5 CONCLUSION AND RECOMMENDATIONS 134

5.1 CONCLUSION 134
5.2 RECOMMENDATIONS 136

REFERENCES 139

APPENDICES 145

LIST OF TABLES

Table 3.1 Major dimensions of test apparatus 109

Table 3.2 Fluid parameters and vibration characteristics of the inside cylinder 110

Table 3.3 Steady diffuser efficiency η_s and dimensionless diffuser performance coefficient δ for finite-length narrow-gap supports 111

Table 3.4 Comparison of the measured and the calculated critical flow velocity for negative damping 112

LIST OF FIGURES

Figure.2.1 (a) Definition of coordinates and symbols of the system in radial direction, and (b) in longitudinal direction. A flexible cylinder of length L and external radius R_d is confined in an annulus with a fluid gap H. The fluid pressure p′, axial flow velocity u′, circumferential flow velocity v′, and vibration amplitude of the rod h′ consist of steady terms P, U, V, and H and perturbation terms p, u, v and h respectively. However, bulk flow in the circumferential direction does not exist because the main flow is in axial direction, so v′ equals zero. 47

Figure 2.2 Pressure ratios of the two-dimensional flow model to the one-dimensional flow model as a function of the radius-to-length ratio and beam eigenfunction mode number. 48

Figure 2.3 Argand diagram for the pinned-pinned cylinder subjected to annular air flow according to Paidoussis theory. The first instability is the first mode buckling at $Uc_1 = 3.14$, the second mode buckling at $Uc_2 = 6.28$, the first and second coupled-mode flutter at $Uc_3 = 6.7$ and the third mode buckling at $Uc_4 = 9.43$ 49

Figure 2.4 Argand diagram for the pinned-pinned cylinder subjected to annular air flow for the one-dimensional flow model without frictional loss. The first instability is the second mode flutter at $Uc_1 = 0.01$ (1.1 m/s), the third mode flutter at $Uc_2 = 0.08$ (9 m/s) 50

Figure 2.5 Argand diagram for the pinned-pinned cylinder subjected to annular air flow for the two-dimensional flow model without frictional loss. The first instability is the first mode buckling at dimensionless $Uc_1 = 2.36$, the second mode buckling at $Uc_2 = 4.72$, the first and second coupled-mode flutter at $Uc_3 = 4.95$, and the third mode buckling at $Uc_4 = 7.15$ 51

Figure 2.6 Real and imaginary parts of friction factor $K_{cf1}^2 = 1 + K_{cf0}/H$ when the inner cylinder vibrates at 10 Hz in the 1st mode, and the dimensionless flow velocities are 0.457, 0.914, 1.827, 2.74, 3.65, and 4.57 52

Figure 2.7 Real and imaginary parts of friction factor $K_{cf1}^2 = 1 + K_{cf0}/H$ when the inner cylinder vibrates at 35 Hz in the 2nd mode, dimensionless flow velocities are 0.457, 0.914, 1.827, 2.74, 3.65, and 4.57 53

Figure 2.8 Real and imaginary parts of friction factor $K_{cf1}^2 = 1 + K_{cf0}/H$ when the inner cylinder vibrates at 75 Hz in the 3rd mode, dimensionless flow velocities are 0.457, 0.914, 1.827, 2.74, 3.65, and 4.57 54

Figure 2.9 (a – c) Real and (d- f) imaginary parts of the perturbation pressure when the inner cylinder vibrates at 10 Hz in the 1st mode. When the vibration amplitude is 1 mm, the different quantities are (a, d) inertia, (b, e) stiffness and (c, f) damping 55

Figure 2.10 (a – c) Real and (d- f) imaginary parts of the perturbation pressure when the inner cylinder vibrates at 35 Hz in the 2nd mode. When the vibration amplitude is 0.2 mm, the different quantities are (a, d) inertia, (b, e) stiffness and (c, f) damping. 56

Figure 2.11 (a – c) Real and (d- f) imaginary parts of the perturbation pressure when the inner cylinder vibrates at 75 Hz in the 3rd mode. When the vibration amplitude is 0.05 mm, the different quantities are (a, d) inertia, (b, e) stiffness and (c, f) damping. 57

Figure 2.12 Real and imaginary parts of the perturbation pressure when the inner cylinder vibrates at 10 Hz, 35 Hz, and 75 Hz in the 1st, 2nd and 3rd modes. Vibration amplitudes are 1 mm for the 1st, 0.2 mm for the 2nd and 0.04 mm for 3rd mode, respectively. (a1), (a2) and (a3) are real parts of the pressure at the 1st, 2nd and 3rd modes, and (b1), (b2) and (b3) are Imaginary parts of the pressure at the 1st, 2nd and 3rd modes, respectively. 58

Figure 2.13 Argand diagram for a simply-supported inner cylinder subjected to unsteady annular flow. The cylinder loses its first stability at 2.36 dimensionless velocity, second at 4.71, third at 7.15 59

Figure 3.1 Schematic drawing of the test section. (a) Inner tube and instrument setup (b) Dimensions near the support 113

Figure 3.2 Vibration amplitude and damping ratio as a function of upstream flow velocity for the inside cylinder in the support with 0.29 mm gap and 20° diffuser angle 114

Figure 3.3 The first and the second natural frequencies as a function of upstream flow velocity for the inside cylinder in the support with 0.29 mm gap and 20° diffuser angle 115

Figure 3.4 X-Y plots for the vibration of the inner cylinder in the support with 0.29 mm gap and 20° diffuser angle. Reynolds numbers (upstream velocity): (a) 1,682 (0.22 m/s), (b) 1,994 (0.26 m/s), (c) 2,262 (0.30 m/s), (d) 2,843 (0.38 m/s) 116

Figure 3.5 RMS amplitude of the inner cylinder as a function of flow velocity upstream of the support for different support gaps

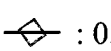 : 0.29 mm /10°  : 0.29 mm /20°

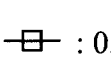 : 0.42 mm /10°  : 0.42 mm /20°

 : 0.67 mm /10° : 0.67 mm /20°

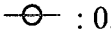 : 2.20 mm /10°  : 2.20 mm /20° 117

Figure 3.6 Analytical model for the inner cylinder with a finite-length gap support ... 118

Figure 3.7 Ratio of total inertia force to structural inertia force as a function of Reynolds number at the gap. S-F: a short-lossless entrance and a free-discharge exit for the gap support. A vibration amplitude of 0.3 mm is assumed. 119

Figure 3.8 Ratio of total stiffness force to structural stiffness force as a function of Reynolds number at the gap for an amplitude of 0.3 mm at the 1st mode.
G 0.29 (1): Annular gap=0.29 mm, Ka=0.1, η=0.1, δ=0.1,
G 0.29 (2): Annular gap=0.29 mm, Ka=0.1, η=0.1, δ=0.5,

G 0.67 (1): Annular gap=0.67 mm, Ka=0.1, η=0.1, δ=0.1,
G 0.67 (2): Annular gap=0.67 mm, Ka=0.1, η=0.1, δ=0.5,
G 2.20 (1): Annular gap=2.20 mm, Ka=0.1, η=0.1, δ=0.1,
G 2.20 (2): Annular gap=2.20 mm, Ka=0.1, η=0.1, δ=0.5,
G 0.29 (S-F): Annular gap=0.29 mm, Short-lossless and free-discharge,
G 0.67 (S-F): Annular gap=0.67 mm, Short-lossless and free-discharge,
G 2.20 (S-F): Annular gap=2.20 mm, Short-lossless and free-discharge . 120

Figure 3.9 Ratio of total damping force to structural damping force as a function of Reynolds number at the gap for a structural damping factor of 0.2% and a max. amplitude of 0.3 mm in the 1st mode.
G 0.29 (1): Annular gap=0.29 mm, Ka=0.1, η=0.1, δ=0.1,
G 0.29 (2): Annular gap=0.29 mm, Ka=0.1, η=0.1, δ=0.5,
G 0.67 (1): Annular gap=0.67 mm, Ka=0.1, η=0.1, δ=0.1,
G 0.67 (2): Annular gap=0.67 mm, Ka=0.1, η=0.1, δ=0.5,
G 2.20 (1): Annular gap=2.20 mm, Ka=0.1, η=0.1, δ=0.1,
G 2.20 (2): Annular gap=2.20 mm, Ka=0.1, η=0.1, δ=0.5,
G 0.29 (S-F): Annular gap=0.29 mm, Short-lossless and free-discharge,
G 0.67 (S-F): Annular gap=0.67 mm, Short-lossless and free-discharge,
G 2.20 (S-F): Annular gap=2.20 mm, Short-lossless and free-discharge . 121

Figure 3.10 Ratio of total damping force to structural damping force as a function of upstream flow velocity for a structural damping factor of 0.2% and a max. amplitude of 0.3 mm in the 1st mode.
G 0.29 (1): Annular gap=0.29 mm, Ka=0.1, η=0.1, δ=0.1,
G 0.29 (2): Annular gap=0.29 mm, Ka=0.1, η=0.1, δ=0.5,
G 0.67 (1): Annular gap=0.67 mm, Ka=0.1, η=0.1, δ=0.1,
G 0.67 (2): Annular gap=0.67 mm, Ka=0.1, η=0.1, δ=0.5,
G 2.20 (2): Annular gap=2.20 mm, Ka=0.1, η=0.1, δ=0.5,
G 0.29 (S-F): Annular gap=0.29 mm, Short-lossless and free-discharge,

G 0.67 (S-F): Annular gap=0.67 mm, Short-lossless and free-discharge,
G 2.20 (S-F): Annular gap=2.20 mm, Short-lossless and free-discharge . 122

Figure 3.11 Ratio of total damping force to structural damping force with a finite-length support of 0.29 mm gap with Ka=0.1, η=0.1, δ=0.1.
■ : Damping force at the entrance of the support
◆ : Damping force at the exit of the support
● : Damping force at mid-way along the support
▲ : Total damping force including the structural damping 123

Figure 3.12 Ratio of total damping force to structural damping force with a finite-length support of 0.29 mm gap with Ka=0.1, η=0.1, δ=0.5
■ : Damping force at the entrance of the support
◆ : Damping force at the exit of the support
● : Damping force at mid-way along the support
▲ : Total damping force including the structural damping 124

Figure 3.13 Pressure recovery measurements as functions of Reynolds number at the supports with 10 degree diffuser angle 125

Figure 3.14 Pressure recovery measurements as functions of Reynolds number at the supports with 20 degree diffuser angle 125

Figure 3.15 Ratio of total stiffness force to structural stiffness force as a function of Reynolds number at the gap. Dotted line and solid line correspond to a short-lossless entrance and a free-discharge exit, and a contraction-loss entrance and a diffuser exit, respectively. In the legend, G x.xx/yy represents a gap size of x.xx mm and a diffuser angle of yy deg..... 126

Figure 3.16 Ratio of total damping force to structural damping force as a function of Reynolds number at the gap for the contraction-loss entrance and the diffuser exit of the support. In the legend, G x.xx/yy represents for gap size of x.xx mm and a diffuser angle of yy deg..... 127

Figure 3.17 Ratio of total damping force to structural damping force as a function of upstream flow velocity for a contraction-loss entrance and a diffuser exit of

the support. In the legend, G x.xx/yy represents a gap size of x.xx mm and diffuser angle of yy deg..... 128

Figure 5.1 Friction loss factor for annular gap as a function of Reynolds number (The notation of Figure 3.15 is used here) 138

LIST OF SYMBOLS

a	vibration amplitude
C	damping coefficient
$C_{f,P}$	perturbation term of friction factor
$C_{f,S}$	steady term of friction factor
$C_{f,total}$	total friction factor (steady + perturbation)
$C_{e,n}$	effective damping coefficient of the n^{th} mode
D_1	coefficient of first order term in differential equation
EI	flexural rigidity
F_f	fluid forces per unit length due to perturbations
$F_{f,D}$	fluid damping force due to perturbation
$F_{f,I}$	fluid inertia force due to perturbation
$F_{f,K}$	fluid stiffness force due to perturbation
F_{frc}	friction force per unit length in axial direction
F_l	fluid force per unit length at support
$F_{S,D}$	inner tube damping force
$F_{S,I}$	inner tube inertia force
$F_{S,K}$	inner tube stiffness force due to perturbation
H	annular gap
h	vibration response of the cylinder
$\overline{h}_n(t)$	vibration response of time (t)
K_0	coefficient of the zeroth order term in differential equation
K_1	contraction loss factor at entrance

K_{cf0}	friction factor
κ_{cf1}	friction parameter ($K_{cf1}{}^2 = 1 + K_{cf0} / H$)
L	length
m	mode number
M_3	coefficient of third order term in differential equation
M_2	coefficient of second order term in differential equation
M_f	added fluid mass
M_s	structural mass per unit length
$M_{e,n}$	modal mass of the nth mode ($M_{e,n} = \int_0^L M_s \cdot \phi_n(x)^2 dx$)
p_f	perturbation pressure
p_c	coefficient of cosine component of perturbation pressure for particular solution
n	mode number
p_s	coefficient of sine component of perturbation pressure for particular solution
P_1	static pressure before diffuser
P_2	static pressure after diffuser
p_{ratio}	ratio of each perturbation pressure terms: 2-D to 1-D flow model
Q_y	flow rate in y direction
ΔQ_y	flow rate perturbation in y direction
q	ratio of radius to length of inner cylinder $[R_d / L]$
Re	Reynolds number ($\mathrm{Re} = \frac{\rho U D_h}{\mu}$)

r	radial coordinate
R_d	radius of inner cylinder
U	mean flow velocity in axial direction
u	perturbation velocity in axial flow velocity
u_c	coefficient of cosine component of axial perturbation velocity for particular solution
u_s	coefficient of sine component of axial perturbation velocity for
v	perturbation velocity in circumferential flow velocity
v_c	coefficient of cosine component of circumferential perturbation velocity for particular solution
v_s	coefficient of sine component of circumferential perturbation velocity for particular solution
x	axial coordinate

Greek

Λ	eigenvalue of matrix equation
δ	dimensionless diffuser performance coefficient $\left[\delta = \frac{d\eta_s}{dh/H}\right]$
ζ_n	damping ratio of n^{th} mode
η	diffuser efficiency
η_s	static recovery coefficient
η_p	perturbation recovery coefficient

θ	circumferential coordinate
ρ	air density (Kg / m^3)
ϕ_n	n eigenfunction of a pinned-pinned cylinder
ϕ_n'	derived eigenfunction with respect to x
τ_x	frictional shear stress in axial direction
τ_θ	frictional shear stress in circumferential direction
ω	angular frequency [rad/s]
ω_n	natural frequency at zero mean flow velocity [rad/s]

Subscripts

a	air
cf	friction coefficient
D	damping
f	fluid
frc	friction
g	gap
I	inertia
K	stiffness
L	length
m	mode number
n	mode number
p	pressure
s	structure

x, X	horizontal direction
y, Y	vertical direction

Abbreviation

AGR	advanced gas-cooled reactor
FIV	flow-induced vibration
PSD	power spectral density
PWR	pressurized water reactor
rms	root mean square

LIST OF APPENDICES

APPENDIX I: Linearization of fluid equations.....145
APPENDIX II: The first order fluid boundary conditions for a diffuser exit.....148
APPENDIX III: Childs' procedures (Childs, 1993).....150
APPENDIX IV: Solution for a short-lossless entrance and a full-discharge exit fluid boundary conditions.....153

CHAPTER 1

INTRODUCTION AND LITERATURE REVIEW

1.1 Review of previous studies

Structures immersed in fluid flow are subjected to forces generated by the flow. When the fluid dynamic force is greater than the flexural rigidity of the structure, the dynamic force causes the structure to move. As a result, the orientation or the form of the structure changes. This deformation may in turn cause the fluid force to change, thus resulting in an interaction between the fluid flow and the structure, what we call, fluid-structure interaction or fluid-structure coupling. All structures in fluid flow are susceptible to flow-induced vibration, sometime even to fluidelastic instabilities.

The types of flows responsible for vibration problems are classified, based on flow configuration, as i) cross-flow, ii) internal axial flow, iii) external axial flow, iv) annular and/or leakage flow, and v) annular flow in finite lengths, irrespective of annular length; sometimes referred to as diffuser configuration. Confined flow may be divided into two types. The first one is relatively confined flow which is called annular flow. The other is tightly confined flow which is called leakage flow. The leakage flow refers not only to cylindrical geometries but also flat plates in rectangular ducts. Annular and/or leakage flow configurations, especially of finite length, are widely encountered in gas and water cooled nuclear reactor components and steam generators. For instance, the primary or secondary coolant flows in narrow annular passages around thermal shields in PWRs, around flow control devices, between fuel stringers and channels on AGRs, and between heat exchange tubes and supports. An important reason for interest in the configuration

is that annular-flow-induced vibration can be mostly observed in inherently flexible systems.

Axial-flow-induced vibration has been of less concern relative to its cross-flow counterpart. The reason for this is understood when considering cross-flow-induced vibrations where even moderate flow velocities may cause large amplitudes. In axial flow, however, the amplitudes of vibrations in industrial structures are generally small. Typical vibration amplitudes due to axial flow would be in the range 10^{-3} < Amplitude/Rod diameter < 10^{-2} (Paidoussis, 2004). The other reason why many researchers have been less concerned is that the phenomenon caused by the axial flow is basically random vibration. For this reason, no dynamic buckling (pitchfork bifurcation) and no flutter (Horf bifurcation) can be easily encountered. Paidoussis (1966) showed that instabilities can occur for cylinders even in axial flow, but at the same time that critical flow velocities are much higher than velocities in normal engineering applications.

The equation of motion for a cylinder in confined axial flow which was derived by Paidoussis (1966, 1973, and 1974) is well known and is popularly cited by researchers. When we consider the confinement effects, the basic mechanism is the same as for unconfined cases. However, the critical flow velocity is now much lower.

It is well known that cylinders in axial flow generally lose stability by divergence in the case of conservative systems such as pinned-pinned or clamped-clamped beam. Paidoussis and Pettigrew (1979) showed experimentally, with a flexible cylinder in confined flow, that cylinders could be significantly destabilized by confinement.

An inviscid analytical model for a body subjected to an external flow was developed by Mateescu and Paidoussis (1985). In this study, a small annular clearance and an axisymmetric rigid body pinned at one point and coaxially mounted in a cylindrical duct

was considered. Potential flow theory was used to determine the unsteady fluid dynamic forces. In a subsequent paper (Mateescu and Paidoussis, 1987), using a simplified form of the Navier-Stokes equations, the effect of fluid viscosity on the flow-induced vibration of the rigid center body was taken into account. In a latter study by Mateescu, et al. (1988), the analytical model was extended to deal with a continuous flexible centerbody in a narrow annular passage. Sim (1987) showed that friction forces contribute to the stability of the system, and that an annular gap generally has a destabilizing effect on the system as the annular gap becomes narrower.

Inada and Hayama (1988, 1990 and 2000) studied one-dimensional leakage-flow-induced vibrations of a rigid plate supported by translational and rotational springs in a narrow tapered passage formed by two fixed plates. In their work, the unsteady fluid force was obtained in terms of the added mass, the added damping and the added stiffness. They showed that single-mode flutter as well as divergence is possible with a divergent channel. Their studies strongly stimulated Japanese research in the field.

The effect of the annular gap on dynamic instability was studied by Tanaka et al. (2001), using small interconnected cylinders to simulate a fast train passing through a tunnel. They showed experimentally that as the annular gap diminished, instability for all test cases was observed, and the critical flow velocity decreased.

The dynamics of train-like articulated systems were recently studied by Sakuma at al. (2008a and 2008b) to investigate the dynamics of a high-speed train travelling in a confined cylindrical tunnel. They showed that the system loses stability by flutter, and that viscous frictional drag has a considerable effect on the stability of the system (2008a). The consecutive study (2008b) showed that no standing wave solution exists in the system, and that the response of the articulated system can be considerably amplified under certain conditions.

Inada (2004) considered the dispersion relation obtained by a travelling wave solution. He found that one component related to a forward travelling wave causes negative damping which is responsible for the onset of flutter for the multi-degree-of-freedom system. He pointed out that this mechanism is different from the flutter caused by a fluid force delay, which can occur in one-degree-of-freedom system in a leakage-flow system as was shown by Inada and Hayama (1988 and 1990) considering a rigid plate which allowed only translational motion.

Li et al. (2002) developed a mathematical model to study flutter instability of leakage-flow-induced vibration for a translational and rotational two-degree-of-freedom system. The mathematical model was extended by Langthjem et al. (2006). In their study, a flexible rod with equilibrium offset (eccentricity) in laminar or turbulent leakage flow was considered. According to their research, a simply supported rod may become unstable by either divergence or flutter. Considering a work-energy balance equation, they found that the centrifugal force is solely responsible for the divergence instability of the pinned-pinned and clamped-clamped rod. In other words, divergence is independent of fluid friction while flutter instability is affected by fluid friction. However, a travelling-wave solution is the only way to formulate the flutter instability.

The first attempt to develop a comprehensive analytical model for leakage-flow induced vibration was made by Hobson (1982). In that study, he considered the 1-D translational motion of a cylindrical center body coaxially positioned in an annular narrow passage. Neglecting the fluid velocity perturbation in the radial direction, the dynamics of the rigid cylindrical body was studied to see what the role of fluid boundary conditions is from the viewpoint of aerodynamic damping. Even though this study did not describe the overall dynamic behavior, it showed that the system can lose stability by flutter with a divergent flow boundary condition at the downstream end. Spur and Hobson (1984) later showed experimentally that negative aerodynamic damping could be possible for a diffuser angle of 4° or more.

Hobson's theory was validated by the experiments of Fujita et al. (1992 and 1994). The researchers made a test apparatus which could be closely controlled to simulate one-degree-of-freedom rigid body motion in a diffuser channel and could measure the fluid dynamic forces both for air and water flow. As a result, they verified that the system lost stability in the cases of a divergent configuration at the upstream end and a diffuser configuration at the downstream end, but not for the straight or convergent channel.

Parkin and Watson (1984) reported the vibration problem of a fuel rod in a gas cooled reactor. They showed experimentally that the instability mechanism in a 30° diffuser is predominantly a forced vibration due to vortex shedding, while that of a 6° diffuser originates from the pressure recovery characteristics of the diffuser. This was a very important discovery which served as a guideline a research on aerodynamic negative damping.

A rigid rod moving periodically in a finite-length annular-gap support was studied by Mulcahy (1980) to investigate fluid forces and hydraulic damping. In his study, tests were preformed in still water, so that a pressure recovery could not be simulated at the exit of the finite-length support. Consequently he found only positive damping in terms of annular gap and length. Hydraulic damping increases with decrease in gap size and increase in annular length. Mulcahy (1984) reported on a cantilevered tube conveying water which showed self-induced-excitation by leakage flow through a slip joint. Interestingly, he found that a limit cycle is attained below the flow rate at which the tube hits the wall, and that at high flow rate the unstable motion switched from first-mode to predominantly second-mode motion. As in Hobson's one-degree-of-freedom study, Mulcahy (1988) studied hydrodynamic negative damping for viscous fluid boundary conditions.

Gorman, et al. (1987) reported the fluid-elastic vibration of a thimble tube in a pressurized water reactor. In the study, a diffuser nozzle, straight hole nozzle and split square nozzle which has four vertical radial grooves were utilized. He found that large vibrations occurred with the diffuser nozzle.

Yasuo and Paidoussis (1989) investigated the flow-induced instability problem of heat exchanger tubes subjected to axial flow in a diffuser-shaped, loose intermediate support which is a problem similar to that studied in this research. In their study, a diffuser of finite length and the potential flow theory to determine fluid forces were considered together with a one-mode approximation of the inner tube. The researchers proposed a critical flow velocity equation for either divergence or flutter.

1.2 Motivation

Since Hobson reported, in 1982, the negative damping of a rod in a divergent channel, studies by Hobson (1984) and Fujita and Ito (1992 and1994) on the aerodynamic damping followed. These studies were all for 1-D translational mode of the rod. A few years later, hinged plates under rotational or rotational plus 1-D translational motion have been studied by Inada & Hayama (1988), then, other Japanese researchers followed the same scheme and extended their theory. Gorman reported, in 1987, that a finite-length diffuser caused the inner rod within it to reach dynamic instability. This work was followed by the study of Yasuo and Paidoussis for a cylinder subjected to axial flow through a finite-length diffuser. The problem that Yasuo and Paidoussis investigated is very practical and applicable to several important piping in power plants. However, the suggested model for critical flow velocity seems to be practically inapplicable for the piping. The critical velocity predicted by the model was too high, much higher than the critical velocity measured by experiments.

Many engineering applications for this subject can be found especially in the power generation plants, for instance, heat exchanger tubes with gap supports in steam generators, UO_2 fuel rods with spacer grids in fuel bundles and fuel pins in gas-cooled reactors during refueling, etc. Nonetheless, few articles can be found on this subject so far. Only a few studies on the dynamical behavior of the cylinder, treated as a continuous system, subjected to annular flow through a finite-length diffuser have been conducted.

Since a finite-length diffuser is a kind of gap support for the inner tube, and the inner tube could be damaged by fretting wear, it is very important not only to understand the physics behind the instability but also to develop a practical model to predict the critical flow velocities.

The foregoing is the motivation for the present work.

1.3 Objectives

Nowadays, numerical simulations such as FEM or BEM are very popular. For many engineering problems, these numerical tools are useful and appropriate. However, in many situations, analytical solutions are valuable, especially to explain an unknown phenomenon, to understand the physics behind it, to give insight on applications and to advance the related engineering field, often leading to unexpected results or applications.

For this reason, firstly, the purpose of this study is to obtain an analytical solution for the perturbation pressure inside of an annulus when a pinned-pinned inner cylinder is subjected to 2-D annular flow. For this study, Hobson's theory has been extended to consider a continuous system and frictional losses by the fluid.

Secondly, comparing the 1-D and 2-D annular flow models, a limitation of the 1-D flow model for a continuous beam will be found.

Thirdly, based on the analytical solution, the finite-length diffuser-induced vibration of a cylinder in axial leakage flow will be investigated by both analytical and experimental approaches.

Fourthly, the final goal of this study is to propose a semi-analytical model to predict the critical flow velocity for a pinned-pinned cylinder in terms of annular gap and diffuser angle of the finite-length gap support.

The expected contributions of this study are:

1. description of the limitation of the 1-D flow model for an annular-flow-induced vibration,

2. development of a frictional loss model for a pinned-pinned tube subjected to annular-flow,
3. development of an analytical model for annular-flow-induced vibration of a pinned-pinned tube,
4. experimental demonstration that a pinned-pinned tube subjected to annular flow in a finite-length gap support loses stability by flutter at low flow velocity,
5. development of an analytical solution for the perturbation pressure in a finite-length narrow-gap support when the inner tube is vibrating.
6. development of a semi-analytical model to predict the critical flow velocity for the tube in the finite-length gap support.

1.4 Thesis outline

This thesis consists of five chapters. Chapter 1 gives an introduction of the whole project. The historical background on this subject is briefly described from axial-flow-induced vibration to the annular- or leakage-flow-induced vibration in a finite-length gap support.

The second and third chapters are represented in the form of papers having their own abstract, introduction, methodology, results and list of references.

In Chapter 2, 1-D and 2-D flow models are developed for the annular-flow-induced vibration of a pinned-pinned tube and compared. With a new friction-loss model, analytical solutions for a perturbation pressure in an annulus are obtained for several flow boundary conditions at the ends of the tube when the inner tube vibrates.

In Chapter 3, the stability of a simply-supported tube subjected to narrow annular flow in a finite-length gap support is experimentally and analytically investigated. Based on the analytical solution, a simple semi-analytical model to predict the critical flow velocity is proposed for the first mode instability.

Chapter 4 is devoted to general discussion consisting of review of objectives, summary of contributions and recommendations for future work.

Final conclusions are presented in Chapter 5, followed by the references that are different from the references in Chapters 2 and 3.

CHAPTER 2

ANALYTICAL SOLUTION FOR A VIBRATING SIMPLY-SUPPORTED CYLINDER SUBJECTED TO 2-D CONCENTRIC ANNULAR FLOW CONSIDERING FRICTION

When an annular-flow-induced vibration of a long slender tube is analyzed, it would seem reasonable that 1-D flow model would be adequate. This is because not only the annular gap but also the radius-to-length ratio is small, so that the radial and circumferential flows can perhaps be considered negligible. Initially, the author, therefore, tried to solve the annular-flow-induced vibration problem by a one-dimensional flow model. However, the 1-D flow model could not correctly reproduce the experimental results.

In Chapter 2, therefore, 1-D and 2-D flow models are developed for the annular-flow-induced vibration of a pinned-pinned tube and compared. It is found that the 1-D model is not applicable for the continuous beam in general.

In addition, with a new friction-loss model, analytical solutions for the perturbation pressure in an annulus are obtained for several flow boundary conditions at the ends of the annulus when the inner tube vibrates. This study shows that the dynamics of annular-flow-induced vibrations obtained by the pressure loss theory is almost the same as by potential flow theory. However, the critical flow velocity is diminished considerably.

The results are presented in the form of a paper submitted to *Journal of Fluids and Structures*. In addition, Appendices containing the detailed derivation of the key equations are included at the end of the thesis.

Nomenclature(i)

$C_{f,P}$	perturbation term of the friction factor
$C_{f,S}$ or C_f	steady term of the friction factor
$C_{f,total}$	total friction factor (steady + perturbation)
EI	flexural rigidity
F_f	fluid forces per unit length due to perturbations
h	vibration response of the cylinder
K_{cf0}	proposed friction factor
κ_{cf1}	modified friction parameter ($K_{cf1}{}^2 = 1 + K_{cf0} / H$)
L	length
m	mode number
M_s	structural mass per unit length
M_f	added fluid mass
p	perturbation pressure
p_c	coefficient of cosine component of perturbation pressure for particular solution
p_s	coefficient of sine component of perturbation pressure for particular solution
p_{ratio}	ratio of each of perturbation pressure terms: 2-D to 1-D flow model
q	ratio of radius to length of the inner cylinder (R_d / L)
r	radial coordinate
R_d	radius of inner cylinder
Re	Reynolds number ($\mathrm{Re} = \frac{\rho U D_h}{\mu}$)
U	mean flow velocity in axial direction

Nomenclature(ii)

ι	perturbation velocity in axial flow velocity
u_c	coefficient of cosine component of axial perturbation velocity for particular solution
u_s	coefficient of sine component of axial perturbation velocity for particular solution
v	perturbation velocity in circumferential flow velocity
v_c	coefficient of cosine component of circumferential perturbation velocity for particular solution
v_s	coefficient of sine component of circumferential perturbation velocity for particular solution
x	axial coordinate
θ	circumferential coordinate
τ_x	frictional shear stress in axial direction
τ_θ	frictional shear stress in circumferential direction
ω	cyclic frequency

2.1 Abstract

An analytical model is proposed based on three main assumptions; (1) small perturbations in flow components, (2) negligible radial flow to reduce the annular flow to two-dimensional flow, and axial flow only for reduction to a one-dimensional flow, and (3) perturbation frictional loss depending on the variation of axial perturbation velocity in terms of space and time. In this study, it is concluded that (1) the difference in fluidelastic forces between two- and one-dimensional flow models mostly depends on cylinder radius, and on whether perturbation flow is mainly allowed in the axial or circumferential direction, (2) the one-dimensional flow model should be limited to 1-d.o.f vibration analysis or the case of a cylinder having a large radius-to-length ratio, and (3) the perturbation assumption makes little change to the dynamics of annular-flow-induced vibrations, however, the critical flow velocity is diminished considerably.

2.2 Introduction

Axial-flow-induced vibration problems have been of less concern than cross-flow-induced vibration problems, largely because the associated instabilities have rarely been encountered in practical applications. However, when axial flows are confined in narrow annular passages, the critical flow velocity may drop to the range of common engineering flow velocities. Recently, it was reported that for some fluid boundary conditions, a rod in annular flow could lose stability by flutter at a relatively low velocity. When low velocity instability is possible, dynamic instability (flutter) is more likely than static instability (divergence). For example, steel piping in practical application generally has low damping, so that fluidelastic forces could possibly overcome damping forces. It has been shown that fluidelastic stiffness needs high flow velocity to overcome rod stiffness.

In order to model the vibration response of a rod in annular viscous flow, Mateescu and Paidoussis (1985) adopted a linearized potential flow theory while Miller (1970), Hobson (1982) and Inada and Hayama (1988) took linearized pressure drop theory. The linearized potential flow theory seems to provide a relatively convenient procedure to obtain analytical solutions for concentric or even eccentric annular flows. However, the potential flow theory cannot model a dynamic instability such as flutter. On the contrary, by the linearized pressure drop theory, the dynamic instability can materialize although it is more difficult and even unlikely to obtain the analytical solution for a continuous system and 2-D flow with friction.

It is known that the first attempt to explain the dynamic instability of annular-flow-induced vibration was by Miller (1970). He used a simple restrictor in an annular channel, moving in a 1-D manner in a direction transverse to the axial flow, to demonstrate flutter instability. Hobson (1982) proposed an analytical model for a cylinder vibrating in an annular flow passage with several fluid boundary conditions. He obtained a closed- form solution, and showed that negative damping is possible for annular flow with an expansion channel at the downstream end. Even though his work was limited to 1-D translational motion of the cylinder, his work gave birth to several studies on this subject. Fujita and Ito (1992 and 1994) scrutinized Hobson's study with precise air and water loop tests. They showed that an annular flow passage with expansion channels, such as an abrupt expansion and diffuser, could lead to 1-D translational and rotational (rocking mode) destabilization and vibration. Porcher and de Langre (1997) proposed an analytical model of 1-D translational and rotational vibration based on 1-D flow considerations. They also carried out an experiment showing that a rod free to vibrate in 1-D rotational motion could lose stability by flutter.

The stability of a narrow tapered passage undergoing translational motion was studied by Inada (1988). The work was later further extended to a 2-d.o.f. vibrational model for translational and rotational motions (1990). It was shown that flutter and divergence are

possible for divergent channels. Since then, Inada and Hayama (2000), Kaneko et al. (2000) and Wu and Kaneko (2005) have tried to explain sheet flutter based on the 2-D plane leakage flow model of Inada (1990). Recently, Langthjem et al. (2007) used the 2-D plane model to analyze the instability mechanism of a flexible rod in leakage flow. The authors used flow rates instead of flow velocities in their analysis.

Many models of annular-flow problems neglect the flow velocity or axial flow distribution in the radial direction. The importance of the radial direction effects increases for annular flow with relatively large gaps, or for centrifugal pump where the inside shaft is rotating in a viscous fluid. In this case, however, circumferential flow consideration is also important. When radial direction effects are not considered, annular flow problems reduce to 2-D flow problems, or may be considered as 1-D if the circumferential flow is also negligible. For this reason, new comers in the field of annular-flow-induced vibration may question whether the 1-D flow model is enough for their analyses in cases where a continuous system is considered, and whether the differences between 1-D and 2-D flow models are important.

It is not easy to obtain an analytical solution particularly when friction is considered. However, once an analytical solution is obtained, a comparison can easily be made between 1-D and 2-D models. The aim of this study is, therefore, (1) to propose an analytical solution for a simply-supported cylinder subjected to two-dimensional concentric annular flow based on a new friction model, (2) based on the solution, to explain the discrepancies in fluidelastic forces between 1-D and 2-D flow models.

2.3 Fluid and structure equations

2.3.1 Equation of motion of a flexible inner cylinder in annular flow

Let's consider an oscillating flexible cylinder subjected to annular flow. The cylinder may be considered as an Euler–Bernoulli beam characterized by a flexural rigidity *EI*, length *L*, and structural mass per unit length M_s. Expressing the added fluid mass as M_f, the small amplitude vibration response of the cylinder by *h*, and fluid forces per unit length due to perturbations by F_f, the equation of motion of the flexible cylinder becomes

$$EI\frac{\partial^4 h}{\partial x^4}+M_f U^2\frac{\partial^2 h}{\partial x^2}+2M_f U\frac{\partial^2 h}{\partial x\partial t}+(M_s+M_f)\frac{\partial^2 h}{\partial t^2}=F_f \tag{2-1}$$

The fluid force F_f coupled to the small amplitude vibrations may be obtained by integrating the fluctuating pressure on the cylinder surface.

2.3.2 Fluid equations and boundary conditions

Consider the two-dimensional unsteady, incompressible annular flow between two concentric cylinders as shown in Fig. 2.1. Assuming small flow perturbations, the first-order continuity and momentum equations may be expressed as

$$H\frac{\partial u}{\partial x}+\frac{H}{r}\frac{\partial v}{\partial \theta}=-\frac{\partial h}{\partial t}-U\frac{\partial h}{\partial x}=0 \tag{2-2}$$

$$\frac{\partial p}{\partial x}+\rho\frac{\partial u}{\partial t}+\rho U\frac{1}{r}\frac{\partial v}{\partial \theta}+2\rho U\frac{1}{r}\frac{\partial u}{\partial x}+\frac{\tau_x}{H}=-\rho\frac{U}{H}\frac{\partial h}{\partial t}-\rho\frac{U^2}{H}\frac{\partial h}{\partial x} \tag{2-3}$$

$$\frac{1}{r}\frac{\partial p}{\partial \theta}+\rho\frac{\partial v}{\partial t}+\rho U\frac{\partial v}{\partial x}+\frac{\tau_\theta}{H}=0 \tag{2-4}$$

In equation (2-3) and (2-4), τ_x, and τ_θ are the non-conservative frictional shear stress. τ_θ may be neglected since there is no bulk flow in the circumferential direction. The reader

is referred to Appendix I for more details on the derivation of linearised equations (2-2) ~ (2-4).

Now, one may express several flow boundary conditions for both ends as follows:

Short loss-less inlet: $p(0)+\rho U u(0)=0$ (2-5)

Contraction loss (K_a) inlet: $p(0)+\rho U u(0)\left(1+K_a\right)=0$ (2-6)

Free discharge outlet: $p(L)=0$ (2-7)

Diffuser of efficiency η and diffuser performance coefficient δ at exit (Hobson, 1982):

$$p(L)+\eta\,\rho U u(L)+\frac{1}{2H}\rho U^2\delta\, h(L)=0 \tag{2-8a}$$

Diffuser of efficiency η and diffuser performance coefficient δ at entrance:

$$p(0)+\eta\,\rho U u(0)+\frac{1}{2H}\rho U^2\delta\, h(0)=0 \tag{2-8b}$$

Irrotational flow at entrance: $v(0)=0$ (2-9)

2.3.3 Two-dimensional flow

The partial differential equations (2-2), (2-3), and (2-4) are not simple since they deal with four functions p, u, v, and h, and two variables, x and θ. Once the support conditions of the inner cylinder are known, a solution may be approximated based on beam eigenfunctions. For a beam simply supported at both ends, one may assume that

the solution consists of a sum of sine functions of the axial variable x, and a sum of sine and cosine functions of the circumferential variable θ.

Considering the pinned-pinned beam, the total channel gap coupled with the vibration amplitude may be expressed as

$$\bar{h}(x,\theta,t) = H + h(x,\theta,t) \tag{2-10}$$

where $h(x,\theta,t) = Y(x,t)cos\theta + Z(x,t)sin\theta$ (2-11)

With the help of equation (2-11), the following solutions are assumed for the dependent perturbation variables.

$$u(x,\theta,t) = u_{1c}(x,t)cos\theta + u_{1s}(x,t)sin\theta \tag{2-12a}$$

$$v(x,\theta,t) = v_{1c}(x,t)cos\theta + v_{1s}(x,t)sin\theta \tag{2-12b}$$

$$p(x,\theta,t) = p_{1c}(x,t)cos\theta + p_{1s}(x,t)sin\theta \tag{2-12c}$$

Substituting the assumed solutions and equations (2-12a) ~ (2-12c) into equations (2-2) ~ (2-4) and collecting and equating the coefficients of $sin\theta$ and $cos\theta$, one obtains six equations. Introducing the four complex variables

$$h = Y + jZ \tag{2-13a}$$

$$u = u_{1c} + ju_{1s} \tag{2-13b}$$

$$v = v_{1c} + jv_{1s} \tag{2-13c}$$

$$p = p_{1c} + jp_{1s} \tag{2-13d}$$

yields the following three complex equations (Childs 1993).

$$\frac{\partial u}{\partial x} - i\frac{1}{r}v = -\frac{1}{H}\frac{\partial h}{\partial t} - \frac{U}{H}\frac{\partial h}{\partial x} \tag{2-14}$$

$$\frac{\partial p}{\partial x} + \rho\frac{\partial u}{\partial t} - i\rho\frac{U}{r}v + 2\rho U\frac{\partial u}{\partial x} + \frac{\tau_x}{H} = -\rho\frac{U}{H}\frac{\partial h}{\partial t} - \rho\frac{U^2}{H}\frac{\partial h}{\partial x} \tag{2-15a}$$

$$\text{or } \frac{\partial p}{\partial x} + \rho\frac{\partial u}{\partial t} + \rho U\frac{\partial u}{\partial x} + \frac{\tau_x}{H} = 0 \tag{2-15b}$$

$$-i\frac{1}{r}p + \rho\frac{\partial v}{\partial t} + \rho U\frac{\partial v}{\partial x} = 0 \tag{2-16}$$

where, τ_x is the fluid friction shear stress. Equation (2-15b) is obtained by substituting equation (2-14) multiplied by ρU into equation (2-15a) to eliminate v and h. Starting with equations (2-11) ~ (2-16) and using the procedure developed by Childs (1993), the partial differential equations are transformed to ordinary differential equations.

The complex displacement of function $h(x,t)$ in equation (2-13a) is expressed in the following form for a simply-supported cylinder.

$$h(x,t) = a\,sin\left(\frac{m\pi}{L}x\right)e^{i\omega t} \tag{2-17}$$

Analytical solutions for u, v and p consist of sum of complementary and particular solutions. For the pinned-pinned cylinder, the solutions may be expressed as

$$u(x,t) = \sum_{j=1}^{3}\overline{u}_j \cdot e^{\Lambda_j x}\cdot e^{i\omega t} + \left(u_s \cdot h + u_c \cdot \frac{dh}{dx}\right)\cdot e^{i\omega t} \tag{2-18}$$

$$p(x,t) = \sum_{j=1}^{3}\overline{p}_j \cdot e^{\Lambda_j x}\cdot e^{i\omega t} + \left(p_s \cdot h + p_c \cdot \frac{dh}{dx}\right)\cdot e^{i\omega t} \tag{2-19}$$

$$v(x,t) = \sum_{j=1}^{3}\overline{v}_j \cdot e^{\Lambda_j x}\cdot e^{i\omega t} + \left(v_s \cdot h + v_c \cdot \frac{dh}{dx}\right)\cdot e^{i\omega t} \tag{2-20}$$

The quentities, u_s, u_c, p_s, p_c, v_s, and v_c are coefficients which must be determined. While the assumed solutions (2-18), (2-19) and (2-20) should satisfy equations (2-14) ~ (2-16), the homogenous and particular solutions can be determined independently. Injecting only the homogeneous solution components in equations (2-18) ~ (2-20) into equations (2-14) ~ (2-16), the following eigenvalue equation for Λ_j and $\left[\overline{u}_j \ \overline{p}_j \ \overline{v}_j\right]^T$ is obtained. For simplicity, the analysis presented in this section is restricted to the frictionless case.

$$\begin{bmatrix} \Lambda_j & 0 & -i\frac{1}{r} \\ \rho\left(i\omega + 2U\Lambda_j\right) & \Lambda_j & -i\frac{\rho U}{r} \\ 0 & -i\frac{1}{r} & \rho(i\omega + U\Lambda_j) \end{bmatrix} \begin{Bmatrix} \overline{u}_j \\ \overline{p}_j \\ \overline{v}_j \end{Bmatrix} = 0 \tag{2-21}$$

Similarly, injecting only the particular solution components into equations (2-14) ~ (2-16) yields the following set of equations for u_s, u_c, p_s, p_c, v_s, and v_c.

$$\frac{\left(Ur + Hru_s - iHv_c\right)}{Hr}\frac{dh}{dx} + \frac{\left(-iHv_s - Hr\lambda_m{}^2 u_c + ir\omega\right)}{Hr}h = 0 \tag{2-22a}$$

$$\frac{r\rho U^2 + H\left(p_s r + 2r\rho U u_s - i\rho U v_c + ir\rho\omega u_c\right)}{Hr}\frac{dh}{dx} - \frac{H\left[r\lambda_m{}^2\left(p_c + 2\rho U u_c\right) + i\rho\left(Uv_s - r\omega u_s\right)\right] - ir\rho\omega U}{Hr}h = 0 \tag{2-22b}$$

$$\frac{-ip_c + \rho r\left(i\omega v_c + Uv_s\right)}{r}\cdot\frac{dh}{dx} + \frac{-ip_s + \rho r\left(i\omega v_s - \lambda_m{}^2 U v_c\right)}{r}\cdot h = 0 \tag{2-22c}$$

where $\lambda_m = \frac{m\pi}{L}$, $m = 1, 2, 3\ldots$

In equation (2-21), the determinant of the matrix must be zero to have a non-trivial solution. One easily arrives at the three conditions, $\Lambda_1 = -\frac{1}{r}$, $\Lambda_2 = \frac{1}{r}$ and $\Lambda_3 = -i\frac{\omega}{U}$ similarly to Hobson (1982). Knowing that $h = \sin(\lambda_m x)$ and $dh/dx = \lambda_m \cos(\lambda_m x)$, equations (2-22a) ~ (2-22c) yield six equations from which six coefficients (, u_s, u_c, p_s, p_c, v_s, and v_c) are determined.

The final three solutions with corresponding relationships are

$$u(x) = \sum_{j=1}^{3} \overline{u}_j \cdot e^{\Lambda_j x} - \left[\frac{r^2 \lambda_m{}^2}{H\left(1 + r^2 \lambda_m{}^2\right)} U \cdot h - i \frac{r^2 \omega}{H\left(1 + r^2 \lambda_m{}^2\right)} \cdot \frac{dh}{dx} \right] \tag{2-23}$$

$$p(x) = \sum_{j=1}^{3} \overline{p}_j \cdot e^{\Lambda_j x} + \left[\frac{\rho r^2 \left(U^2 \lambda_m{}^2 + \omega^2\right)}{H\left(1 + r^2 \lambda_m{}^2\right)} \cdot h - i \frac{2 \rho r^2 \omega U}{H\left(1 + r^2 \lambda_m{}^2\right)} \cdot \frac{dh}{dx} \right] \tag{2-24}$$

$$v(x) = \sum_{j=1}^{3} \overline{v}_j \cdot e^{\Lambda_j x} + \left[\frac{r\omega}{H\left(1 + r^2 \lambda_m{}^2\right)} \cdot h - i \frac{rU}{H\left(1 + r^2 \lambda_m{}^2\right)} \cdot \frac{dh}{dx} \right] \tag{2-25}$$

with

$$(1)\ \Lambda_1 = -\frac{1}{r} :\ i\overline{u}_1 - \overline{v}_1 = 0,\ \overline{p}_1 + \rho\left(U - ir\omega\right) \cdot \overline{u}_1 = 0 \tag{2-26}$$

$$(2)\ \Lambda_2 = \frac{1}{r} :\ i\overline{u}_2 + \overline{v}_2 = 0,\ \overline{p}_2 + \rho\left(U + ir\omega\right) \cdot \overline{u}_2 = 0 \tag{2-27}$$

$$(3)\ \Lambda_3 = -i\frac{\omega}{U} :\ \overline{v}_3 + \frac{r\omega}{U} \cdot \overline{u}_3 = 0,\ \overline{p}_3 = 0 \tag{2-28}$$

As noted by Hobson (1982), the first two conditions (2-26, 2-27) represent irrotational velocities associated with pressure fields while the third stands for a vortical velocity. However, once the friction term is considered in equation (2-15a) or (2-15b), the three

conditions are not as simple as equation (2-26) ~ (2-28) owing to the existence of non-conservative energy loss.

Final solutions are obtained by using the non-triviality conditions, equations (2-26) ~ (2-28), and two flow boundary conditions among equations (2-5) to (2-9).

For instance, when an annular flow is coupled with a short-lossless inlet and a free-discharge outlet, equation (2-5) with equations (2-23) and (2-24) give

$$\overline{p}_1 + \overline{p}_2 - i\frac{2\rho r^2 \omega U}{H\left(1+r^2\lambda_m{}^2\right)} \cdot \left.\frac{dh}{dx}\right|_{x=0} + \rho U\left(\overline{u}_1 + \overline{u}_2 + i\frac{r^2\omega}{H\left(1+r^2\lambda_m{}^2\right)} \cdot \left.\frac{dh}{dx}\right|_{x=0}\right) = 0 \qquad (2\text{-}29)$$

In addition, $\overline{u}_3$ is zero because the inlet flow is irrotational so that the vortical velocity is zero. For a free discharge at the exit, equation (2-7) together with equations (2-23) and (2-24) give

$$e^{-\frac{L}{r}} \cdot \overline{p}_1 + e^{\frac{L}{r}} \cdot \overline{p}_2 - i\frac{2\rho r^2 \omega U}{H\left(1+r^2\lambda_m{}^2\right)} \cdot \left(\frac{dh}{dx}\right)_{x=L} = 0 \qquad (2\text{-}30)$$

Equations (2-26), (2-27), (2-29), (2-30) with $\overline{u}_3 = 0$ give

$$\begin{bmatrix} -\rho(ir\omega - U) & 0 & 0 & 1 & 0 \\ 0 & \rho(ir\omega + U) & 0 & 0 & 1 \\ 0 & 0 & 1 & 0 & 0 \\ \rho U & \rho U & 0 & 1 & 1 \\ 0 & 0 & 0 & e^{-\frac{L}{r}} & e^{\frac{L}{r}} \end{bmatrix} \begin{Bmatrix} \overline{u}_1 \\ \overline{u}_2 \\ \overline{u}_3 \\ \overline{p}_1 \\ \overline{p}_2 \end{Bmatrix} = \begin{bmatrix} 0 \\ 0 \\ 0 \\ ir^2\omega\dfrac{\rho U + 1}{H\left(1+r^2\lambda_m{}^2\right)} \cdot \left.\dfrac{dh}{dx}\right|_{x=0} \\ i\dfrac{2\rho r^2 \omega U}{H\left(1+r^2\lambda_m{}^2\right)} \cdot \left(\dfrac{dh}{dx}\right)_{x=L} \end{bmatrix} \qquad (2\text{-}31)$$

where $\left(\frac{dh}{dx}\right)_{x=L} = (-1)^m \cdot a \cdot (\lambda_m), \quad \lambda_m = \frac{m\pi}{L}, \quad m = 1,\ 2,\ 3,\ldots$ (2-32)

and a is the vibration response amplitude.

Solving equation (2-31) for each $\overline{u}_j$ and $\overline{p}_j$, substituting these into equation (2-24), and following some mathematical operations, one obtains the following equation:

$$\begin{aligned} p(x) = & \frac{\rho r^2 \left(\lambda_m{}^2 U^2 + \omega^2\right)}{H\left(1 + r^2 \lambda_m{}^2\right)} \cdot h - i \frac{2\rho r^2 \omega U}{H\left(1 + r^2 \lambda_m{}^2\right)} \cdot \frac{dh}{dx} \\ & - \frac{\rho r U (U + i r\omega)(U - ir\omega) \cdot e^{(2L-x)/r}}{H\left(1 + r^2 \lambda_m{}^2\right)\left[\left(1 + e^{2L/r}\right)U + i\left(-1 + e^{2L/r}\right) r\omega\right]} \cdot \left|\frac{dh}{dx}\right|_{x=0} \\ & + i\omega \frac{2\rho r^2 U (U - ir\omega) \cdot e^{(-L+x)/r}}{H\left(1 + r^2 \lambda_m{}^2\right)\left[\left(1 + e^{2L/r}\right)U + i\left(-1 + e^{2L/r}\right) r\omega\right]} \cdot \left|\frac{dh}{dx}\right|_{x=L} \end{aligned} \quad (2\text{-}33)$$

For the mathematical operations, the Mathematica (2007) software was utilized with the assumptions that $r \ll L$ and $e^{L/r} \ll e^{2L/r}$. When $e^{-(L+x)/r} \ll 1$ is considered, equation (2-33) becomes

$$\begin{aligned} p(x) = & \frac{\rho r^2 \left(\lambda_m{}^2 U^2 + \omega^2\right)}{H\left(1 + r^2 \lambda_m{}^2\right)} \cdot h - i \frac{2\rho r^2 \omega U}{H\left(1 + r^2 \lambda_m{}^2\right)} \cdot \frac{dh}{dx} \\ & - \frac{\rho r U (U - ir\omega)}{H\left(1 + r^2 \lambda_m{}^2\right)} \cdot e^{-x/r} \cdot \left|\frac{dh}{dx}\right|_{x=0} + i\omega \frac{2\rho r^2 U}{H\left(1 + r^2 \lambda_m{}^2\right)} \cdot \left|\frac{dh}{dx}\right|_{x=L} \cdot e^{(-L+x)/r} \end{aligned} \quad (2\text{-}34)$$

The procedure for the other fluid boundary conditions is described in Appendix A.

Once the pressure is determined, the fluid force per unit length F_f in equation (2-1) is calculated by integrating the perturbation pressure $p(x,t)$ over the surface of the cylinder as follows:

$$F_f = -\int_0^{2\pi} (p\cos\theta)\cdot(rd\theta)\cos\theta d\theta = -\int_0^{2\pi} p\cdot r\left(\cos\theta\right)^2 d\theta \tag{2-35}$$

2.3.4 One-dimensional flow

When it comes to one-dimensional flows, by eliminating the circumferential components from equation (2-2), (2-3) and (2-4), the following two simple equations emerge:

$$H\frac{\partial u}{\partial x}+\frac{\partial h}{\partial t}+U\frac{\partial h}{\partial x}=0 \tag{2-36}$$

$$\frac{\partial p}{\partial x}+\rho\frac{\partial u}{\partial t}+\rho U\frac{\partial u}{\partial x}+\frac{\tau_x}{H}=0 \tag{2-37}$$

Now, the vibration response of the cylinder may be expressed by

$$h'(x,t) = H + h(x)\cdot e^{i\omega t} \tag{2-38}$$

Using the technique of separation-of-variables, substituting equation (2-38) into (2-36) and integrating with respect to the spatial variable x, one obtains an expression for $u(x)$, then, with equation (2-37), the pressure function may be obtained. If the cylinder is simply-supported, $u(x)$ and $p(x)$ are, respectively,

$$u(x)=\frac{i\omega}{H\lambda_m{}^2}\frac{dh}{dx}-\frac{Uh}{H}+C_1 \tag{2-39}$$

$$p(x)=\rho\frac{U^2\lambda_m{}^2+\omega^2}{H\lambda_m{}^2}h-\frac{i2\rho\omega U}{H\lambda_m{}^2}\frac{dh}{dx}-i\rho\omega xC_1+C_2 \tag{2-40}$$

where C_1 and C_2 are integration constants which may be determined from the fluid boundary conditions of equations (2-5) ~ (2-9). One finds four solutions for the pressure function with respect to the spatial variable x.

For instance, in the case of the short loss-less inlet and free discharge outlet, the pressure function is giving by

$$\begin{aligned}p(x)=&\rho\frac{U^2\lambda_m{}^2+\omega^2}{H\lambda_m{}^2}\cdot h-\frac{i2\rho U\omega}{H\lambda_m{}^2}\cdot\frac{dh}{dx}\\&+\rho\frac{U^2\lambda_m{}^2(U+i(L-x)\omega)+\omega^2(U+i(L-x)\omega)}{H\lambda_m{}^2(U+iL\omega)}\cdot|h|_{x=0}\\&-\rho U\cdot\frac{(L-x)}{H\lambda_m{}^2(U+iL\omega)}\omega^2\cdot\left|\frac{dh}{dx}\right|_{x=0}\\&+\rho\frac{U^2\lambda_m{}^2(U+ix\omega)+\omega^2(U+ix\omega)}{H\lambda_m{}^2(U+iL\omega)}\cdot|h|_{x=L}+i\omega\frac{2\rho U(U+ix\omega)}{H\lambda_m{}^2(U+iL\omega)}\cdot\left.\frac{dh}{dx}\right|_{x=L}\end{aligned} \tag{2-41}$$

where a is the vibration amplitude. Since $|h|_{x=0}=0$ and $|h|_{x=L}=0$, equation (2-41) becomes

$$\begin{aligned}p(x)=&\rho\frac{U^2\lambda_m{}^2+\omega^2}{H\lambda_m{}^2}\cdot h-\frac{i2\rho U\omega}{H\lambda_m{}^2}\cdot\frac{dh}{dx}\\&-\rho U\cdot\frac{(L-x)}{H\lambda_m{}^2(U+iL\omega)}\omega^2\cdot\left.\frac{dh}{dx}\right|_{x=0}+i\omega\frac{2\rho U(U+ix\omega)}{H\lambda_m{}^2(U+iL\omega)}\cdot\left.\frac{dh}{dx}\right|_{x=L}\end{aligned} \tag{2-42}$$

The reader is referred to Appendix B for the pressure functions corresponding to other fluid boundary conditions.

2.4 Comparison of 1-D with 2-D flow equations

As shown in equation (2-34) and Appendix A, the pressure functions for the two-dimensional flow model may be divided into two groups; one having the displacement function $h(x)$, or $h'(x)$ and the other consisting of the exponential functions, $e^{(-x/r)}$, or $e^{(x-L)/r}$. The effect of the exponential functions is most important at the annular entrance ($e^{-x/r}$) or at the exit ($e^{(x-L)/r}$). In the rest of the region, their effects are almost negligible. The simply-supported cylinder does not vibrate at the ends, so that the entrance and exit effects are insignificant despite the exponential terms in the solutions.

Similarly, as shown in equation (2-42) and Appendix B, solutions for one-dimensional flow consist of the same functions $h(x)$, or $h'(x)$ *as* for the two-dimensional model, and of some linear functions, such as, x and L-x, of the cylinder length x which are equivalent to the entrance and the exit effects of the two-dimensional flow model.

Comparing equation (2-34) and (2-42), it can be noted that the difference between the models comes mainly from the term $r^2 / H\left(1+r^2\lambda_m{}^2\right)$ and $1/H\lambda_m{}^2$ for 2-D and 1-D flow, respectively. Knowing that $\lambda_m = m\pi / L$, the two terms may be rewritten as $\frac{L^2}{H\left[(L/r)^2 + m^2\pi^2\right]}$ and $\frac{L^2}{Hm^2\pi^2}$. Therefore, they may be approximately equated only if $\frac{L^2}{r^2} + (m\pi)^2 \approx (m\pi)^2$, which means that the higher the mode number and the larger the cylinder radius, the better the approximation. In other words, a 1-D flow model may be inappropriate for real piping since the cylinder radius is small, and a few low modes are important.

In the next two sections, comparison is made in two ways; one is for the case where the entrance and exit effects are neglected, which we call a simplified comparison, the second when all terms are included, thus a full comparison.

2.4.1 Simplified Comparison

For a simply-supported cylinder, since both ends do not vibrate, the entrance and the exit effects are negligible, so that a simple comparison could be effective even for different fluid boundary conditions.

Neglecting the terms having $e^{-x/r}$ and $e^{(x-L)/r}$, for all flow boundary conditions, the pressure perturbation solutions reduce to one case, which can be confirmed in Appendices. There are three added terms; fluid inertia term, fluid damping term, and stiffness term. In order to make a comparison of each of the pressure terms, we divide each term of the 1-D flow by the equivalent 2-D term. In the three cases, the following equation is obtained.

$$p_{ratio} = \frac{p(x)_{1-D}}{p(x)_{2-D}} = \frac{R_d^{\,2}\lambda_m^{\,2}}{1+R_d^{\,2}\lambda_m^{\,2}} \tag{2-43}$$

where, R_d is the radius of the inner cylinder.

Since $\lambda_m = m\pi / L, \quad (m = 1,2,3,\ldots)$, where m is the mode number of the beam eigenfunction, introducing a new parameter q which is the ratio of radius to length of the inner cylinder, equation (2-43) becomes

$$p_{ratio} = \frac{q^2 m^2 \pi^2}{1 + q^2 m^2 \pi^2} \tag{2-44}$$

where $q = R_d / L$.

The variation of p_{ratio} is shown in Fig. 2.2 as a function of q and m. As shown in Fig. 2.2, when the radius-to-length ratio is small, the pressure ratio is small as well, which means that the one-dimensional model exaggerates the three fluidelastic forces for small radius-to-length ratios. Generally, for most engineering applications, e.g. piping system such as tubes in steam generators and the fuel tubes of Pressurized Water Reactors (PWR), the ratio q is 0.03 at the most. The overstatement worsens with decreasing mode number.

2.4.2 Full Comparison

When the exponential terms are included, there are additional terms involving $U \pm ir\omega$ in the pressure equations (2-33), (2A-3), (2A-5) and (2A-8) for the two-dimensional model, and $U \pm iL\omega$ in the denominator of the pressure equations (2-42), (2B-1), (2B-2) and (2B-3) for the one-dimensional model. It is, therefore, hard to separate every term according to ω^2, ω or other, and to make the direct comparison in terms of inertia, damping and stiffness forces.

It is, however, worth noting that the two terms, $U \pm iL\omega$ in the one-dimensional model and $U \pm ir\omega$ in the two-dimensional model, have velocity dimensions, and the second terms $iL\omega$, and $ir\omega$ are added due to the vibration of the inner cylinder. Since the one-dimensional model does not allow the flow to be squeezed in the circumferential direction, when the inner cylinder moves toward the wall of the outer cylinder during vibration, the perturbed flow can only move in the axial direction while for the two-dimensional model flow in the circumferential direction occurs as well. This may be the

reason why the vibration frequency ω is coupled with the inner rod length L in the 1-D model. Physically, however, only some mid-length part of the whole length reaches close to the wall. Some fluid near the mid-length region probably moves in the axial direction, and the fluid flows relatively easily when the radius of the inner cylinder is considerably large. Therefore, the one-dimensional model may be suitable for an inner cylinders of large diameter and short length which vibrates in the manner of a rigid body. However, generally speaking, fluid squeezing in the circumferential direction is more plausible for many engineering applications. $U \pm i r \omega$ and $U \pm i L \omega$ are included in the terms which give strong effects at the ends, so that the effects may be exaggerated when the cylinder vibrates in a one-dimensional manner, without any support at the ends.

In order to separate and collect the terms with respect to the order of ω, with consideration of the structure equation (2-1), one may make the equation third order in terms of frequency ω by multiplying every numerator on the right side by $U \pm i L \omega$ for 1-D flow or $U \pm i r \omega$ for 2-D flow. For instance, for the case of the two-dimensional flow model with short loss-less and free discharge boundary conditions, one obtains

$$-i M_3 \cdot \omega^3 - M_2 \cdot \omega^2 + i D_1 \cdot \omega + K_0 = 0 \tag{2-45}$$

where,

$$M_3 = r \cdot \left[\left(M_t \right) + \frac{\rho \pi r^3}{H(1 + r^2 \lambda_m{}^2)} \right] \cdot h \tag{2-46a}$$

$$M_2 = U\left(M_t + \frac{\rho\pi r^3}{H(1+r^2\lambda_m{}^2)}\right)\cdot h + 2U\,r\left(M_f + \frac{\rho\pi r^3}{H(1+r^2\lambda_m{}^2)}\right)\cdot\frac{dh}{dx}$$
$$+\frac{\rho\pi r^4 U}{H(1+r^2\lambda_m{}^2)}\cdot\left|\frac{dh}{dx}\right|_{x=0}\cdot e^{-x/r} - \frac{2\rho\pi r^4 U}{H(1+r^2\lambda_m{}^2)}\cdot\left|\frac{dh}{dx}\right|_{x=L}\cdot e^{(-L+x)/r} \qquad (2\text{-}46b)$$
$$+\frac{2\rho\pi r^4 U}{H(1+r^2\lambda_m{}^2)}\cdot\left|\frac{dh}{dx}\right|_{x=L}\cdot e^{-(L+x)/r}$$

$$D_1 = r\lambda_m{}^2\left[EI\,\lambda_m{}^2 - \frac{\rho\pi r^3U^2}{H(1+r^2\lambda_m{}^2)}\right]\cdot h + 2U^2\left[M_f + \frac{\rho\pi r^3}{H(1+r^2\lambda_m{}^2)}\right]\cdot\frac{dh}{dx}$$
$$+ rU^2 M_f\cdot\frac{d^2h}{dx^2} - \frac{2a\rho\pi r^3U^2}{H(1+r^2\lambda_m{}^2)}\cdot e^{(-L+x)/r}\cdot\left|\frac{dh}{dx}\right|_{x=L} \qquad (2\text{-}46c)$$
$$-\frac{2a\rho\pi r^3U^2}{H(1+r^2\lambda_m{}^2)}\cdot e^{-(L+x)/r}\cdot\left|\frac{dh}{dx}\right|_{x=L}$$

$$K_0 = \lambda_m{}^2U\left[EI\,\lambda_m{}^2 - \frac{\rho\pi r^3U^2}{H(1+r^2\lambda_m{}^2)}\right]\cdot h + U^3M_f\cdot\frac{d^2h}{dx^2}$$
$$+\frac{\rho\pi r^2U^3}{H(1+r^2\lambda_m{}^2)}\cdot e^{-x/r}\cdot\left|\frac{dh}{dx}\right|_{x=0} \qquad (2\text{-}46d)$$

For the one-dimensional model for the same boundary conditions, the equivalent terms are

$$M_3 = L\cdot\left[\left(M_t\right) + \frac{\rho\pi r^3}{H\lambda_m{}^2}\right]\cdot h \qquad (2\text{-}47a)$$

$$M_2 = U\left(M_t + \frac{\rho\pi r^3}{H\lambda_m{}^2}\right)\cdot h + 2U\,L\left(M_f + \frac{\rho\pi r^3}{H\lambda_m{}^2}\right)\cdot\frac{dh}{dx}$$
$$-\frac{2\rho\pi rU}{H\lambda_m}\cdot x\cdot\left|\frac{dh}{dx}\right|_{x=L} - \frac{\rho\pi rU}{H\lambda_m}\cdot(L-x)\cdot\left|\frac{dh}{dx}\right|_{x=0} \qquad (2\text{-}47b)$$

$$D_1 = L\lambda_m{}^2\left[EI\,\lambda_m{}^2 - \frac{\rho\pi r^3U^2}{H\lambda_m{}^2}\right]\cdot h + 2U^2\left[M_f + \frac{\rho\pi r^3}{H\lambda_m{}^2}\right]\cdot\frac{dh}{dx} + LU^2\,M_f\cdot\frac{d^2h}{dx^2} - \frac{2\rho\pi rU^2}{H\lambda_m}\cdot\left|\frac{dh}{dx}\right|_{x=L} \tag{2-47c}$$

$$K_0 = \lambda_m{}^2U\left[EI\,\lambda_m{}^2 - \frac{\rho\pi r^3U^2}{H\lambda_m{}^2}\right]\cdot h + U^3M_f\cdot\frac{d^2h}{dx^2} \tag{2-47d}$$

When it comes to the third order equation, there are some similarities between equation (2-46a) ~ (2-46d) for the two-dimensional model and equation (2-47a) ~ (2-47d) of the one-dimensional model, relative to the variables *"r"* and *" L"*. The overall expressions are, however, very different. Multiplication by the length L, instead of the radius r, makes the coefficients of each term very large when $r << L$.

Numerical simulations

For the short loss-less inlet and free-discharge outlet, utilizing equation (2-45), (2-46a) ~ (2-46d) and (2-47a) ~ (2-47d), a Galerkin projection may be used to grasp and to compare the dynamics provided by the one-dimensional and the two-dimensional flow models. A state-space algorithm is employed to solve the third order equations and to depict the solution in Argand diagrams. The parameters used for the numerical computations are

(1) ratio of radius to length (r / L): 0.00364 (= 0.008/2.2)

(2) inner diameter of cylinder: 14.2 mm

(3) annular gap (H) : 5.15 mm

(4) Young's modulus (E): 2.1×10^{11} Pascal

(5) compressed air density (ρ): 10 kg/m^3

(6) inner cylinder density: 7,800 kg/m^3

For definition of the dimensionless flow velocity, the expression $\bar{U} = LU\sqrt{\frac{M_f}{EI}}$ is used. Not only inviscid hydrodynamic mass ($M_{virtual} = \rho \cdot A$) but also annular confinement are considered to yield a fluid mass per unit length M_f (Paidoussis, 2004).

A pinned-pinned cylinder subjected to annular-flow-induced vibrations is known to lose stability consecutively by divergence at a dimensionless flow velocity of 3.14 for the first mode and 6.28 for the second mode when the same parameters are used. Coupled-mode flutter is then observed. Fig. 2.3 shows the dynamics based on linear theory, reproduced according to Paidoussis' theory (Paidoussis, 2004).

However, completely different predictions are made with the one-dimensional flow model as shown in Fig.2.4. First of all, the inner cylinder loses stability in the second mode by flutter at dimensionless velocity $\bar{U} = 0.01 (= 1.1$ m/s). Since then, this model gives divergence instability at the first mode. These critical flow velocities are, however, too low. It is believed that these implausible results occur because flow is not allowed in the circumferential direction but only in the axial direction, so that the fluid effects from the cylinder vibration are coupled only with the cylinder length.

The two-dimensional flow model gives results similar to those of the axial flow theory (Paidoussis 1966 and 1969) as shown in Fig. 2.5. In accordance with the theory which is proposed here, the inner rod loses stability by divergence in the first mode and the second mode consecutively at dimensionless flow velocities of 2.36 and 4.71, respectively. As the flow velocity is increased coupled-mode flutter occurs at 4.95 dimensionless flow velocity. The two first modes undergo divergence, and then experience coupled-mode flutter at much higher flow. This is a linear dynamics

approach based on a linear theory, so that, strictly, it may not be applicable to the behavior beyond the first instability.

2.5 Friction

2.5.1 Perturbation pressure and axial flow velocity

In developing the analytical model, the most difficult part is implementation of the friction loss. Since the friction loss has the form $K_{cf}\frac{\rho}{H}Uu$, the eigenvalues for a nontrivial solution do not have a simple form as in section 2.3. In order to avoid this complexity and to have a simpler form of solution, equation (2-3) or equation (2-15) is written as

$$\frac{\partial p}{\partial x}+\rho\frac{\partial u}{\partial t}+\rho U\frac{\partial u}{\partial x}+K_{cf0}\frac{\rho}{H}\left(U\frac{\partial u}{\partial x}+\frac{\partial u}{\partial t}\right)=0 \qquad (2\text{-}48)$$

In equation (2-48), the last term represents the rate of change of turbulent friction momentum per unit length, in which the operator $\left(U\frac{\partial}{\partial x}+\frac{\partial}{\partial t}\right)$ is assumed to have a similar definition as in Paidoussis (2004, chapter 8.2). Differently from conventional steady friction loss, the frictional loss due to flow perturbations is assumed to be proportional not only to the product of the mean flow velocity and the spatial variation of the perturbation flow velocity but also proportional to its time variation.

Equating the friction term in equation (2-48) to equation (2-15b), the friction term becomes

$$\frac{\tau_x}{H} = \frac{\rho}{H} K_{cf0} \left(U \frac{\partial u}{\partial x} + \frac{\partial u}{\partial t} \right) \tag{2-49}$$

Here, regarding equation (2-49), a definition of the friction factor K_{cf0} is needed. This is done in section 2.5.2 below.

Substituting equation (2-49) into (2-15b), and rewriting equation (2-15b), the following matrix equation can be written which is equivalent to equation (2-21) for the frictionless case:

$$\begin{bmatrix} \Lambda_j & 0 & -i\frac{1}{r} \\ \rho\left[i\omega\left(\kappa_{cf1}{}^2\right) + U\Lambda_j\left(\kappa_{cf1}{}^2\right)\right] & \Lambda_j & 0 \\ 0 & -i\frac{1}{r} & \rho(i\omega + U\Lambda_j) \end{bmatrix} \begin{Bmatrix} \overline{u}_j \\ \overline{p}_j \\ \overline{v}_j \end{Bmatrix} = 0 \tag{2-50}$$

where $\kappa_{cf1}{}^2 = 1 + K_{cf0} / H$ (2-51a)

or $\kappa_{cf1}{}^2 = 1 + \hat{K}_{cf0}$ (2-51b)

Complementary solutions can be obtained for the three conditions; $\Lambda_1 = -\frac{\kappa_{cf1}}{r}$, $\Lambda_2 = \frac{\kappa_{cf1}}{r}$ and $\Lambda_3 = -i\frac{\omega}{U}$. For each, one obtains three relationships between the coefficients of pressure $\overline{p}_i$, circumferential flow velocity $\overline{v}_i$ and the axial flow velocity $\overline{u}_i$ as follows:

$$(1)\ \Lambda_1 = -\frac{\kappa_{cf1}}{r}:\ i\kappa_{cf1}\overline{u}_1 - \overline{v}_1 = 0,\ \overline{p}_1 + \rho\kappa_{cf1}\left[U\kappa_{cf1} - i\,r\omega\right]\cdot\overline{u}_1 = 0 \tag{2-51}$$

$$(2)\ \Lambda_2 = \frac{\kappa_{cf1}}{r}:\ i\kappa_{cf1}\overline{u}_2 + \overline{v}_2 = 0,\ \overline{p}_2 + \rho\kappa_{cf1}\left(\kappa_{cf1}U + ir\omega\right)\cdot\overline{u}_2 = 0 \tag{2-52}$$

$$(3)\ \Lambda_3 = -i\frac{\omega}{U}:\ \overline{v}_3 + \frac{r\omega}{U}\cdot\overline{u}_3 = 0,\ \overline{p}_3 = 0 \tag{2-53}$$

Similarly to the case without friction effects, following the procedure from equation (2-23) to equation (2-27) and equation (2-29) to (2-33), the following equations are obtained for the perturbation flow velocity and perturbation pressure *p(x,t)* considering friction loss.

$$\begin{aligned} p(x) = {} & \frac{\rho r^2 \kappa_{cf1}{}^2\left(\lambda_m{}^2 U^2 + \omega^2\right)}{H\left(\kappa_{cf1}{}^2 + r^2\lambda_m{}^2\right)}\cdot h - i\frac{2\rho r^2 \kappa_{cf1}{}^2\,\omega U}{H\left(\kappa_{cf1}{}^2 + r^2\lambda_m{}^2\right)}\cdot\frac{dh}{dx} \\ & + i\omega\frac{\rho r^2\cdot e^{-x\kappa_{cf1}/r}}{H\left(1+r^2\lambda_m{}^2\right)}\cdot\frac{U\kappa_{cf1}\left(U\kappa_{cf1} - i r\omega\right)}{\left[\left(-1+\kappa_{cf1}{}^2\right)U - i\kappa_{cf1} r\omega\right]}\left[\frac{dh}{dx}\right]_{x=0} \\ & + i\omega\frac{2\rho r^2 U\cdot e^{(-L+\kappa_{cf1}\cdot x)/r}}{H\left(1+r^2\lambda_m{}^2\right)}\left[\frac{dh}{dx}\right]_{x=L} \end{aligned} \tag{2-54}$$

$$\begin{aligned} u(x) = {} & \frac{r^2 U}{H\left(\kappa_{cf1}{}^2 + r^2\lambda_m{}^2\right)}\cdot\frac{d^2h}{dx^2} + i\omega\frac{r^2}{H\left(\kappa_{cf1}{}^2 + r^2\lambda_m{}^2\right)}\cdot\frac{dh}{dx} \\ & - i\omega\frac{r^2 U}{H\left(1+r^2\lambda_m{}^2\right)}\cdot\frac{e^{-\kappa_{cf1}x/r}}{\left[\left(-1+\kappa_{cf1}{}^2\right)U - i\kappa_{cf1} r\omega\right]}\cdot\left|\frac{dh}{dx}\right|_{x=0} \\ & + i\omega\frac{2e^{(-L+\kappa_{cf1}x)/r}\cdot r^2}{H\left(1+r^2\lambda_m{}^2\right)\kappa_{cf1}\left(\kappa_{cf1}U + i\,r\omega\right)}\cdot\left|\frac{dh}{dx}\right|_{x=L} \end{aligned} \tag{2-55}$$

The first term in equation (2-54) dominates the real pressure field while the second term dominates the imaginary pressure component. Both terms have a strong effect over the entire channel length while the last two terms have an effect at the entrance (third term) and at the exit (fourth term) of the annular channel. Knowing that the simply-supported cylinder does not allow displacement at either end, the perturbation pressure field is unlikely to have significant effect on the dynamics of the cylinder. Equation (2-54) is

equivalent to equation (2-34) for the short-lossless inlet and the free-discharge exit with no friction consideration.

2.5.2 Perturbation friction factor

The steady friction factor may be described by a single variable which is the mean flow velocity U. The perturbation friction factor, however, needs more variables such as the perturbation flow velocity and the vibration frequency. Knowing that the fluid and structure are coupled, one may reasonably assume that the perturbation and its friction factor come not only from the flowing fluid but also from the vibrating structure. There is no available experimental data so far, and it may not be easy to determine the perturbation friction factor by experiment. In the present work, the commonly used steady friction factor has been divided into real and imaginary components as described below.

It is widely accepted that the steady friction factor is dependent on the Reynolds number. For instance, Langthjem (2006) used the experimental results of Shimoyama and Yamada (1957) in which $C_f = 0.26 \times \mathrm{Re}^{-0.24}$ for turbulent flow, and $C_f = 48 \times \mathrm{Re}^{-1}$ for laminar flow. In this study, K_{cf0} is defined to be a friction factor for perturbation flow. The perturbation flow frictional loss cannot be easily predicted or obtained by a simple experiment.

Let's introduce the work of Langthjem(2006), which is developed based on the work of Shimoyama and Yamada (1957). The total friction factor is expressed as

$$C_{f,total} = C_{f,S} + C_{f,P} \left(= C_{f,Steady} + C_{f,Pertub.} \right)$$

$$= 48 \cdot \mathrm{Re}^{-1} (1 - \frac{\Delta Q_y}{\bar{Q}_y}), \quad \mathrm{Re} \le 1300 \quad \text{(Langthjem ,2006)}$$

$$= 0.26 \cdot \mathrm{Re}^{-0.24}(1 - 0.24\frac{\Delta Q_y}{\bar{Q}_y}), \quad \mathrm{Re} \geq 2000 \text{ (Langthjem ,2006)}$$

The flow rate Q is used in place of flow velocity. Considering concentric annular flow, the perturbation friction factor in terms of flow velocity may be rewritten as

$$C_{f,total} \simeq 48 \cdot \mathrm{Re}^{-1}(1 - \frac{u}{U}), \quad \mathrm{Re} \leq 1300 \tag{2-56}$$

$$C_{f,total} \simeq 0.26 \cdot \mathrm{Re}^{-0.24}(1 - 0.24\frac{u}{U}), \quad \mathrm{Re} \geq 2000 \tag{2-57}$$

In accordance with the assumption that every term has a perturbation component, the friction loss (F_{frc}) in the axial momentum equation (2-15b) is written as

$$\frac{\tau_x}{H} = \frac{1}{2} \cdot \left(C_{f,s} + C_{f,p}\right) \cdot \rho(U+u)^2 \cdot \frac{1}{H} \simeq C_{f,s}\frac{\rho}{H}Uu + C_{f,p}\frac{\rho}{2H}U^2 \tag{2-58}$$

For laminar flow, equation (2-58) becomes

$$\begin{aligned} \frac{\tau_x}{H} &= 48 \cdot \mathrm{Re}^{-1} \cdot \frac{\rho}{H}Uu + 48 \cdot \mathrm{Re}^{-1} \cdot \left(-\frac{u}{U}\right)\frac{\rho}{2H}U^2 \\ &= 24 \cdot \mathrm{Re}^{-1} \cdot \frac{\rho}{H}Uu, \end{aligned} \tag{2-59}$$

and for turbulent flow, equation (2-58) gives

$$\begin{aligned} \frac{\tau_x}{H} &= 0.26 \cdot \mathrm{Re}^{-0.24} \cdot \frac{\rho}{H}Uu + 0.26 \cdot \mathrm{Re}^{-0.24} \cdot \left(-0.24\frac{u}{U}\right)\frac{\rho}{2H}U^2 \\ &= 0.2288 \cdot \mathrm{Re}^{-0.24} \cdot \frac{\rho}{H}Uu \end{aligned} \tag{2-60}$$

Substituting equation (2-59) and (2-60) into equation (2-49), one obtains two equations as follows:

(1) Laminar flow, $\mathrm{Re} \le 1300$:

$$24 \cdot \frac{\rho U}{H} \cdot \mathrm{Re}^{-1} \cdot \frac{\rho U}{H} u(x,t) \simeq \frac{\rho}{H} K_{cf0} \left(U \frac{\partial}{\partial x} + \frac{\partial}{\partial t} \right) u(x,t) \tag{2-61}$$

(2) Turbulent flow, $\mathrm{Re} \ge 2000$:

$$0.2288 \cdot \mathrm{Re}^{-0.24} \frac{\rho U}{H} u(x,t) \simeq \frac{\rho}{H} K_{cf0} \left(U \frac{\partial}{\partial x} + \frac{\partial}{\partial t} \right) u(x,t) \tag{2-62}$$

When a simply supported beam having eigenfunctions $\phi_n(x) = Sin(n\pi / L)$ is considered, the axial perturbation flow velocity equation (2-55) becomes

$$u(x) = \frac{r^2}{H\left(\kappa_{cf1} + r^2 \lambda_m{}^2\right)} \cdot \left(U\phi''(x) + i\omega\phi'(x) \right) \tag{2-63}$$

Introducing the operators $\left(U \frac{\partial^2}{\partial x^2} + \frac{\partial^2}{\partial x \partial t} \right)$, or $\frac{\partial}{\partial x}\left(U \frac{\partial}{\partial x} + \frac{\partial}{\partial t} \right)$ and $\frac{d}{dx}\left(U \frac{d^2}{dx^2} + i\omega \frac{d}{dx} \right)$, and using equation (2-63), equations (2-61) and (2-62) become

$$\begin{aligned} &24 \cdot \mathrm{Re}^{-1} U \cdot \left(U \frac{d^2}{dx^2} + i\omega \frac{d}{dx} \right) \phi(x) \\ &- K_{cf0} \left[U \frac{d}{dx} \left(U \frac{d^2}{dx^2} + i\omega \frac{d}{dx} \right) \phi(x) + i\omega \left(U \frac{d^2}{dx^2} + i\omega \frac{d}{dx} \right) \phi(x) \right] \simeq 0 \end{aligned} \tag{2-64}$$

$$0.2288 \cdot \mathrm{Re}^{-0.24} U \cdot \left(U \frac{d^2}{dx^2} + i\omega \frac{d}{dx} \right) \phi(x) - K_{cf0} \left[U \frac{d}{dx} \left(U \frac{d^2}{dx^2} + i\omega \frac{d}{dx} \right) \phi(x) + i\omega \left(U \frac{d^2}{dx^2} + i\omega \frac{d}{dx} \right) \phi(x) \right] \simeq 0 \tag{2-65}$$

Cancelling out the common terms, one obtains

$$24 \cdot \mathrm{Re}^{-1} U \cdot \phi(x) - K_{cf0} \left(U \frac{d\phi(x)}{dx} + i\omega\phi(x) \right) \simeq 0, \tag{2-66}$$

and

$$0.2288 \cdot \mathrm{Re}^{-0.24} U \cdot \phi(x) - K_{cf0} \left(U \frac{d\phi(x)}{dx} + i\omega\phi(x) \right) \simeq 0 \tag{2-67}$$

The final equations are

$$K_{cf0} \simeq \frac{24 \cdot \mathrm{Re}^{-1}}{\left[U \left(\phi'(x)/\phi(x) \right) + i\omega \right]} \cdot U \quad \text{for } \mathrm{Re} \le 1300 \tag{2-68}$$

$$K_{cf0} \simeq \frac{(0.2288) \cdot \mathrm{Re}^{-0.24}}{\left[U \left(\phi'(x)/\phi(x) \right) + i\omega \right]} \cdot U \quad \text{for } \mathrm{Re} \ge 2000 \tag{2-69}$$

The friction factor for laminar flow, equation (2-68), is small and almost flat over the total cylinder length and flow velocity, which is generally less than a few m/s for moderate gap size annular flows. The friction factor for turbulent flow, equation (2-69), depends significantly on the axial position and flow velocity.

Strictly speaking, however, K_{cf0} is actually not a dimensionless factor anymore. K_{cf0} has length dimensions, so that $1 + K_{cf0}/H$ or $1 + \hat{K}_{cf0}$ in equation (2-51a, 2-51b) can,

practically, be interpreted as a friction factor. When K_{cf0} is zero, the matrix equation (2-50) reduces to the frictionless case. Therefore, the new friction factor becomes

$$K_{cf1}{}^2 = 1 + \hat{K}_{cf0} \simeq 1 + \frac{24 \cdot \mathrm{Re}^{-1} \cdot U}{H\left[U\left(\phi'(x)/\phi(x)\right) + i\omega\right]} \quad \text{for } \mathrm{Re} \le 1300 \tag{2-70}$$

$$K_{cf1}{}^2 = 1 + \hat{K}_{cf0} \simeq 1 + \frac{(0.2288) \cdot \mathrm{Re}^{-0.24} \cdot U}{H\left[U\left(\phi'(x)/\phi(x)\right) + i\omega\right]} \quad \text{for } \mathrm{Re} \ge 2000 \tag{2-71}$$

Equations (2-70) and (2-71) suggest that the perturbation friction factor is dependent not only on the flow velocity but also on the vibration frequency of the inner cylinder. It is also not constant, depending on the axial location on the cylinder.

Numerical simulations

For the numerical simulations of the short loss-less entrance and free-discharge exit, the following parameters are used.

(1) ratio of radius to length (r/L): 0.00364
(2) inner diameter of cylinder: 14.2 mm
(3) annular gap (H): 5.15 mm
(4) Young's modulus of the cylinder: 2.1×10^{11} Pascal
(5) inner cylinder density: 7,800 kg/m^3
(6) hydraulic diameter: 10.3 mm
(7) compressed air density: 10 kg/m^3

Fig. 2.6 to 2.8 shows the variation of the new friction factor $K_{cf1}{}^2$ over the inner cylinder length as a function of air flow velocity for the first three modes when the frequency $\omega = \omega_n$, and the flow boundary conditions are a short loss-less entrance and a

full discharge exit. Fig. 2.6 shows that first friction factor is not flat over the cylinder length but coupled somehow with the mode shape of the inner cylinder, and the shape becomes sharper and magnitudes bigger as flow velocity increases. Interestingly, the real part of the first friction factor shows a similarity to the second mode shape of the cylinder, and the real peak-to-peak values are almost the same as the absolute imaginary values. The second and the third friction factors show similar trends to the first one in terms of flow velocity except that the real part of the second friction factor resembles the fourth mode shape of the cylinder while the third one is similar to the 6^{th} mode. The second and third imaginary friction factors have two and three peaks, respectively, which are shown in Figs. 2.7 and 2.8.

Substituting the perturbation friction factor developed for the simply-supported cylinder in equation (2-71) into equation (2-54), one may obtain the perturbation pressure distribution as a function of the cylinder length, frequency and flow velocity. The pressure function, as seen in equation (2-54), can be divided into three terms; ω^2 related terms, ω related terms and ω independent terms, which may be called inertia, damping, and stiffness terms, respectively. The three terms are shown in Fig. 2.9 ~ 2.11 for the case where the entrance and exit effects are not considered.

As seen in the figures, even though the mass and stiffness terms have imaginary components, they are negligibly small hence the two terms have mostly real values. Conversely, the damping term has predominantly imaginary values. It is physically true that the phase difference between mass and stiffness is 180°, and between mass and damping, or stiffness and damping is 90°. The stiffness term is the most predominant among the three terms.

What is the meaning of the imaginary part of the mass and the stiffness term, and the real part of the damping term? It is believed that the terms are perturbations coming from system complexity. The strongly coupled system may not be clearly distinguished

into the three terms. Our new friction factor in equations (2-70) and (2-71) turns out to be coupled with vibration frequency (imaginary) as well as flow velocity (real), so that, as far as the mass and stiffness terms are concerned, imaginary parts could come from the frequency-coupled components while the real part of the damping could come from the flow velocity-dependent term. As seen in Fig. 2.9, each term of the first perturbation pressure is strongly coupled with the first beam mode; although the damping term does not seem to correspond to the first mode, it matches a 90-degree-shifted first mode. Similarly, each term of the second and third perturbation pressure is coupled with the second mode and the third mode, respectively.

Fig. 2.12 shows the total perturbation pressure, real and imaginary components, normalized for the different modes. As expected, stiffness terms are predominant in the real part while the damping term is dominant in the imaginary part. Comparing the real and imaginary parts, 90^{o} phase differences are clearly seen.

The dynamic behavior of the simply-supported cylinder in annular flow is shown in Fig. 2.13. The dynamics of the present model is basically similar to the model of axial-flow-induced vibration developed by Paidoussis (1966, 1969). Beyond the first instability, the second mode divergence is found, then, the converged first and second modes undergo coupled-mode flutter as the third instability. One may predict that, since the stiffness term of the perturbation pressure is negatively predominant, the system loses stability by divergence. The cylinder is estimated to lose its first stability at $\bar{U}$ =2.36 while the non-perturbation-based model predicts a critical flow velocity of 3.14. Even though the overall dynamics proposed by the friction-based model is somewhat different, the first critical flow velocity is very close to the velocity predicted by the previous model neglecting friction.

2.6 Conclusions

In this study, Hobson's work is further extended to be applicable to annular-flow-induced vibration of a pinned-pinned cylinder based on a two-dimensional flow model with friction. For the friction consideration, a new concept of a perturbation friction factor is introduced, which consists of a real and imaginary part. By using the proposed friction model, friction effects can be analyzed and applied for all the vibration modes. It is shown that not only the friction factor but also the perturbation pressure is strongly coupled with the mode shapes of the simply-supported cylinder.

By the proposed new friction factor, the theoretical solutions for unsteady pressure and flow velocities are easily obtained. In addition, the perturbation pressure can reasonably be analyzed as three terms; ω^2 related terms, ω related terms and ω independent terms. The ω independent term, which is a fluidelastic stiffness force, is the most predominant among the three terms, so that static-type instability could be expected.

The proposed two-dimensional flow model shows that the predicted fluid forces are significantly different from those of a one-dimensional fluid model for a pinned-pinned cylinder subjected to annular flow. It is believed that the large difference is attributable to the cylinder radius-to-length ratio and to whether or not circumferential flow is allowed. Considering that the one-dimensional flow model does not allow for fluid to be squeezed in the circumferential direction, utilization of the one-dimensional flow model is probably limited to radius-to-length ratios larger than 0.8, or to one-dimensional vibrations such as 1-d.o.f translational or rotational (rocking) motion (Hobson 1982, Fujita and Ito, 1992 and 1994, Porcher and de Langre, 1997).

The flow perturbation theory does lead to some change of dynamics of the annular-flow-induced vibrations of a cylinder as compared to the confined mean flow velocity theory

which does not consider perturbations. It turns out that small perturbations decrease the first dimensionless critical flow velocity down to 2.36 from 3.14 when only mean flow is considered.

The proposed friction-based model is expected to give solutions for different support conditions of a cylinder such as cantilevered and fixed-fixed cylinders. Also, it may further be extended to give an analytical solution to the problem of a finite-length annular gap support.

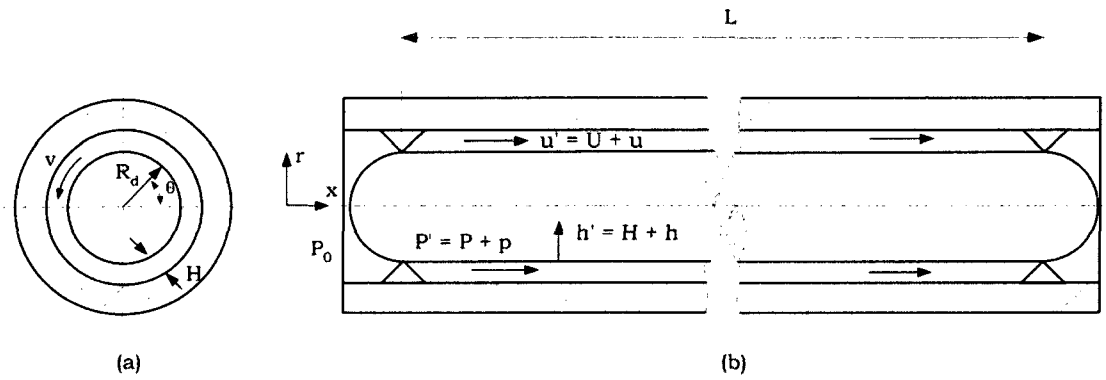

Figure.2.1 (a) Definition of coordinates and symbols of the system in radial direction, and (b) in longitudinal direction. A flexible cylinder of length L and external radius R_d is confined in an annulus with a fluid gap H. The fluid pressure p′, axial flow velocity u′, circumferential flow velocity v′, and vibration amplitude of the rod h′ consist of steady terms P, U, V, and H and perturbation terms p, u, v and h respectively. However, bulk flow in the circumferential direction does not exist because the main flow is in axial direction, so v′ equals zero.

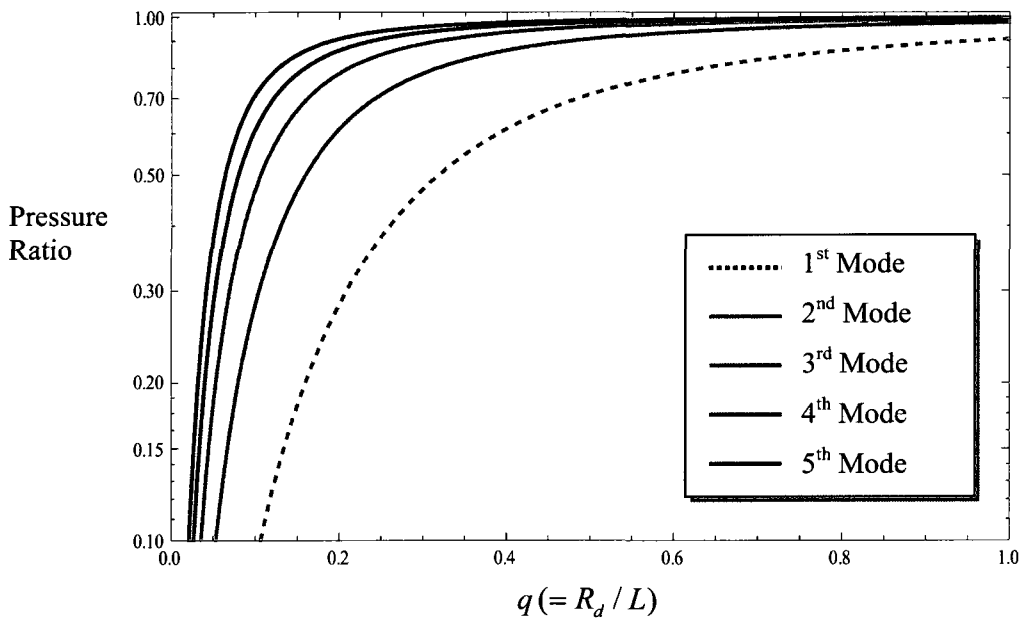

Figure 2.2 Pressure ratios of the two-dimensional flow model to the one-dimensional flow model as a function of the radius-to-length ratio and beam eigenfunction mode number.

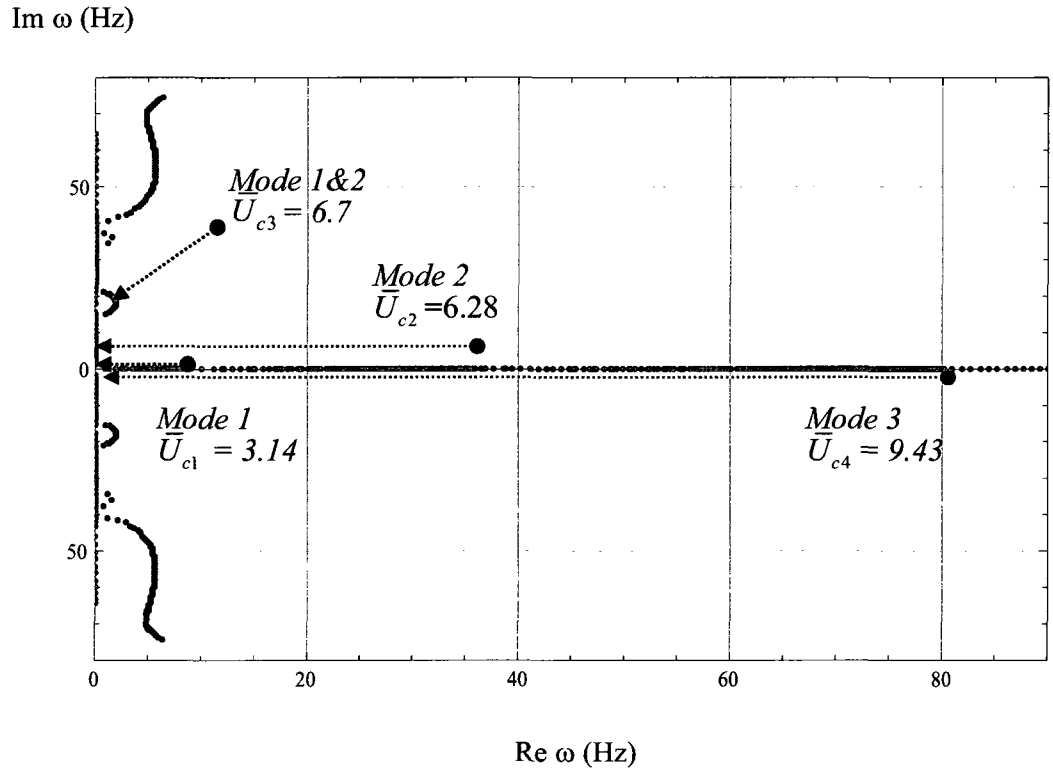

Figure 2.3 Argand diagram for the pinned-pinned cylinder subjected to annular air flow according to Paidoussis theory. The first instability is the first mode buckling at $Uc_1 = 3.14$, the second mode buckling at $Uc_2 = 6.28$, the first and second coupled-mode flutter at $Uc_3 = 6.7$ and the third mode buckling at $Uc_4 = 9.43$

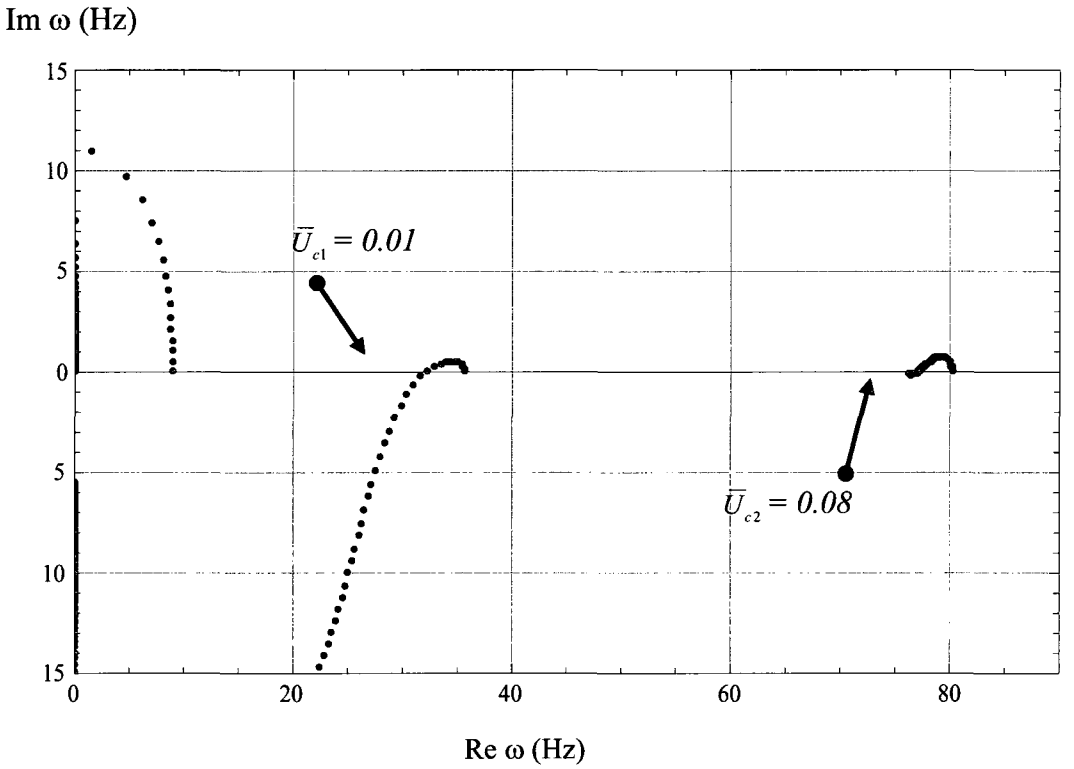

Figure 2.4 Argand diagram for the pinned-pinned cylinder subjected to annular air flow for the one-dimensional flow model without frictional loss. The first instability is the second mode flutter at Uc_1 = 0.01 (1.1 m/s), the third mode flutter at Uc_2 =0.08 (9 m/s).

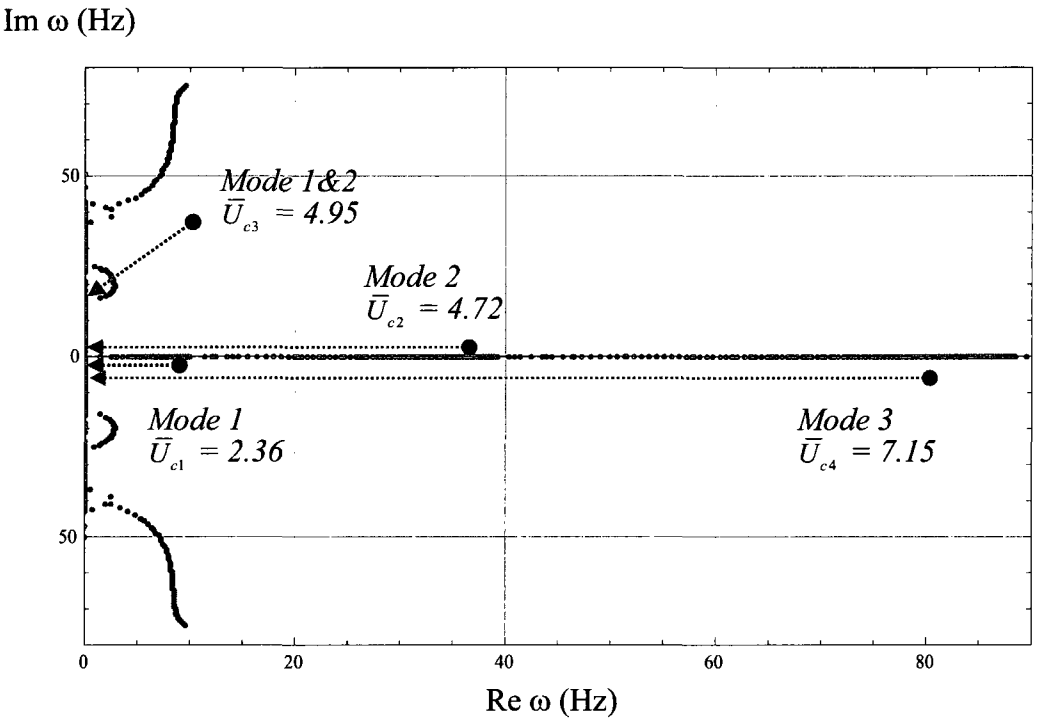

Figure 2.5 Argand diagram for the pinned-pinned cylinder subjected to annular air flow for the two-dimensional flow model without frictional loss. The first instability is the first mode buckling at dimensionless Uc_1 = 2.36, the second mode buckling at Uc_2 =4.72, the first and second coupled-mode flutter at Uc_3 = 4.95, and the third mode buckling at Uc_4 =7.15

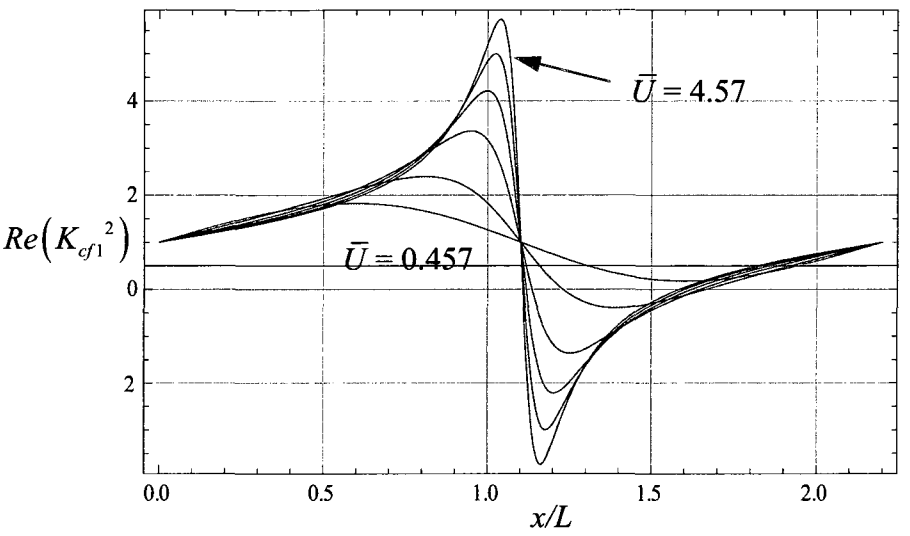

(a) Real Part

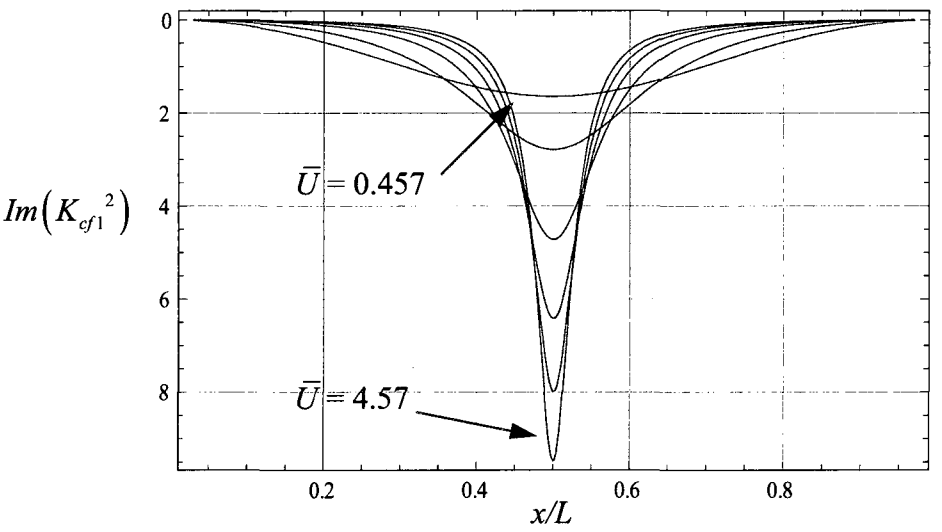

(b) Imaginary Part

Figure 2.6 Real and imaginary parts of friction factor $K_{cf1}{}^2\left(=1+\hat{K}_{cf0}\right)$ when the inner cylinder vibrates at 10 Hz in the 1st mode, and the dimensionless flow velocities are 0.457, 0.914, 1.827, 2.74, 3.65, and 4.57

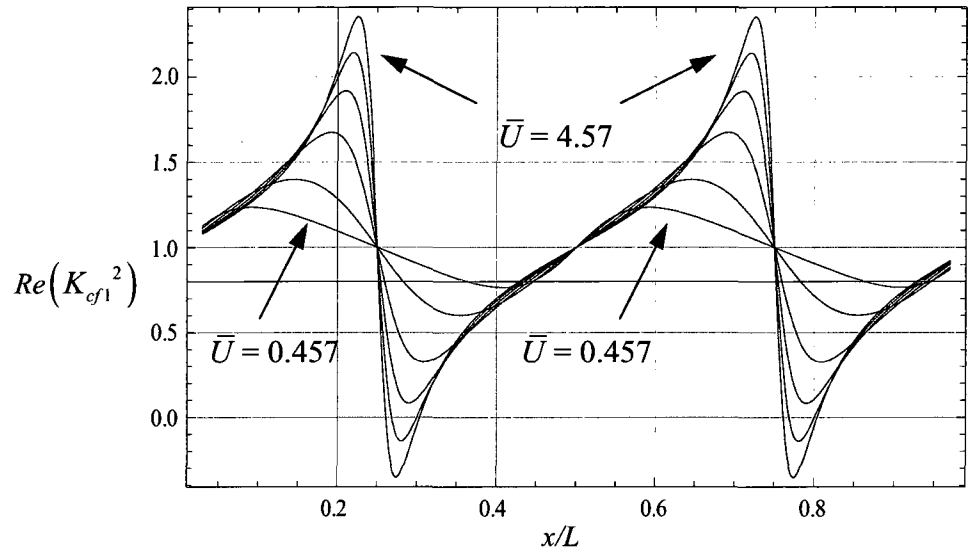

(a) Real Part

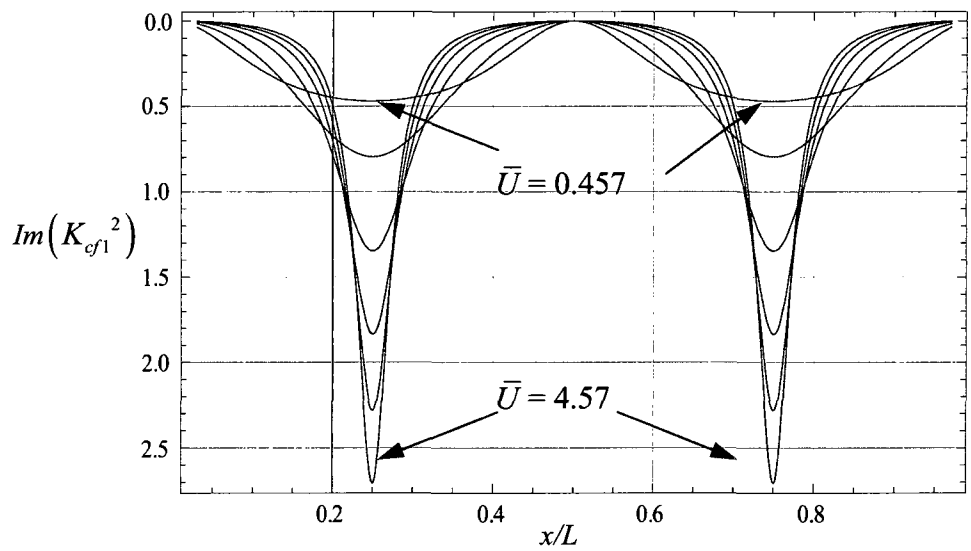

(b) Imaginary Part

Figure 2.7 Real and imaginary parts of friction factor $K_{cf1}{}^2\left(=1+\hat{K}_{cf0}\right)$ when the inner cylinder vibrates at 35 Hz in the 2nd mode, dimensionless flow velocities are 0.457, 0.914, 1.827, 2.74, 3.65, and 4.57

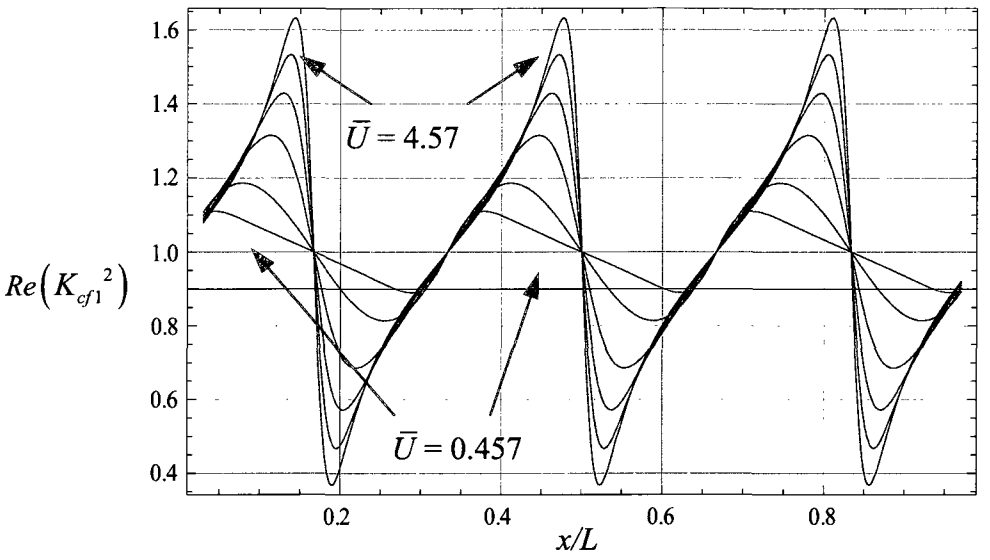

(a) Real Part

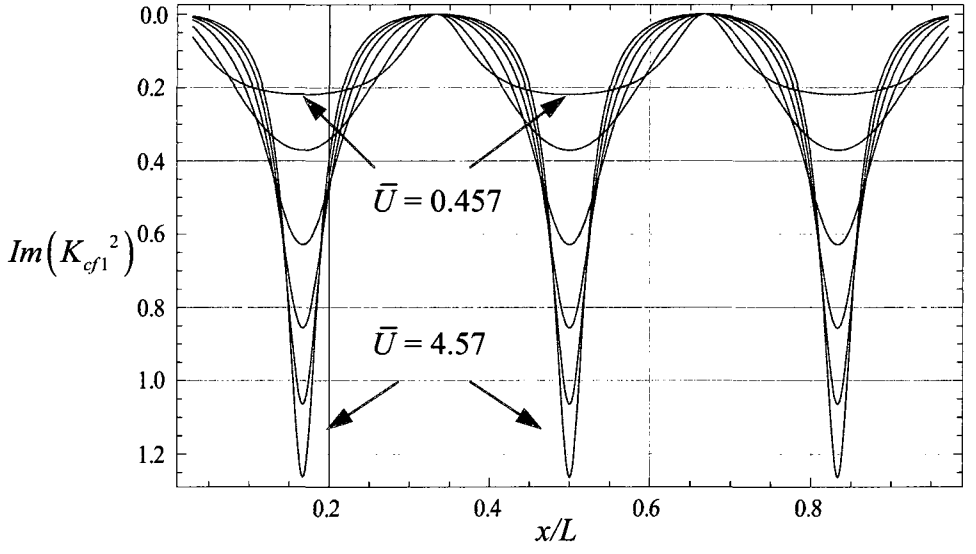

(b) Imaginary Part

Figure 2.8 Real and imaginary parts of friction factor $K_{cf1}{}^2\left(=1+\hat{K}_{cf0}\right)$ when the inner cylinder vibrates at 75 Hz in the 3rd mode, dimensionless flow velocities are 0.457, 0.914, 1.827, 2.74, 3.65, and 4.57

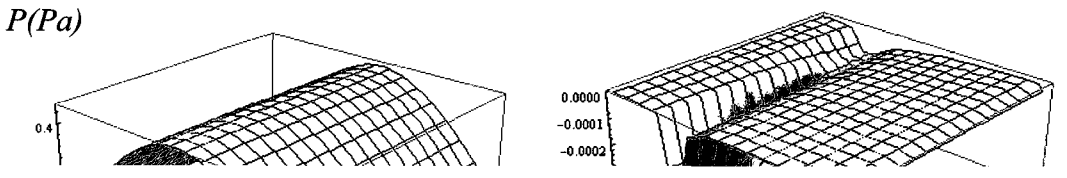

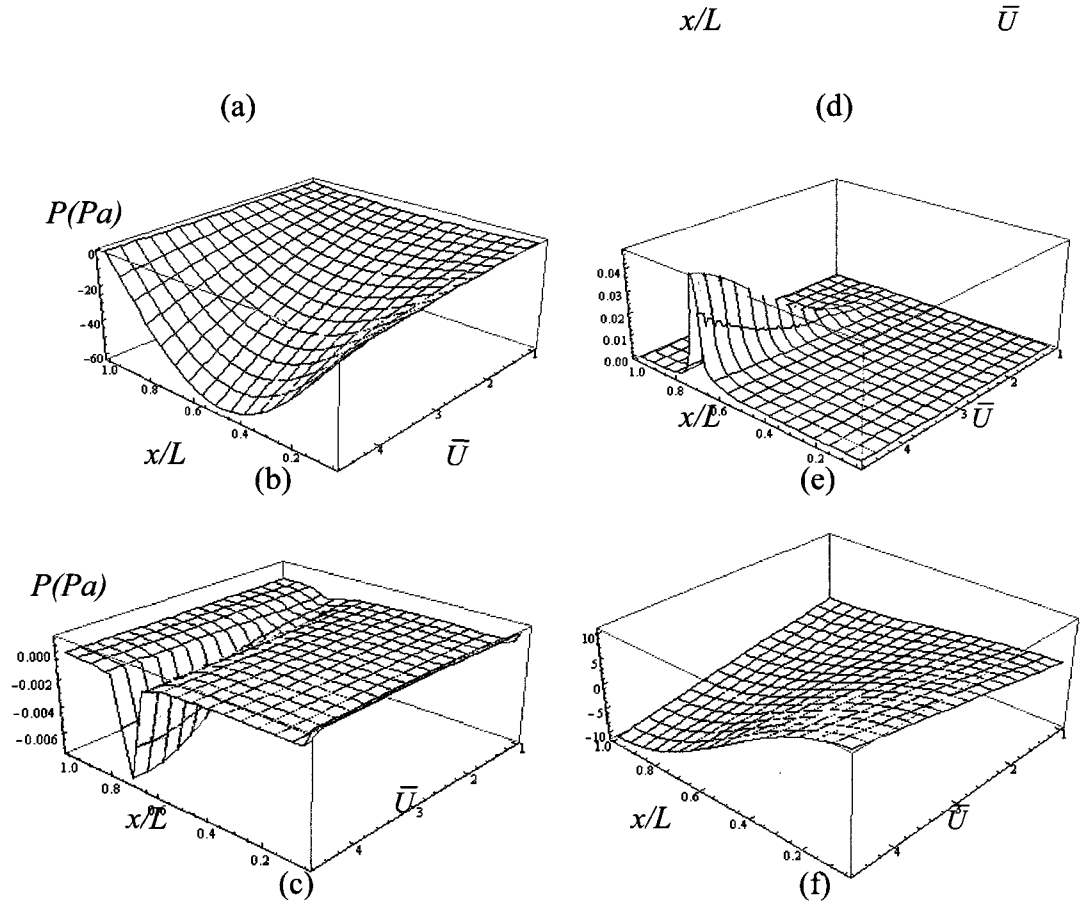

Figure 2.9 (a – c) Real and (d- f) imaginary parts of the perturbation pressure when the inner cylinder vibrates at 10 Hz in the 1st mode. When the vibration amplitude is 1 mm, the different quantities are (a, d) inertia, (b, e) stiffness and (c, f) damping

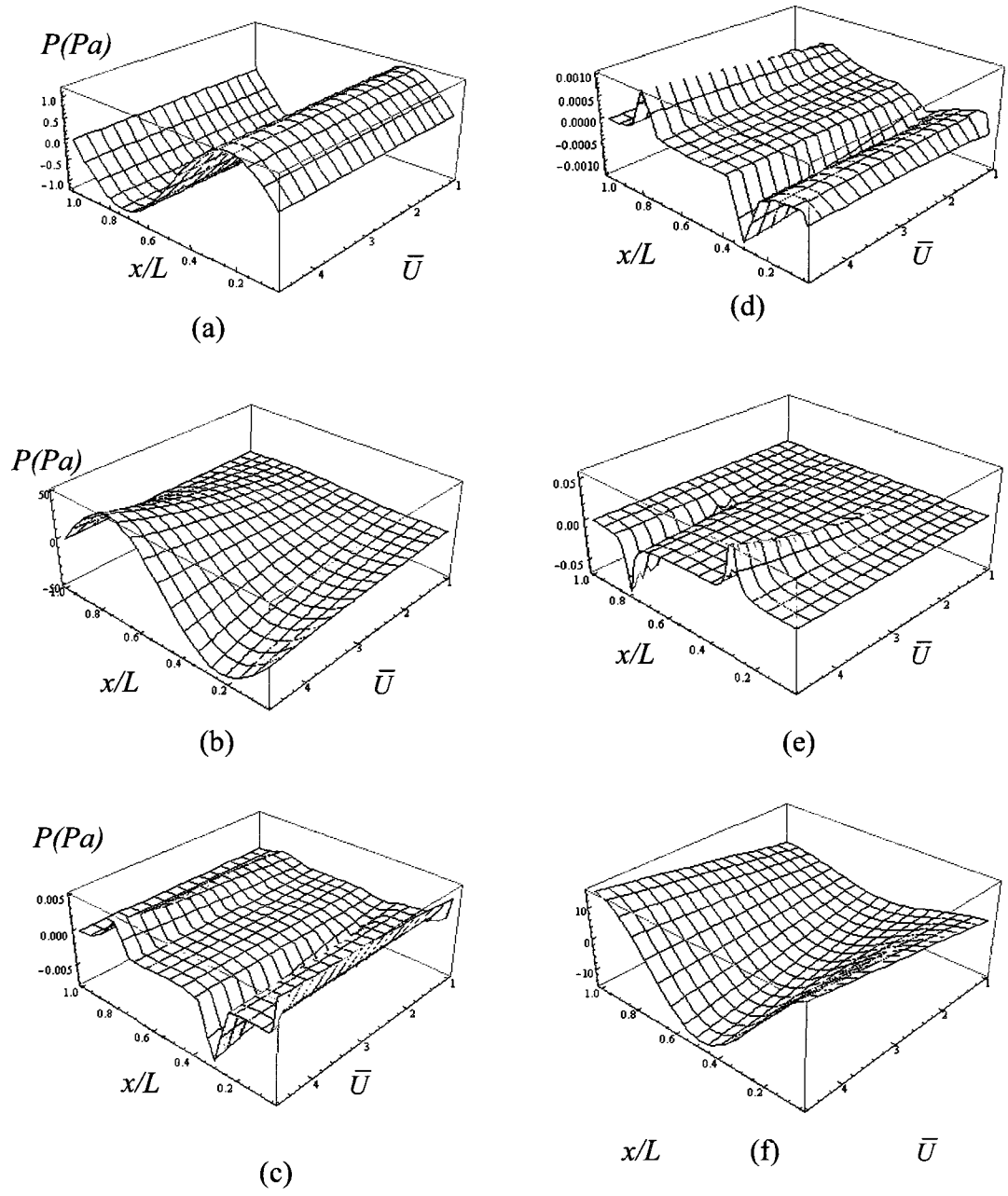

Figure 2.10 (a – c) Real and (d- f) imaginary parts of the perturbation pressure when the inner cylinder vibrates at 35 Hz in the 2nd mode. When the vibration amplitude is 0.2 mm, the different quantities are (a, d) inertia, (b, e) stiffness and (c, f) damping.

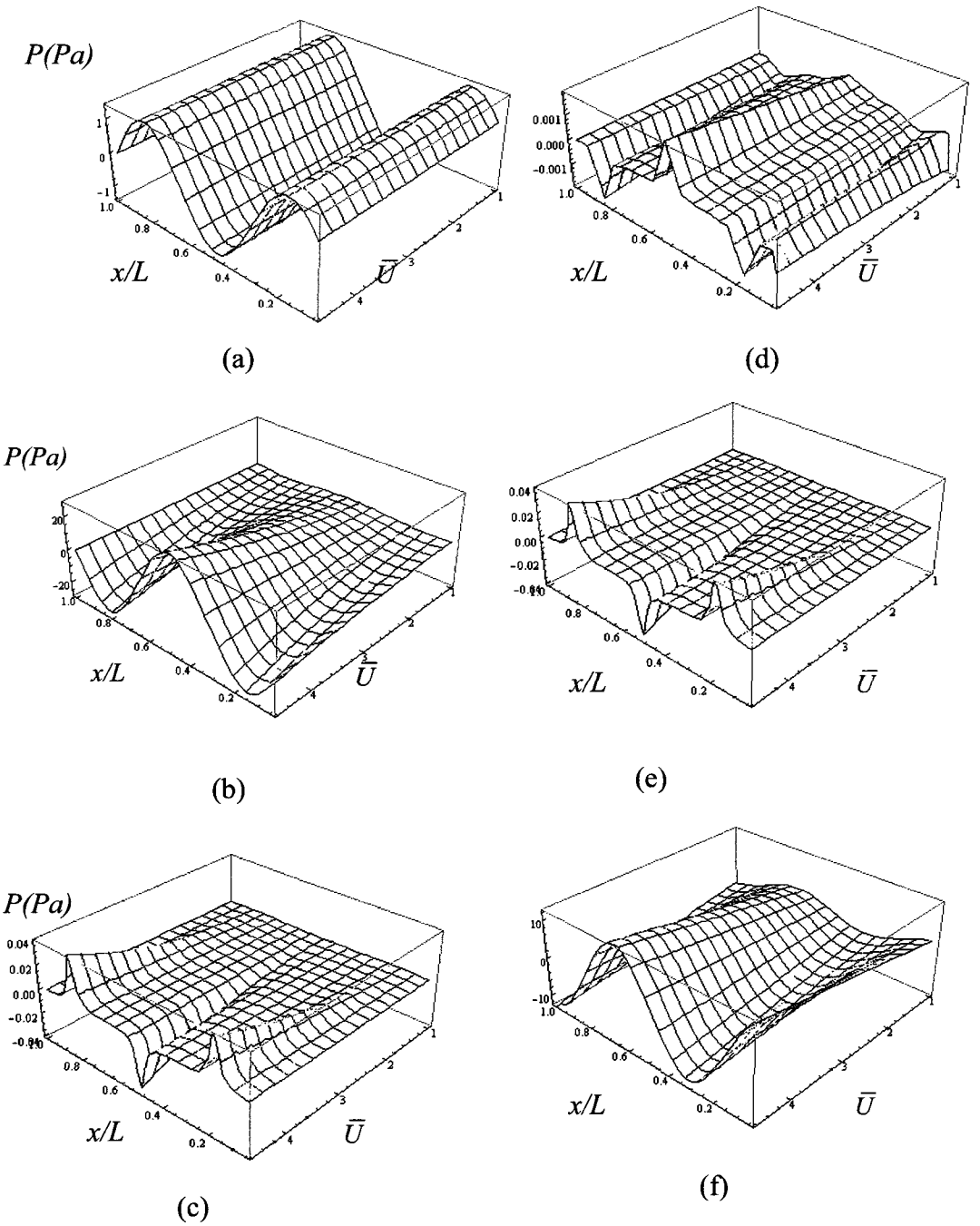

Figure 2.11 (a – c) Real and (d- f) imaginary parts of the perturbation pressure when the inner cylinder vibrates at 75 Hz in the 3rd mode. When the vibration amplitude is 0.05 mm, the different quantities are (a, d) inertia, (b, e) stiffness and (c, f) damping.

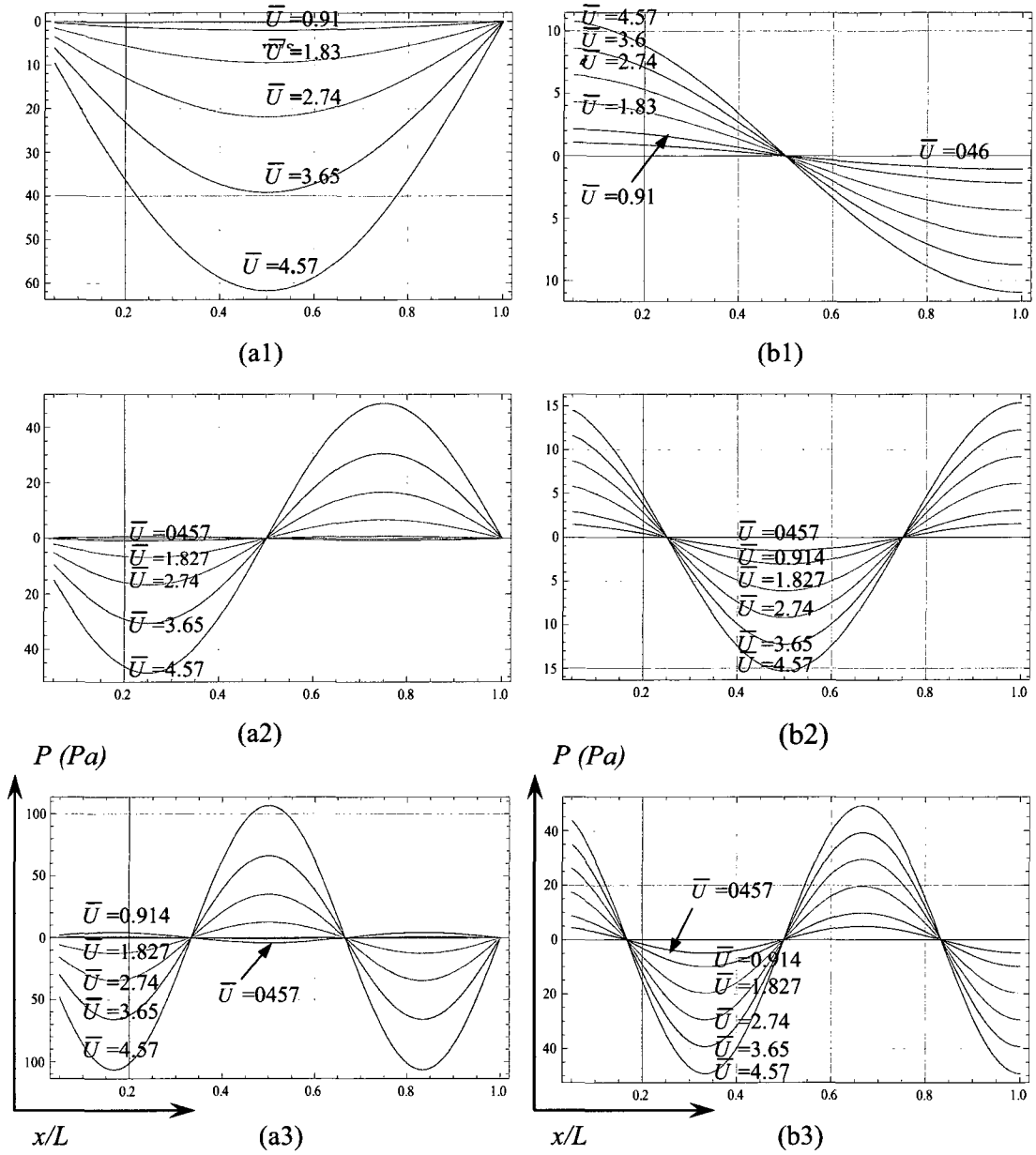

Figure 2.12 Real and imaginary parts of the perturbation pressure when the inner cylinder vibrates at 10 Hz, 35 Hz, and 75 Hz in the 1st, 2nd and 3rd modes. Vibration amplitudes are 1 mm for the 1st, 0.2 mm for the 2nd and 0.04 mm for 3rd mode, respectively. (a1), (a2) and (a3) are real parts of the pressure at the 1st, 2nd and 3rd modes, and (b1), (b2) and (b3) are Imaginary parts of the pressure at the 1st, 2nd and 3rd modes, respectively.

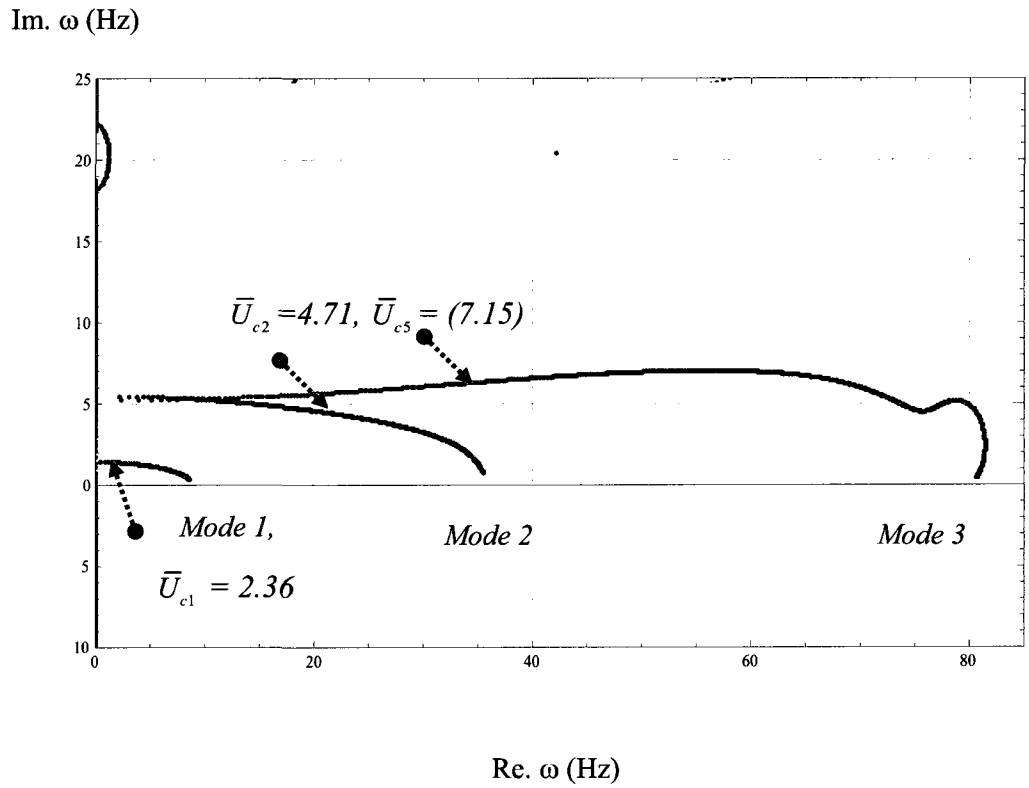

Figure 2.13 Argand diagram for a simply-supported inner cylinder subjected to unsteady annular flow. The cylinder loses its first stability at 2.36 dimensionless velocity, second at 4.71, third at 7.15.

APPENDIX 2A: PRESSURE FUNCTIONS FOR 2-D FLOWS FOR SEVERAL FLOW BOUNDARY CONDITIONS WITHOUT FRICTION TERM

(1) Contraction loss inlet and free discharge outlet

In the case of a contraction loss factor K_a at the entrance, the flow boundary conditions equation (2-6) with equation (2-23) and (2-24) give

$$\begin{aligned}&\overline{p}_1+\overline{p}_2-i\frac{2\rho r^2\omega U}{H\left(1+r^2\lambda_m{}^2\right)}\cdot\left.\frac{dh}{dx}\right|_{x=0}\\&\quad+\rho U\left(\overline{u}_1+\overline{u}_2+\overline{u}_3+i\frac{r^2\omega}{H\left(1+r^2\lambda_m{}^2\right)}\cdot\left.\frac{dh}{dx}\right|_{x=0}\right)\cdot\left(1+K_a\right)=0\end{aligned}\tag{2A-1}$$

In this case, the flow downstream of the contraction is not irrotational, so that

$$\overline{v}(0)=0\tag{2A-2}$$

Equation (2-6), (2-23), (2-24), (2-25), (2-30) and (2A-1) yield the following matrix equation.

$$\begin{bmatrix}-\rho(ir\omega-U) & 0 & 0 & 1 & 0 & 0 & 0 & 0\\ 0 & \rho(ir\omega+U) & 0 & 0 & 1 & 0 & 0 & 0\\ 0 & 0 & -r\omega/U & 0 & 0 & 0 & 0 & 1\\ \rho U(1+K_a) & \rho U(1+K_a) & \rho U(1+K_a) & 1 & 1 & 0 & 0 & 0\\ 0 & 0 & 0 & e^{-L/r} & e^{L/r} & 0 & 0 & 0\\ i & 0 & 0 & 0 & 0 & -1 & 0 & 0\\ 0 & i & 0 & 0 & 0 & 0 & 1 & 0\\ 0 & 0 & 0 & 0 & 0 & 1 & 1 & 1\end{bmatrix}\begin{Bmatrix}\overline{u}_1\\ \overline{u}_2\\ \overline{u}_3\\ \overline{p}_1\\ \overline{p}_2\\ \overline{v}_1\\ \overline{v}_2\\ \overline{v}_3\end{Bmatrix}=$$

$$\begin{bmatrix} 0 \\ 0 \\ 0 \\ (1-K_a)\cdot\rho r\omega\cdot\left.\dfrac{dh}{dx}\right|_{x=0} \\ 2\rho r\omega\cdot\left.\dfrac{dh}{dx}\right|_{x=L} \\ 0 \\ 0 \\ \left.\dfrac{dh}{dx}\right|_{x=0} \end{bmatrix} \cdot \frac{irU}{H\left(1+r^2\lambda_m{}^2\right)} \tag{2A-3}$$

where $\lambda_m = \dfrac{m\pi}{L}, \quad m = 1,\ 2,\ 3,\ldots$

Solving equation (2A-3) for $\overline{u}_j$, $\overline{p}_j$ and $\overline{v}_j$, and then, substituting them into equation (2-24), the following equation is obtained:

$$p(x) = \frac{\rho r^2\left(\lambda_m{}^2U^2+\omega^2\right)}{H\left(1+r^2\lambda_m{}^2\right)}\cdot h - i\frac{2\rho r^2\omega U}{H\left(1+r^2\lambda_m{}^2\right)}\cdot\frac{dh}{dx} - i\omega\frac{2\rho r^2\,U}{H\left(1+r^2\lambda_m{}^2\right)}\cdot e^{(-L+x)/r}\cdot\left|\frac{dh}{dx}\right|_{x=L}$$
$$-\frac{\rho rU\left[-(1+K_a)U^2+\left(-1+K_a\right)r^2\omega^2\right]}{H\left(1+r^2\lambda_m{}^2\right)\left[U(1+K_a)+ir\omega\right]}\cdot\left|\frac{dh}{dx}\right|_{x=0}\cdot e^{-x/r} \tag{2A-3}$$

(2) Short-lossless inlet and diffuser outlet

When a short loss-less entrance and a diffuser at the exit are considered, the flow boundary condition (2-5) and (2-8a) with equation (2-23) ~ (2-28) give equation (2-29) and

$$e^{-\frac{L}{r}}\cdot\overline{p}_1+e^{\frac{L}{r}}\cdot\overline{p}_2-i\frac{2\rho r^2\omega U}{H\left(1+r^2\lambda_m{}^2\right)}\cdot\left(\frac{dh}{dx}\right)_{x=L}$$
$$+\eta\rho U\left(e^{-\frac{L}{r}}\cdot\overline{u}_1+e^{\frac{L}{r}}\cdot\overline{u}_2+i\frac{r^2\omega}{H\left(1+r^2\lambda_m{}^2\right)}\cdot\left(\frac{dh}{dx}\right)_{x=L}\right)=0 \qquad \text{(2A-4)}$$

Equation (2-9), (2-23), (2-24), (2-25), (2-29) and (2A-4) yield matrix equation as follows:

$$\begin{bmatrix}-\rho(ir\omega-U) & 0 & 1 & 0 & 0 & 0\\ 0 & \rho(ir\omega+U) & 0 & 1 & 0 & 0\\ \rho U & \rho U & 1 & 1 & 0 & 0\\ \rho U\eta e^{-L/r} & \rho U\eta e^{L/r} & e^{-L/r} & e^{L/r} & 0 & 0\\ i & 0 & 0 & 0 & -1 & 0\\ 0 & i & 0 & 0 & 0 & 1\end{bmatrix}\begin{Bmatrix}\overline{u}_1\\ \overline{u}_2\\ \overline{p}_1\\ \overline{p}_2\\ \overline{v}_1\\ \overline{v}_2\end{Bmatrix}$$
$$=\begin{Bmatrix}0\\ 0\\ \rho r\omega\cdot\left.\frac{dh}{dx}\right|_{x=0}\\ \rho r\omega(2-\eta)\cdot\left.\frac{dh}{dx}\right|_{x=L}\\ 0\\ 0\end{Bmatrix}\cdot\frac{irU}{H\left(1+r^2\lambda_m{}^2\right)} \qquad \text{(2A-5)}$$

where, $\lambda_m=\dfrac{m\pi}{L}$, $m=1,\ 2,\ 3,\ldots$

Solving equation (2A-5) for each $\overline{u}_j$, $\overline{p}_j$ and $\overline{v}_j$, and then, substituting them into equation (2-24), one may obtain the following equation:

$$p(x)=\frac{\rho r^2\left(\lambda_m{}^2U^2+\omega^2\right)}{H\left(1+r^2\lambda_m{}^2\right)}\cdot h-i\frac{2\rho r^2\omega U}{H\left(1+r^2\lambda_m{}^2\right)}\cdot\frac{dh}{dx}-\frac{\rho rU\left(U-ir\omega\right)}{H\left(1+r^2\lambda_m{}^2\right)}\cdot\left|\frac{dh}{dx}\right|_{x=0}\cdot e^{-x/r}$$
$$+i\frac{\rho r^2\omega\, U\left(U+ir\omega\right)\left(\eta-2\right)}{H\left(1+r^2\lambda_m{}^2\right)\left[\left(\eta-1\right)U-ir\omega\right]}\cdot\left|\frac{dh}{dx}\right|_{x=L}\cdot e^{(-L+x)/r} \qquad \text{(2A-5)}$$

(3) Diffuser inlet and free discharge outlet

When a diffuser at the entrance and a free discharge at the exit are considered, flow boundary conditions (2-8b) and (2-7) with equations (2-23) ~ (2-28) give

$$\overline{p}_1+\overline{p}_2-\frac{i2a\rho r^2\omega U}{H\left(1+r^2\lambda_m{}^2\right)}\cdot\left|\frac{dh}{dx}\right|_{x=0}+\eta\rho U\left(\overline{u}_1+\overline{u}_2+\frac{ir^2\omega}{H\left(1+r^2\lambda_m{}^2\right)}\cdot\left|\frac{dh}{dx}\right|_{x=0}\right)=0 \qquad \text{(2A-6)}$$

Equation (2-9), (2-23), (2-24), (2-25), (2-30) and (2A-6) yield a matrix equation as follows:

$$\begin{bmatrix}-\rho\left(ir\omega-U\right) & & 1 & & & \\ & \rho\left(ir\omega+U\right) & & 1 & & \\ \eta\rho U & \eta\rho U & 1 & 1 & & \\ & & e^{-L/r} & e^{L/r} & & \\ i & & & & -1 & \\ & i & & & & 1\end{bmatrix}\begin{Bmatrix}\overline{u}_1\\ \overline{u}_2\\ \overline{p}_1\\ \overline{p}_2\\ \overline{v}_1\\ \overline{v}_2\end{Bmatrix}$$
$$=\begin{bmatrix}0\\ 0\\ \rho r\omega(2-\eta)\cdot\left.\frac{dh}{dx}\right|_{x=0}\\ 2\rho r\omega\cdot\left.\frac{dh}{dx}\right|_{x=L}\\ 0\\ 0\end{bmatrix}\cdot\frac{irU}{H\left(1+r^2\lambda_m{}^2\right)} \qquad \text{(2A-7)}$$

where, $\lambda_m = \dfrac{m\pi}{L}, \quad m = 1,\ 2,\ 3,\ldots$

Solving equation (2A-7) for each $\overline{u}_j$, $\overline{p}_j$ and $\overline{v}_j$, and then, substituting them into equation (2-24), one may obtain the following equation:

$$p(x) = \frac{\rho r^2\left(\lambda_m{}^2 U^2 + \omega^2\right)}{H\left(1 + r^2\lambda_m{}^2\right)} \cdot h - i\frac{2\rho r^2 \omega U}{H\left(1 + r^2\lambda_m{}^2\right)} \cdot \frac{dh}{dx}$$
$$+ i\omega\frac{2\rho r^2 U}{H\left(1 + r^2\lambda_m{}^2\right)} \cdot e^{(-L+x)/r} \cdot \left|\frac{dh}{dx}\right|_{x=L} + i\frac{\rho r^2 U\omega(\eta - 2)[U - ir\omega]}{H\left(1 + r^2\lambda_m{}^2\right)[U(\eta - 1) + ir\omega]} \cdot e^{-x/r} \cdot \left|\frac{dh}{dx}\right|_{x=0}$$

(2A-8)

APPENDIX 2B: PRESSURE FUNCTIONS FOR 1-D FLOWS FOR SEVERAL FLOW BOUNDARY CONDITIONS

(1) Contraction loss inlet and free discharge outlet

In the case that the contraction loss factor K_a is considered at the entrance, flow boundary condition (2-6) and (2-7) with equations (2-39) and (2-40) give the pressure function $p(x)$ as follows:

$$p(x)=\rho\frac{U^2\lambda_m{}^2+\omega^2}{H\lambda_m{}^2}\cdot h-\frac{i2\rho\omega U}{H\lambda_m{}^2}\cdot\frac{dh}{dx}-\frac{\rho U\omega^2(K_a-1)(L-x)}{H\lambda_m{}^2\left[U(1+K_a)+iL\omega\right]}\cdot\left|\frac{dh}{dx}\right|_{x=0}$$
$$+i\cdot\frac{2\rho\omega U\left[U(1+K_a)+ix\omega\right]}{H\lambda_m{}^2\left[U(1+K_a)+iL\omega\right]}\cdot\left|\frac{dh}{dx}\right|_{x=L} \qquad \text{(2B-1)}$$

(2) Short-lossless inlet and diffuser outlet

In the case of pressure recovery, the recovery efficiency η, is considered at the exit and flow boundary conditions (2-5) and (2-8a) with equation (2-39) and (2-40) give the pressure function $p(x)$ as follows:

$$p(x)=\rho\frac{U^2\lambda_m{}^2+\omega^2}{H\lambda_m{}^2}\cdot h-\frac{i2\rho\omega U}{H\lambda_m{}^2}\cdot\frac{dh}{dx}$$
$$+i\omega\rho U\cdot\frac{-U\eta+i(L-x)\omega}{H\lambda_m{}^2\left[U(1-\eta)+iL\omega\right]}\cdot\left|\frac{dh}{dx}\right|_{x=0} \qquad \text{(2B-2)}$$
$$+i\rho\omega U\cdot\frac{(2-\eta)(U+ix\omega)}{H\lambda_m{}^2\left[U(1-\eta)+iL\omega\right]}\cdot\left|\frac{dh}{dx}\right|_{x=L}$$

(3) Diffuser inlet and free discharge outlet

In the case of pressure recovery, the recovery efficiency η, occurs at the entrance and flow boundary condition (2-8b) and (2-7) with equations (2-39) and (2-40) give the pressure function $p(x)$ as follows:

$$p(x) = \rho \frac{U^2 \lambda_m^{\,2} + \omega^2}{H \lambda_m^{\,2}} \cdot h - \frac{i 2 \rho \omega U}{H \lambda_m^{\,2}} \cdot \frac{dh}{dx} - \frac{\rho U \omega^2 (2-\eta)(L-x)}{H \lambda_m (U\eta + iL\omega)} \cdot \left|\frac{dh}{dx}\right|_{x=0} + i \frac{2 \rho U \omega (U\eta + ix\omega)}{H \lambda_m (U\eta + iL\omega)} \cdot \left|\frac{dh}{dx}\right|_{x=L} \qquad \text{(2B-3)}$$

2.7 References

Childs, D., 1993. Turbomachinery rotodynamics, Chapter 4, John Wiley & Sons, Inc.

Fujita, K and Ito, T., 1992. Study of leakage-flow-induced vibration of an axisymmetric cylindrical rod due to axial flow, S*ymposium on Flow-Induced Vibration and Noise*, ASME. PVP **244**, 33-43.

Fujita, K, Ito, T. Kawata, Y and Izumi, H., 1994. Axial leakage-flow-induced vibration of a long flexible rod with small gaps, Flow-Induced Vibration, ASME, PVP-Vol. 273, pp.133-143.

Hobson, D.E., 1982. Fluid-elastic instabilities caused by flow in an annulus, Proceedings of 3rd International Conference on Vibration of Nuclear Plant, Keswick, UK, BNES, London (1982), pp. 460–463.

Inada, F., 1988. A study on leakage-flow-induced vibrations (fluid dynamic forces acting on the walls of a one dimensional , narrow passage, *JSME international J.* Series III, 31, 39-47.

Inada, F. and Hayama, S., 1990. A study on leakage-flow-induced vibrations. Part 1: fluid dynamic forces and moments acting on the walls of a narrow tapered passage. Part 2: stability analysis and experiments for two-degree of freedom systems combining translational and rotational motions, Journal of Fluids and Structures Vol. 4, pp. 395–412 and 413–428.

Kaneko, S., Tanaka, S., Watanabe, T., 2000. Leakage-flow-induced flutter of highly flexible structures, In: Ziada, S., Staubli, T. (Eds.), Flow-induced vibration 2000, pp. 837-844.

Langthjem, M. A., Morita, H. Nakamura, T. and Nakano, M., 2006, A flexible rod in annular leakage flow: Influence of turbulence and equilibrium offset, and analysis of instability mechanism, Journal of Fluids and Structures, **22** 617-645.

Mateescu and Païdoussis, 1985 D. Mateescu and M.P. Païdoussis, The unsteady potential flow in an axially-variable annulus and its effect on the dynamics of the oscillating rigid center-body, ASME Journal of Fluids Engineering 107 (1985), pp. 412–427.

Miller, D.R., 1970. Generation of positive and negative damping with a flow restrictor in axial flow. In: Proceedings of the Conference on Flow-Induced Vibrations in Reactor System Components. Argonne National Laboratory Report ANL7685, Argonne IL, USA, pp. 304–311.

Paidoussis, M.J., 1966, Vibrations of cylinders with supported ends, induced by axial flow, Proceedings Institution of Mechanical Engineers, **180**, 268-278.
Paidoussis, M.J., 1969, An experimental study of vibrations of flexible cylinders induced by nominal axial flow, Nuclear Science and Engineering, **35**, 127-138.

Paidoussis, M.J., 2004, Fluid-structure interactions: Slender structures and axial flows, Chapter 8.2, Elsevier academic press.

Porcher, G., de Langre, E., 1997. A friction-based model for fluidelastic forces induced by axial flow. In: M.P. Païdoussis, et al. (Eds.), Proceedings 4th Int'l Symposium on Fluid–Structure Interactions, Aeroelasticity, Flow-Induced Vibration and Noise, Vol. II, AD-Vol. 53-2. ASME, New York, pp. 67–74.

Shimoyama, y, Yamada, y., 1957. Experiments on the labyrinth packing (1st report). Transactions of Japan Society of Mechanical Engineers, Part 3 23, 44-49 (in Japanese).

Wu, X., Kaneko. S., 2005. linear and nonlinear analyses of sheet flutter induced by leakage flow, Journal of Fluids and Structures, 20, 927-948.

CHAPTER 3

ANNULAR-FLOW-INDUCED VIBRATIONS OF A SIMPLY-SUPPORTED TUBE IN A FINITE-LENGTH NARROW-GAP SUPPORT

The stability of a simply-supported tube subjected to narrow annular flow in a finite-length gap support is experimentally and analytically investigated in this Chapter. Numerous experiments show that a pinned-pinned tube subjected to leakage flow in a finite-length narrow-gap support first loses stability by flutter, and the critical flow velocity is low.

The problem is analytically solved based on the solution obtained in Chapter 2. In the analytical solution, the exit boundary condition for pressure recovery is found to be predominant for flutter instability. Based on the analytical solution, a simple semi-analytical model to predict the critical flow velocity is proposed for the first mode instability. The prediction of the semi-analytical model agrees reasonably well with the experimental results.

Nomenclature(i)

C	damping coefficient
$C_{e,n}$	effective damping coefficient of the nth mode
EI	flexural rigidity
F_f	fluid forces per unit length due to perturbations
$F_{f,D}$	fluid damping force due to perturbation
$F_{f,I}$	fluid inertia force due to perturbation
$F_{f,K}$	fluid stiffness force due to perturbation
F_l	fluid force per unit length at support
$F_{S,D}$	inner tube damping force
$F_{S,I}$	inner tube inertia force
$F_{S,K}$	inner tube stiffness force due to perturbation
h	vibration response of the cylinder
$\overline{h}_n(t)$	vibration response of time (t)
K_{cf0}	friction factor
κ_{cf1}	friction parameter ($K_{cf1}{}^2 = 1 + K_{cf0}/H$)
L	length
m	mode number
M_f	added fluid mass
M_s	structural mass per unit length
$M_{e,n}$	modal mass of the nth mode ($M_{e,n} = \int_0^L M_s \cdot \phi_n(x)^2 dx$)
p_f	perturbation pressure

Nomenclature(ii)

p_c	coefficient of cosine component of perturbation pressure for particular solution
n	mode number
p_s	coefficient of sine component of perturbation pressure for particular solution
P_1	static pressure before diffuser
P_2	static pressure after diffuser
Re	Reynolds number ($\mathrm{Re} = \frac{\rho U D_h}{\mu}$)
r	radial coordinate
R_d	radius of inner cylinder
U	mean flow velocity in axial direction
u	perturbation velocity in axial flow velocity
u_c	coefficient of cosine component of axial perturbation velocity for particular solution
u_s	coefficient of sine component of axial perturbation velocity for
v	perturbation velocity in circumferential flow velocity
v_c	coefficient of cosine component of circumferential perturbation velocity for particular solution
v_s	coefficient of sine component of circumferential perturbation velocity for particular solution
x	axial coordinate
θ	circumferential coordinate
ω	cyclic frequency
ω_n	natural frequency at zero mean flow velocity

Nomenclature (iii)

ζ_n	damping ratio of the n^{th} mode
δ	dimensionless diffuser performance coefficient
η	recovery coefficient
η_s	static recovery coefficient
η_p	perturbation recovery coefficient
ρ	air density (Kg/m^3)
τ_x	frictional shear stress in axial direction
τ_θ	frictional shear stress in circumferential direction

3.1 Abstract

The stability of a simply-supported tube subjected to narrow annular flow in a finite-length gap support is experimentally and analytically investigated. For the experiment, a 2.5 m test section and several finite-length gap supports have been made considering different gap size and diffuser angles of the support. The tube was observed to lose stability by flutter. The critical flow velocity was strongly dependent on the annular gap size and the diffuser angle at the downstream end of the support. A solution for the perturbation pressure on the tube is analytically obtained considering the friction loss, the contraction loss at the entrance, and the pressure recovery at the exit of the support. In the analytical solution, the exit boundary condition for pressure recovery is found to be predominant for flutter instability. However, flutter instability does not materialize for lossless boundaries such as short-lossless inlet and free-discharge outlet. Based on the analytical solution, a simple semi-analytical model to predict the critical flow velocity is proposed for the first mode instability. The prediction of the semi-analytical model agrees reasonably with the experimental results. However, it is judged that the pressure recovery at the diffuser should be experimentally measured more accurately to have even better prediction.

3.2 Introduction

Considerable effort has been made to develop methodologies to predict the instabilities of a flexible rod subjected to annular or leakage flow. As a result, several methods to predict the dynamic behavior have been developed, such as the linearized potential flow theory based model (Mateescu, Paidoussis and Sim, 1985, 1987, 1988), and the pressure-loss models (Hobson, 1982; Spurr and Hobson, 1984; Fujita and Ito, 1992; and Langthjem et al., 2006). The basic dynamics due to annular flow are known by virtue of these models.

On the other hand, to tackle industrial problems such as heat exchanger tube and control rod vibrations in gas and water cooled reactors, the practical conditions provided by the tube-support plate geometry should be considered. For heat exchanger tubes, the support causes leakage flow (highly confined annular flow) and sometimes, additional divergent or convergent flow at the exit or the entrance of the support, which is due to chamfering of the support hole for manufacturing convenience. The tube has therefore no positive contact support when centered within the loose support. Therefore, when it comes to heat exchangers, leakage flow over a finite length and divergent or convergent fluid boundary conditions should be considered in addition to the basic annular flow. For brevity, the term 'support' is used here to mean a 'loose support'.

Unlike the basic annular flow case, a rigid rod translating periodically in a finite length annular region of confined flow was studied by Mulcahy (1980). He studied the fluid forces and hydraulic damping. However, since the study was done for still water, only positive damping was found. Later, Yasuo and Paidoussis (1989) considered the flow-induced instability problem of heat exchanger tubes subjected to axial flow in a diffuser-shaped, loose intermediate support which is the same problem as this study examines. In their study, potential flow theory was considered with a one-mode approximation of the tube. They suggested critical flow velocity equation for divergence and flutter. Application of this theory to practical problems is, however, limited because of the one-mode approximation and inaccurate prediction of the critical flow velocity.

It is not easy to obtain an analytical solution particularly when friction loss is considered. However, once an analytical solution is obtained, numerous applications are possible. The aim of this study is, therefore, (1) with an experimental approach, to measure the critical flow velocity for several annular gaps and diffuser angles, (2) to propose an analytical solution for the fluctuating pressure on the surface of a simply-supported cylinder subjected to the annular flow at the finite-length narrow-gap support, (3) based

on the solution, to propose a simple calculation procedure to predict the critical flow velocity for the first vibration mode of the tube.

3.3 Experiments

3.3.1 Description of apparatus

The test section with associated instrumentations is schematically shown in Figures 3.1 (a) and (b). Experiments were conducted in a 2.5m long test section in which the flow rate ranged up to flow velocity of 12 *m/s*. A 2.2 m long and 15.9 mm (0.627 inch) diameter inner tube was used with a mid-support (finite-length narrow-gap support) having a length of 38.7 mm (1.525 inch). Several geometries of the axisymmetric mid-support were investigated. The inner tube was supported by four pins at one end, therefore, a total of eight contact points for both ends to simulate pinned-pinned boundary conditions. The gaps between the inner tube and supports were 0.29 mm, 0.42 mm, 0.67 mm, 2.2 mm, and the annular gap between the inner tube and outer plexiglass glass tube is 5.15 mm. Diffuser angles of 10° and 20° were provided at the downstream end of the support. All dimensions are summarized in Table 3.1.

Fluid parameters and vibration characteristics of the inner cylinder are summarized in Table 3.2. Compressed air comes into the test loop through a pressure regulator connected to the building services air supply. The air meets a contraction at the entrance to the test section due to the tube support, enters the annulus provided by the lower glass tube, and then, flows into the much smaller annular channel provided by the replaceable support. The air flow is controlled by a valve at the end of the test loop, so that higher flow velocities can be obtained by opening the valve.

As seen in Figures 3.1 (a) and (b), two static pressures are measured at locations just upstream and downstream of the diffuser so that the pressure recovery can be calculated. Unfortunately, with this pressure gage setup, the expansion loss at the downstream end

of the support cannot be measured. Vibration amplitudes are measured with four laser sensors (reflex sensor, Wenglor Company), in two directions near the support, at mid-span and at the one-fourth position along the test section. The measurement signals were acquired and analyzed using an Oros data acquisition system.

3.3.2 Experimental results

The inner pinned-pinned cylinder loses its first mode stability at very low flow velocity for all support cases. The first instability is clearly observed in the first mode. The instability is believed to be a dynamic instability, not a static one. The reasons are that the critical flow velocity is too low to overwhelm the stiffness of the steel cylinder by negative fluid stiffness, the natural frequencies do not change before the inner cylinder starts impacting the support, and limit cycles are clearly observed for all the supports below or above the critical flow velocities.

Figure 3.2 shows the measured *rms* vibration amplitude and damping factor as functions of the upstream flow velocity for the support having a 0.29 mm gap with a 20° diffuser angle. The vibration amplitude starts increasing rapidly from 0.2 m/s. At the same time, the damping ratio has decreased to nearly zero. Then, as the inner cylinder starts impacting the support, the amplitude decreases while the "effective" damping ratio increases. The damping ratio is estimated by curve fitting the response spectrum in the neighborhood of the first mode frequency. All measurements for the different support geometries show the same trend as in Figure 3.2.

While the vibration amplitude and the damping change, the natural frequency of the cylinder does not change at all before the onset of impacting, as shown in Figure 3.3. The 12.5 Hz and 40.2 Hz components are, respectively, the first and the second natural

frequencies. When the inner cylinder starts impacting, the first natural frequency increases to 14.5 Hz. Physically impacting increases the effective stiffness of the tube.

Figure 3.4 shows X-Y plots of the cylinder motion at the support elevation. As the amplitude increases, whirling motions are clearly observed, which is believed to be a limit cycle. It is well known that the limit cycle is the result of a dynamic instability. Once impacting starts, the limit cycle disappears. When the cylinder contacts the support, the cylinder seems to vibrate in a one-dimensional motion. This is a very typical vibration behavior for all the supports with increasing flow velocity.

The vibration amplitudes for different gaps and diffuser angles as functions of flow velocity are shown in Figure 3.5. The lowest critical flow velocity of 0.10 m/s (equivalent to 2.38 m/s or 790 Reynolds number at the support) is obtained with the support having a 0.29 mm gap and a 10° diffuser while the highest critical flow velocity of 2.82 m/s (equivalent to 7.6 m/s or 17,000 Reynolds number at the support) is observed with a 2.20 mm gap and a 10° diffuser. Generally speaking, the smaller the gap and the diffuser angle the lower the critical flow velocity. However, for the 0.68 mm gap support, the critical flow velocity of 0.12 m/s is obtained with the 10° diffuser, which is significantly lower than that of the 0.42 mm gap support. The upstream critical flow velocity of 0.12 m/s is equivalent to 1.14 m/s or 870 Reynolds number at the support. For the largest gap (2.2 mm) support, interestingly, the critical flow velocity of the 20° support is much lower. Critical flow velocities for all the supports are summarized in Table 3.4.

3.4 Analytical model

3.4.1 Assumptions

For the development of an analytical model, the following assumptions are made:

1. Although fluid flows in an annular confinement before and after the support, the fluid effects from such confinements are considered to be negligible at low flow velocity. Therefore, the analytical model to be solved is as illustrated in Figure 3.6.
2. The mechanical damping of the inside cylinder is assumed to be small; the damping ratio (ξ) in the experiments is 0.2%.
3. For the inner cylinder, the radius-to-length ratio is assumed to be so small that shell-type vibration may be neglected.
4. Every flow-related term may be expressed as the sum of an average (steady) component plus a small perturbation component.

3.4.2 Equation of motion of a flexible inner-cylinder

The oscillating flexible inner-cylinder simply supported at the ends is considered as an Euler-Bernoulli beam having flexural rigidity EI, length L, mass per unit length M_s, and damping coefficient C. The cylinder is subjected to distributed external forces which occur due to the fluid motion. Since the fluid forces are coupled to the inner-cylinder motion, the equation of transverse motion $h(x,t)$ of the cylinder is expressed as

$$M_s \frac{d^2h(x,t)}{dt^2} + C\frac{dh(x,t)}{dt} + EI\frac{d^4h(x,t)}{dx^4} = F_f(x,t) \tag{3-1}$$

where $F_f(x,t) = F_l(x)\cdot e^{i\omega t} = -\int_0^{2\pi} P_f(x,t)\cdot e^{i\omega t}\left(\cos\theta\right)^2 r d\theta$, (3-2)

The following modal expansion solution is assumed.

$$h(x,t) = \sum_{n=1}^{\infty}\phi_n(x)\cdot\bar{h}_n(t) = \sum_{n=1}^{\infty}\phi_n(x)\cdot a_n\cdot e^{i\omega t} \tag{3-3}$$

It is assumed that the pressure perturbation varies as a cosine function around the circumference of the inner cylinder. Figure 3.6 shows that an arbitrary perturbation pressure p acting on the inner cylinder surface when the cylinder moves in the positive y direction. $\phi_n(x)$ and a_n in equation (3-3) are the nth eigenfunction and the vibration amplitude, respectively. F_f and $P_f(x,t)$ in equation (3-2) are the fluidelastic *force/unit length* and the pressure on the cylinder surface, respectively. For a simply-supported beam, the eigenfunctions are

$$\phi_n(x) = sin\left(\lambda_n x\right),\ \lambda_n = \frac{n\pi}{L};\ n = 1,2,3... \tag{3-4}$$

Substituting equations (3-3) and (3-4) into equation (3-1) gives

$$\sum_{n=1}^{\infty}\left[M_s \ddot{\bar{h}}_n(t) + C\dot{\bar{h}}_n(t) + EI\lambda_n{}^4 \bar{h}_n(t) \right] \cdot \phi_n(x) = F_f(x,t) \tag{3-5}$$

Multiplying equation (3-5) by $\phi_m(x)$ in order to use the mode orthogonality property, and integrating over the length gives

$$M_{e,n}\ddot{\bar{h}}_n(t) + 2\zeta_n \omega_n M_{e,n}\dot{\bar{h}}_n(t) + \omega_n{}^2 M_{e,n}\bar{h}_n(t) = \int_{L1}^{L2} \phi_n(x) \cdot F_f(x,t)\, dx \tag{3-6}$$

where , $M_{e,n} = \int_0^L M_s \cdot \phi_n(x)^2 dx$, (3-7a)

$$\bar{h}_n(t) = a_n e^{i\omega t}, \tag{3-7b}$$

$$\zeta_n = \frac{C_{e,n}}{2M_{e,n}\omega_n}, \tag{3-7c}$$

$$\omega_n{}^2 = \frac{\int_0^L EI\lambda_n{}^4 \cdot \phi_n(x)^2 dx}{M_{e,n}} \tag{3-7d}$$

When a finite-length narrow-gap support is considered, the entrance and exit locations at L_1, and L_2, respectively, shown in Figure 3.6 demarcate the forcing region, thus

$$F_f \neq 0 \text{ for } L_1 \leq x \leq L_2, \text{ and otherwise, } F_f = 0 \tag{3-8}$$

Since the cylinder motion is coupled with the fluid motion, the cylinder vibration leads to increased pressure fluctuations. The fluctuating pressure may be separated into three terms related to fluid added mass ($P_{f,I}$), damping ($P_{f,D}$) and stiffness ($P_{f,K}$) and written as follows:

$$F_f(x,t) = -\pi r\left[-\omega^2 P_{f,I}\phi_n(x) + i\omega P_{f,D}\phi_n(x) + P_{f,K}\phi_n(x)\right]\bar{P}_f(t) \tag{3-9}$$

Substituting equation (3-9) into equation (3-6) and using (3-7b) ~ (3-7d) gives

$$\begin{aligned} -\omega^2\left(1 + Q\int_{L1}^{L2} P_{f,I}\phi_n(x)^2\,dx\right) + i\omega\left(2\zeta_n\omega_n + Q\cdot\int_{L1}^{L2} P_{f,D}\phi_n(x)^2\,dx\right) \\ + \left(\omega_n{}^2 + Q\cdot\int_{L1}^{L2} P_{f,K}\phi_n(x)^2\,dx\right) = 0 \end{aligned} \tag{3-10}$$

where $Q = \pi r / M_{e,n}$, (3-11)

and $P_{f,I} \neq P_{f,D} \neq P_{f,K} \neq 0$ for $L_1 \leq x \leq L_2$, otherwise. $P_{f,I} = P_{f,D} = P_{f,K} = 0$.

3.4.3 Fluid equations and boundary conditions

Consider a two-dimensional unsteady, incompressible, annular flow between two concentric cylinders. Assuming small perturbations of the flow, the first-order continuity and momentum equations may be expressed as

$$H\frac{\partial u}{\partial x}+\frac{H}{r}\frac{\partial v}{\partial \theta}=-\frac{\partial h}{\partial t}-U\frac{\partial h}{\partial x} \tag{3-12}$$

$$\frac{\partial p}{\partial x}+\rho\frac{\partial u}{\partial t}+\rho U\frac{1}{r}\frac{\partial v}{\partial \theta}+2\rho U\frac{\partial u}{\partial x}+\frac{\tau_x}{H}=-\rho\frac{U}{H}\frac{\partial h}{\partial t}-\rho\frac{U^2}{H}\frac{\partial h}{\partial x} \tag{3-13}$$

$$\frac{1}{r}\frac{\partial p}{\partial \theta}+\rho\frac{\partial v}{\partial t}+\rho U\frac{\partial v}{\partial x}+\frac{\tau_\theta}{H}=0 \tag{3-14}$$

In equation (3-13) and (3-14), τ_x and τ_θ are non-conservative friction shear stresses. τ_θ may be neglected since there is no bulk flow in the circumferential direction.

In this study, the three fluid equations together with two boundary conditions for the entrance and the exit are considered. A short lossless entrance and a free discharge exit are considered as ideal conditions. As realistic conditions, a contraction-loss entrance and a diffuser exit are taken into account.

For the short-lossless entrance and the free-discharge exit boundary conditions, the following equations are obtained:

$$p(L_1)+\rho U\,u(L_1)=0 \tag{3-15}$$

for the entrance, and

$$p(L_2)=0 \tag{3-16}$$

for the exit of the finite-length support.

For the realistic fluid boundary conditions, we consider a contraction loss factor K_1 at the entrance, and a diffuser efficiency η at the exit of the finite-length support. For the contraction loss at the entrance of the support, one obtains

$$p(L_1) + \rho U\, u(L_1)(1 + K_1) = 0 \tag{3-17}$$

Considering Bernoulli's equation just before and after the exit gives

$$\frac{P_2 - P_1}{0.5\rho U_1^2} = \eta_s \tag{3-18}$$

$$p_1 + \eta_s \rho U_1 u_1 + \eta_p \frac{1}{2} \rho U_1^2 = 0 \tag{3-19}$$

In equation (3-18), P_1 and P_2 are the static pressures immediately before and after the diffuser, respectively. η_s is the static pressure recovery coefficient at the diffuser. In equation (3-19), p_1 and u_1 represent the perturbation pressure and flow velocity upstream of the diffuser. Linearizing and assuming that the perturbation recovery coefficient η_p is a function of *h(x)*, one can write

$$\eta_p = \frac{\Delta \eta_s}{\Delta h} \cdot h \tag{3-20}$$

As proposed by Hobson (1982), a dimensionless diffuser performance coefficient δ is introduced as follows:

$$\delta = \frac{\Delta \eta_s}{\Delta h / H} \tag{3-21}$$

Then, substituting into equation (3-19), one obtains

$$p_1 + \eta_s \rho U_1 u_1 + \delta \frac{\rho U_1^{\,2}}{2H} \cdot h = 0 \tag{3-22}$$

3.4.5 Friction coefficient and friction loss

A new concept to consider friction has been proposed by Kang et al. (2009). To take the friction term in the momentum equation (3-13) into account, the axial momentum loss due to friction is expressed in the form

$$\frac{\tau_x}{H} = \frac{\rho}{H} K_{cf0} \left(U \frac{\partial u}{\partial x} + \frac{\partial u}{\partial t} \right) \tag{3-23}$$

Setting $K_{cf1}{}^2 = 1 + K_{cf0}/H$ simplifies the solution procedure, and the analytical solutions for perturbation flows can be obtained without difficulties. Using the friction coefficient of the Shimoyama and Yamada (1957) model, K_{cf0}, and $K_{cf1}{}^2$ are obtained as follows:

$$K_{cf0} \simeq \frac{(0.2288)\cdot \mathrm{Re}^{-0.24}}{\left[U\left(\phi_n'(x)/\phi_n(x)\right)+i\omega\right]}\cdot U \quad \text{for } \mathrm{Re} \geq 2000, \tag{3-24}$$

$$K_{cf1}{}^2 \simeq 1 + \frac{(0.2288)\cdot \mathrm{Re}^{-0.24}}{H\left[U\left(\phi_n'(x)/\phi_n(x)\right)+i\omega\right]}\cdot U \quad \text{for } \mathrm{Re} \geq 2000. \tag{3-25}$$

3.4.6 Analytical solution for pressure perturbation

The authors proposed an analytical solution for annular-flow-induced vibration considering a new friction concept in Kang et al. (2009). For a brief description of the solution, we start with substituting equations (3-23) and (3-25) into equation (3-13). By virtue of equation (3-12), equation (3-13) becomes

$$\frac{\partial p}{\partial x} + \rho\left(K_{cf1}\right)^2 \frac{\partial u}{\partial t} + \rho U\left(K_{cf1}\right)^2 \frac{\partial u}{\partial x} = 0 \tag{3-26}$$

Equations (3-12) and (3-14) may be expressed as first order complex differential equations.

$$\frac{\partial u}{\partial x} - i\frac{1}{r}v = -\frac{1}{H}\frac{dh}{dt} - \frac{U}{H}\frac{dh}{dx} \tag{3-27}$$

$$-i\frac{1}{r}p + \rho\frac{\partial v}{\partial t} + \rho U\frac{\partial v}{\partial x} = 0 \tag{3-28}$$

The vibration response of a simply-supported inner cylinder vibrating in mode n can be written as

$$h_n(x,t) = \phi_n(x)\cdot a_n\, e^{i\omega t}. \tag{3-29}$$

where $\phi_n(x) = sin\left(\frac{n\pi}{L}x\right)$

The solutions of (3-26) ~ (3-28) for $u_n(x,t)$, $v_n(x,t)$ and $p_n(x,t)$ may be expressed as

$$u_n(x,t) = \sum_{j=1}^{3}\overline{u}_j\cdot e^{\Lambda_j x}\cdot e^{i\omega t} + \left(u_s\cdot\phi_n + u_c\cdot\phi_n'\right)\cdot\overline{h}_n(t) \tag{3-30}$$

$$v_n(x,t) = \sum_{j=1}^{3}\overline{v}_j\cdot e^{\Lambda_j x}\cdot e^{i\omega t} + \left(v_s\cdot\phi_n + v_c\cdot\phi_n'\right)\cdot\overline{h}_n(t) \tag{3-31}$$

$$p_n(x,t) = \sum_{j=1}^{3}\overline{p}_j\cdot e^{\Lambda_j x}\cdot e^{i\omega t} + \left(p_s\cdot\phi_n + p_c\cdot\phi_n'\right)\cdot\overline{h}_n(t) \tag{3-32}$$

Substituting equations (3-29) ~ (3-32) into equation (3-26) ~(3-28), collecting the homogeneous terms (independent of $\overline{h}_n$) of equations (3-30) ~(3-32), and setting to zero yields

$$\begin{bmatrix} \Lambda_j & 0 & -i\frac{1}{r} \\ \rho\left[i\omega\left(\kappa_{cf1}{}^2\right)+U\Lambda_j\left(\kappa_{cf1}{}^2\right)\right] & \Lambda_j & 0 \\ 0 & -i\frac{1}{r} & \rho(i\omega+U\Lambda_j) \end{bmatrix} \begin{Bmatrix} \overline{u}_j \\ \overline{p}_j \\ \overline{v}_j \end{Bmatrix} = 0 \qquad (3\text{-}33)$$

where $K_{cf1}{}^2 = 1 + K_{cf0}/H$.

In order to have a non-trivial solution for equation (3-33), the determinant of the matrix should be zero. The resulting characteristic equation yields the following three eigenvalues; $\Lambda_1 = -\frac{K_{cf1}}{r}$, $\Lambda_2 = \frac{K_{cf1}}{r}$ and $\Lambda_3 = -i\frac{\omega}{U}$. Utilizing each eigenvalue, three relationships between the coefficients of pressure $\overline{p}_i$, circumferential flow velocity $\overline{v}_i$ and axial flow velocity $\overline{u}_i$ are determined.

$$(1)\ \Lambda_1 = -\frac{K_{cf1}}{r},\quad i\kappa_{cf1}\overline{u}_1 - \overline{v}_1 = 0,\quad \overline{p}_1 + \rho\kappa_{cf1}\left[U\kappa_{cf1} - i\,r\,\omega\right]\cdot\overline{u}_1 = 0 \qquad (3\text{-}34)$$

$$(2)\ \Lambda_2 = \frac{K_{cf1}}{r},\ i\kappa_{cf1}\bar{u}_2 + \bar{v}_2 = 0,\ \bar{p}_2 + \rho\kappa_{cf1}\left(\kappa_{cf1}U + ir\omega\right)\cdot\bar{u}_2 = 0 \tag{3-35}$$

$$(3)\ \Lambda_3 = -i\frac{\omega}{U},\ \bar{v}_3 + \frac{r\omega}{U}\cdot\bar{u}_3 = 0,\ \bar{p}_3 = 0 \tag{3-36}$$

As noted by Hobson (1982), the first two conditions, (3-34) and (3-35), represent irrotational velocities and pressure fields while the third stands for a vortical velocity field convecting with the fluid without an associated perturbation pressure field.

In the equations (3-30) ~ (3-32), u_s, u_c, p_s, p_c, v_s, and v_c are coefficients to be determined. By substituting equations (3-29) ~ (3-32) into equations (3-26) ~ (3-28), with equation (3-33), the following three equations are obtained:

$$\frac{\left(Ur + Hru_s - iHv_c\right)}{Hr}\phi_n' + \frac{\left(-iHv_s - Hr\lambda_n^2 u_c + ir\omega\right)}{Hr}\phi_n = 0 \tag{3-37}$$

$$\frac{r\rho U^2 + H\left(p_s r + 2r\rho U u_s - i\rho U v_c + ir\rho\omega u_c\right)}{Hr}\phi_n' - \frac{H\left[r\lambda_n^2\left(p_c + 2\rho U u_c\right) + i\rho\left(Uv_s - r\omega u_s\right)\right] - ir\rho\omega U}{Hr}\phi_n = 0 \tag{3-38}$$

$$-\frac{ip_c + r\rho\left(Uv_s + i\omega v_c\right)}{r}\phi_n' - \frac{p_s + r\rho\left(-iU\lambda_n^2 v_c - \omega v_s\right)}{r}\phi_n = 0 \tag{3-39}$$

where $\lambda_n = \frac{n\pi}{L}$, $n = 1, 2, 3\ldots$

Knowing that $h(x,t)$ is a sine function in x and the derivative of $h(x,t)$ is a cosine function, the first and the second terms in equation (3-37) ~ (3-39) may be separated and set to zero independently, so that the six coefficients can be determined.

The three final solutions are

$$u(x)=\left\{\sum_{j=1}^{3}\overline{u}_j\cdot e^{\Lambda_j x}-\left[\frac{r^2{\lambda_n}^2}{H\left({K_{cf1}}^2+r^2{\lambda_n}^2\right)}U\cdot\phi_n-i\frac{r^2\omega}{H\left({K_{cf1}}^2+r^2{\lambda_n}^2\right)}\cdot\phi_n'\right]\right\}, \tag{3-40}$$

$$v(x)=\left\{\sum_{j=1}^{3}\overline{v}_j\cdot e^{\Lambda_j x}+\left[\frac{{K_{cf1}}^2 r\omega}{H\left({K_{cf1}}^2+r^2{\lambda_n}^2\right)}\cdot\phi_n-i\frac{{K_{cf1}}^2 rU}{H\left({K_{cf1}}^2+r^2{\lambda_n}^2\right)}\cdot\phi_n'\right]\right\}, \tag{3-41}$$

$$p(x)=\left\{\sum_{j=1}^{3}\overline{p}_j\cdot e^{\Lambda_j x}+\left[\frac{{K_{cf1}}^2\rho r^2\left(U^2{\lambda_n}^2+\omega^2\right)}{H\left({K_{cf1}}^2+r^2{\lambda_n}^2\right)}\cdot\phi_n-i\frac{2{K_{cf1}}^2\rho r^2\omega U}{H\left({K_{cf1}}^2+r^2{\lambda_n}^2\right)}\cdot\phi_n'\right]\right\} \tag{3-42}$$

with three conditions, equations (3-34) ~ (3-36), for $\mathbf{\Lambda}_1$, $\mathbf{\Lambda}_2$ and $\mathbf{\Lambda}_3$.

For the short lossless entrance and free discharge, equations (3-15) and (3-16) can be rewritten as

$$\begin{aligned}&\overline{p}_1\cdot e^{-\frac{K_{cf1}\cdot L_1}{r}}+\overline{p}_2\cdot e^{\frac{K_{cf1}\cdot L}{r}}+\frac{\rho r^2{K_{cf1}}^2\left[\left(U^2{\lambda_n}^2+\omega^2\right)\cdot\phi_n\big|_{x=L_1}-i2\omega U\cdot\phi_n\big|_{x=L_1}\right]}{H\left({K_{cf1}}^2+r^2{\lambda_n}^2\right)}\cdot\overline{h}_n(t)\\&+\rho\mathrm{U}\left(\overline{u}_1\cdot e^{-\frac{K_{cf1}\cdot L_1}{r}}+\overline{u}_2\cdot e^{\frac{K_{cf1}\cdot L}{r}}\right)+\frac{\rho\mathrm{U}r^2\left(-{\lambda_n}^2U\cdot\phi_n\big|_{x=L_1}+i\omega\cdot\phi_n\big|_{x=L_1}\right)}{H\left({K_{cf1}}^2+r^2{\lambda_n}^2\right)}\cdot\overline{h}_n(t)=0\end{aligned} \tag{3-43}$$

and

$$\bar{p}_1 \cdot e^{-\frac{K_{cf1} \cdot L_2}{r}} + \bar{p}_2 \cdot e^{\frac{K_{cf1} \cdot L_2}{r}} + \frac{K_{cf1}{}^2 \rho r^2 \left(U^2 \lambda_n{}^2 + \omega^2\right)}{H\left(K_{cf1}{}^2 + r^2 \lambda_n{}^2\right)} \cdot \phi_n\big|_{x=L_2} \cdot \bar{h}_n(t) - i \frac{2 K_{cf1}{}^2 \rho r^2 \omega U}{H\left(K_{cf1}{}^2 + r^2 \lambda_n{}^2\right)} \cdot \phi_n'\Big|_{x=L_2} \cdot \bar{h}_n(t) = 0 \tag{3-44}$$

In the case of the short lossless entrance, the flow is assumed to be irrotational, so that $\bar{u}_3 = 0$. This is the reason why there is no $\bar{u}_3$ in equation (3-43).

Combining equations (3-34), (3-35), (3-43) and (3-44), one obtains the matrix equation

$$\begin{vmatrix} \kappa_{cf1}\left(U\kappa_{cf1} - ir\omega\right) & 0 & 1 & 0 \\ 0 & \kappa_{cf1}\left(U\kappa_{cf1} - ir\omega\right) & 0 & 1 \\ Ue^{\frac{KL_1}{r}} & Ue^{\frac{KL_1}{r}} & e^{\frac{KL_1}{r}} & e^{\frac{KL_1}{r}} \\ 0 & 0 & e^{\frac{KL_2}{r}} & e^{\frac{KL_2}{r}} \end{vmatrix} \cdot \begin{Bmatrix} \bar{u}_1 \\ \bar{u}_2 \\ \bar{p}_1/\rho \\ \bar{p}_2/\rho \end{Bmatrix}$$

$$= -r^2 \begin{Bmatrix} 0 \\ 0 \\ \dfrac{\left(K_{(L1)}{}^2 - 1\right)U^2\lambda_n{}^2 + K_{(L1)}{}^2\omega^2}{H\left(K_{(L1)}{}^2 + r^2\lambda_n{}^2\right)} \cdot \phi_{nL1} + i\omega U \dfrac{\left(1 - 2K_{(L1)}{}^2\right)}{H\left(K_{(L1)}{}^2 + r^2\lambda_n{}^2\right)} \cdot \phi_{nL1}{}' \\ \dfrac{K_{(L2)}{}^2\left(U^2\lambda_n{}^2 + \omega^2\right)}{H\left(K_{(L2)}{}^2 + r^2\lambda_n{}^2\right)} \cdot \phi_{nL2} - i\omega U \dfrac{2K_{(L2)}{}^2}{H\left(K_{(L2)}{}^2 + r^2\lambda_n{}^2\right)} \cdot \phi_{nL2}{}' \end{Bmatrix} \cdot \bar{h}_n(t) \tag{3-45}$$

where $\frac{KL_1}{r}=\left.\frac{K_{cf1}\cdot x}{r}\right|_{x=L1}$, $\frac{KL_2}{r}=\left.\frac{K_{cf1}\cdot x}{r}\right|_{x=L2}$, $\phi_{nL1}=\phi_n(x)\big|_{x=L1}$, $\phi_{nL2}=\phi_n(x)\big|_{x=L2}$,

$K_{(L1)}{}^2=\left.K_{cf1}{}^2\right|_{x=L1}$, $K_{(L2)}{}^2=\left.K_{cf1}{}^2\right|_{x=L2}$, $\phi'_{nL1}=\left.\frac{d\phi_n}{dx}\right|_{x=L1}$, and $\phi'_{nL2}=\left.\frac{d\phi_n(x)}{dx}\right|_{x=L2}$.

For the contraction-loss entrance and diffuser exit, equation (3-17) and (3-19) can be rewritten as equations (3-43) and (3-44), then, with equations (3-34) and (3-35), one can obtain the matrix equation below

$$\begin{vmatrix} \kappa_{cf1}\left(U\kappa_{cf1}-ir\omega\right) & 0 & 1 & 0 \\ 0 & \kappa_{cf1}\left(U\kappa_{cf1}-ir\omega\right) & 0 & 1 \\ (1+K_1)Ue^{-\frac{KL_1}{r}} & (1+K_1)Ue^{\frac{KL_1}{r}} & e^{-\frac{KL_1}{r}} & e^{\frac{KL_1}{r}} \\ U\eta e^{-\frac{KL_2}{r}} & U\eta e^{-\frac{KL_2}{r}} & e^{-\frac{KL_2}{r}} & e^{\frac{KL_2}{r}} \end{vmatrix} \cdot \begin{Bmatrix} \bar{u}_1 \\ \bar{u}_2 \\ \bar{p}_1/\rho \\ \bar{p}_2/\rho \end{Bmatrix}$$

$$= -r^2 \begin{Bmatrix} 0 \\ 0 \\ \frac{\left[\left(K_{(L1)}{}^2-K_a\right)U^2\lambda_n{}^2+K_{(L1)}{}^2\omega^2\right]}{H\left(K_{(L1)}{}^2+r^2\lambda_n{}^2\right)}\phi_{nL1}+i\omega U\cdot\frac{K_a-2K_{(L1)}{}^2}{H\left(K_{(L1)}{}^2+r^2\lambda_n{}^2\right)}\phi'_{nL1} \\ \frac{\left(K_{(L2)}{}^2-\eta\right)U^2\lambda_n{}^2+K_{(L2)}{}^2\omega^2}{H\left(K_{(L2)}{}^2+r^2\lambda_n{}^2\right)}\cdot\phi_{nL2}+i\omega U\cdot\frac{\eta-2K_{(L2)}{}^2}{H\left(K_{(L2)}{}^2+r^2\lambda_n{}^2\right)}\cdot\phi'_{nL2} \end{Bmatrix}\cdot\bar{h}_n(t) \qquad (3\text{-}46)$$

where $K_a=1+K_1$.

The two simultaneous equations in matrix forms may be solved with the help of a symbolic computer softwares such as Mathematica or Maple. Mathematica 6.0 (2007) was utilized to obtain solutions for perturbation pressures, based on the relations

$$e^{2K_{cf1}\cdot x/r}\Big|_{x=L1} \ll e^{2K_{cf1}\cdot x/r}\Big|_{x=L2}, \text{ and } e^{K_{(L1)}\cdot(2L_1+x)/r} \ll e^{K_{(L2)}\cdot(2L_2+x)/r}.$$

The resulting perturbation pressures at the narrow annulus are

$$\begin{aligned} p(x) = {} & \frac{\rho r^2 K_{cf1}{}^2}{H\left(K_{cf1}{}^2 + r^2\lambda_n{}^2\right)} \times \left[-i2\omega U\cdot\phi_n' - U^2\cdot\phi_n'' + \omega^2\phi_n\right] \\ & - \left\{\frac{\rho r^2}{H\left(K_{(L1)}{}^2 + r^2\lambda_n{}^2\right)}\cdot\left[\left((K_{L1}{}^2 - 1)\cdot U^2\lambda_n{}^2 + K_{L1}{}^2\omega^2\right)\cdot\phi_{nL1} + i\omega U\left(1 - 2K_{L1}{}^2\right)\cdot\phi_{nL1}'\right]\right\} \\ & \times \frac{K_{cf1}\left(UK_{cf1} - ir\omega\right)}{\left[U\left(K_{cf1}{}^2 - 1\right) - ir\omega K_{cf1}\right]}\cdot e^{\frac{KL_1 - K_{cf1}x}{r}} \\ & - \frac{\rho r^2\cdot K_{L2}{}^2}{H\left(K_{(L2)}{}^2 + r^2\lambda_n{}^2\right)} \times \left[\left(U^2\lambda_n{}^2 + \omega^2\right)\cdot\phi_{nL2} - i2\omega U\cdot\phi_{nL2}'\right]\cdot e^{\frac{-KL_2 + K_{cf1}x}{r}} \end{aligned} \quad (3\text{-}47)$$

for the short-lossless entrance and free-discharge exit, and

$$p(x)=\frac{\rho r^2 {K_{cf1}}^2}{H\left({K_{cf1}}^2+r^2{\lambda_n}^2\right)}\times\left[-i2\omega U\cdot\phi_n'-U^2\cdot\phi_n''+\omega^2\phi_n\right]$$
$$-\left\{\frac{\rho r^2}{H\left({K_{(L1)}}^2+r^2{\lambda_n}^2\right)}\cdot\left[\left(({K_{L1}}^2-K_a)\cdot U^2{\lambda_n}^2+{K_{L1}}^2\omega^2\right)\cdot\phi_{nL1}+i\omega U\left(K_a-2{K_{L1}}^2\right)\cdot\phi_{nL1}'\right]\right\}$$
$$\times\frac{\cdot K_{cf1}\left(UK_{cf1}-ir\omega\right)}{\left[U\left({K_{cf1}}^2-K_a\right)-ir\omega K_{cf1}\right]}\cdot e^{\frac{KL_1-K_{cf1}x}{r}}$$
$$-\frac{\rho r^2}{H\left({K_{(L2)}}^2+r^2{\lambda_n}^2\right)}\times\frac{e^{\frac{-KL_2+K_{cf1}x}{r}}\cdot K_{cf1}\left(UK_{cf1}+ir\omega\right)}{\left[U\left({K_{cf1}}^2-\eta\right)+ir\omega K_{cf1}\right]}\times$$
$$\left\{\left[\left(\delta+2({K_{L2}}^2-\eta)\right)r^2{\lambda_n}^2U^2+{K_{L2}}^2\left(\delta U^2+2r^2\omega^2\right)\right]\cdot\phi_{nL2}+i2\omega r^2U\left(\eta-2{K_{L2}}^2\right)\cdot\phi_{nL2}'\right\}$$

(3-48)

for the contraction-loss entrance and diffuser exit.

Equations (3-47) and (3-48) may be divided into three terms; a term proportional to $e^{(KL_1-x\cdot K_{cf1})/r}$, a term proportional to $e^{(-KL_2+x\cdot K_{cf1})/r}$ and a term independent of these two exponential functions. The function $e^{(KL_1-x\cdot K_{cf1})/r}$ has a peak at the entrance ($x=L_1$). The magnitude of this function decreases rapidly with increment of the variable x beyond the entrance, so that this term multiplied by $e^{(KL_1-x\cdot K_{cf1})/r}$ may be called the *'entrance effect'*. Similarly, $e^{(-KL_2+x\cdot K_{cf1})/r}$ may be called the *'exit effect'*. Unlike these two terms, the first term, in equations (3-47) and (3-48) consist of eigenfunction and derivatives of the eigenfunction, so that the latter term has an effect in the whole spatial domain. For this reason, the latter term may be called the *'mid-way effect'*. It is not difficult to identify

the three fluid effects in the three terms: inertia (ω^2), Coriolis ($i\omega$) and, centrifugal effects, respectively.

Recognizing that the fluid mass is independent of the fluid velocity, it is true that small effective lengths of entrance and exit are insufficient to induce significant fluid inertia forces. Therefore, it is assumed that the real part of the entrance and exit effects is limited to fluidelastic stiffness while the imaginary part is fluidelastic damping ($i\omega$ terms).

The fluidelastic force per unit length may be calculated by integrating the pressure field which is given by equation (3-2). Accordingly, equation (3-47) gives

$$F_l(x)=\frac{-\rho\pi r^3 K_{cf1}{}^2}{H\left(K_{cf1}{}^2+r^2\lambda_n{}^2\right)}\times\left[-i2\omega U\cdot\phi_n'-U^2\cdot\phi_n''+\omega^2\phi_n\right] \\ +\left[F_{lET1}\right]\times e^{\frac{KL_1-K_{cf1}x}{r}}+\left[F_{lEX1}\right]\times e^{\frac{-KL_2+K_{cf1}x}{r}} \tag{3-49}$$

where $F_{lET1}=\mathbb{R}_1\cdot\left[\left((K_{L1}{}^2-1)\cdot U^2\lambda_n{}^2+K_{L1}{}^2\omega^2\right)\cdot\phi_{nL1}+i\omega U\left(1-2K_{L1}{}^2\right)\cdot\phi_{nL1}'\right]$

$$\times\frac{K_{cf1}\left(UK_{cf1}-ir\omega\right)}{\left[U\left(K_{cf1}{}^2-1\right)-ir\omega K_{cf1}\right]}\cdot e^{\frac{KL_1-K_{cf1}x}{r}}, \tag{3-50}$$

$$F_{lEX1}=\mathbb{R}_2\cdot\left[\left(U^2\lambda_n{}^2+\omega^2\right)\cdot\phi_{nL2}-i2\omega U\cdot\phi_{nL2}'\right]\cdot e^{\frac{-KL_2+K_{cf1}x}{r}}, \tag{3-51}$$

$$\mathbb{R}_1=\frac{\rho\pi r^3}{H\left(K_{(L1)}{}^2+r^2\lambda_n{}^2\right)}, \tag{3-52}$$

$$\mathbb{R}_2 = \frac{\rho\pi r^3 \cdot {K_{L2}}^2}{H\left({K_{(L2)}}^2 + r^2{\lambda_n}^2\right)}. \tag{3-53}$$

Similarly, equation (3-48) gives

$$\begin{aligned} F_l(x) = & \frac{-\rho\pi r^3 {K_{cf1}}^2}{H\left({K_{cf1}}^2 + r^2{\lambda_n}^2\right)} \times \left[-i2\omega U \cdot \phi_n' - U^2 \cdot \phi_n'' + \omega^2\phi_n\right] \\ & + \left[F_{lET2}\right] \times e^{\frac{KL_1 - K_{cf1}x}{r}} + \left[F_{lEX2}\right] \times e^{\frac{-KL_2 + K_{cf1}x}{r}} \end{aligned} \tag{3-54}$$

where $F_{lET2} = \mathbb{R}_1 \cdot \left[\left(({K_{L1}}^2 - K_a) \cdot U^2{\lambda_n}^2 + {K_{L1}}^2\omega^2\right) \cdot \phi_{nL1} + i\omega U\left(K_a - 2{K_{L1}}^2\right) \cdot \phi_{nL1}'\right]$

$$\times \frac{K_{cf1}\left(UK_{cf1} - ir\omega\right)}{\left[U\left({K_{cf1}}^2 - K_a\right) - ir\omega K_{cf1}\right]} \cdot e^{\frac{KL_1 - K_{cf1}x}{r}} \tag{3-55}$$

$$\begin{aligned} F_{lEX2} = & \left\{\begin{array}{l} \left[\left(\delta + 2({K_{L2}}^2 - \eta)\right)r^2{\lambda_n}^2U^2 + {K_{L2}}^2\left(\delta U^2 + 2r^2\omega^2\right)\right] \cdot \phi_{nL2} \\ + i2\omega r^2 U\left(\eta - 2{K_{L2}}^2\right) \cdot \phi_{nL2}' \end{array}\right\} \\ & \times \mathbb{R}_2 \cdot \frac{K_{cf1}\left(UK_{cf1} + ir\omega\right)}{\left[U\left({K_{cf1}}^2 - \eta\right) + ir\omega K_{cf1}\right]} \cdot e^{\frac{-KL_2 + K_{cf1}x}{r}} \end{aligned} \tag{3-56}$$

It is not easy to formulate one fluid-structure coupled equation similar to equation (3-10) by identifying every single term in equation (3-49) and (3-50) in terms of factors of $\omega^2, \omega,$ and ω^0. A single equation may be obtained from the denominators of the two equations, which renders the equation of motion a third-order differential equation. Also, it is not easy to utilize Galerkin's projection for the whole dynamic behavior in terms of mean flow velocity due to the complexity of the fluidelastic force equations.

However, if the inner cylinder first loses stability by flutter at low flow velocity, the imaginary part of the fluidelastic force may be used to see if damping becomes negative, and overcomes the structural damping forces. From equations (3-6), (3-7a) and (3-7b), one may set a damping balance condition for the negative damping force.

$$i\omega\left(2\zeta\omega_n\int_0^L M_s\phi_n(x)^2\,dx\right)\bar{h}_n(t)-\mathrm{Im}\int_{L1}^{L2}\phi_n(x)\cdot F_l(x,t)\,dx\le 0 \tag{3-57}$$

By utilizing equations (3-49) – (3-56) considering the earlier discussion on the entrance and exit effects, the fluid damping force in equation (3-57) becomes

$$-\int_{L1}^{L2}\mathrm{Im}\left[F_l(x)\right]\phi_n dx=-\int_{L1}^{L2}\frac{2\rho\pi r^3 {K_{cf1}}^2\omega U}{H\left({K_{cf1}}^2+r^2{\lambda_n}^2\right)}\cdot\phi_n'\phi_n dx-\int_{L1}^{L2}\mathrm{Im}\left(F_{lET1}+F_{lEX1}\right)\phi_n dx \tag{3-58}$$

for the short-lossless entrance and free-discharge exit, and

$$-\int_{L1}^{L2}\mathrm{Im}\left[F_l(x)\right]\phi_n dx=-\int_{L1}^{L2}\frac{2\rho\pi r^3 {K_{cf1}}^2\omega U}{H\left({K_{cf1}}^2+r^2{\lambda_n}^2\right)}\cdot\phi_n'\phi_n dx-\int_{L1}^{L2}\mathrm{Im}\left(Fl_{ET2}+Fl_{EX2}\right)\phi_n dx \tag{3-59}$$

for the contraction-loss entrance and diffuser exit. One may add a Coriolis' term to equation (3-58) and (3-59) when the flow velocity is not negligible.

By virtue of the discussion above on the fluidelastic forces, the modal fluid mass may be expressed by

$$F_{f,I} = \omega^2 \left[\frac{\rho \pi r^3 K_{cf1}{}^2}{H\left(K_{cf1}{}^2 + r^2 \lambda_n{}^2\right)} \cdot \int_{L1}^{L2} \phi_n(x)^2 dx \right] \tag{3-60}$$

The fluid stiffness forces are

$$F_{f,K} = \int_0^L M_f U^2 \phi_n''(x) \phi_n dx + \frac{\rho \pi r^3 K_{cf1}{}^2 U^2 \lambda_n{}^2}{H\left(K_{cf1}{}^2 + r^2 \lambda_n{}^2\right)} \cdot \int_{L1}^{L2} \left[\phi_n(x) - \mathrm{Re}\left(F_{lET1} + F_{lEX1}\right)\right] \phi_n dx \tag{3-61}$$

for the short-lossless entrance and the free-discharge exit, and

$$F_{f,K} = \int_0^L M_f U^2 \phi_n''(x) \phi_n dx + \frac{\rho \pi r^3 K_{cf1}{}^2 U^2 \lambda_n{}^2}{H\left(K_{cf1}{}^2 + r^2 \lambda_n{}^2\right)} \cdot \int_{L1}^{L2} \left[\phi_n(x) - \mathrm{Re}\left(F_{lET2} + F_{lEX2}\right)\right] \phi_n dx \tag{3-62}$$

for the contraction-loss entrance and diffuser exit.

3.5 Numerical calculations

For a one-mode approximation, the first mode can be utilized since the inner tube was observed to lose stability in the first mode.

The dimensions of the physical properties and fluid characteristics are summarized in Table 3.1 and Table 3.2. All the properties and the dimensions are selected to model the experimental test setup.

The finite-length gap support having a 38.1 *mm* length is considered to be positioned at the mid length of the inner cylinder as shown in Figure 3. 6. The mid point of the support coincides with the mid length of the inner cylinder. For the upstream end of the support, a contraction loss factor K_a is considered. On the other hand, for the downstream diffuser exit, the diffuser efficiency η and a dimensionless diffuser performance coefficient δ are considered.

The calculated fluidelastic forces, inertia, damping and stiffness, were normalized by structural damping force for the convenience.

3.5.1 Parametric study

The calculated fluidelastic inertia ratios are plotted in Figure 3. 7. Since the inertia force is independent of the annular-flow velocity, as Blevins (1990) indicated, the added mass becomes large as the gap decreases, so that a larger inertia force results from the smaller annulus.

The entrance and exit effects are assumed to be limited to fluidelastic stiffness (Real) and fluidelastic damping (Imaginary) components of the fluid force, so that the inertia effects at the entrance and exit are neglected. Based on this assumption, Figure 3. 8 illustrates the normalized fluidelastic stiffness as a function of Reynolds number for different fluid boundary conditions and annular gap sizes. For the lossless entrance and exit, the stiffness varies little with the fluid boundary conditions and Reynolds number. However, for the loss and recovery boundaries, depending on gap size, the normalized fluidelastic stiffness changes significantly. The fluidelastic stiffness decreases much more with the smaller annular gap as the Reynolds number decreases.

In addition to the annular gap, the other important parameter is the dimensionless diffuser performance coefficient δ. The coefficient δ has much more effect than the diffuser efficiency η on the fluidelastic stiffness. The two factors are related to the diffuser angle at the downstream end. However, It must be understood that η is a static coefficient while δ is a dynamic coefficient. One can appreciate the difference from

equations (3-18) and (3-20). With K_a, δ =0.1 and η =0.8, the stiffness is almost the same as the stiffness with K_a= δ =0.1 and η =0.1 for all supports. However, when K_a= η =0.1 and δ =0.5, the fluidelastic stiffness decreases much more than when K_a=η =0.1 and δ =0.1 for all gap sizes.

In equation (3-57), the negative total damping force means that the fluid energy absorbed by the inner cylinder is larger than the energy dissipated through damping. Normalized total damping variations are shown in Figure 3. 9. In order to obtain Figure 3. 9, a structural damping ratio of 0.2 % is assumed. The damping ratio of fuel rods in Pressurized Water Reactor PWR (PWR) and of steam generator tubes in nuclear power plants are known to be near or less than 0.2% (excluding damping introduced by loose support). For the lossless entrance and exit, the total damping forces do not change much as Reynolds number is varied. However, in the case of the contraction loss at the entrance and diffuser at the exit, the total damping forces may become negative. As the annular gap decreases, or the diffuser performance coefficient δ increases, the total damping force decreases rapidly. For the support having 0.29 mm gap with K_a= δ = η =0.1, the fluid damping overcomes the structural damping at a Reynolds number of 4,790 or 0.54 m/s upstream flow velocity, which is equivalent to 12.3 m/s at the gap. On the other hand, for the same parameters with δ =0.5, negative damping is obtained at a Reynolds number of 1,850 or 0.21 m/s upstream flow velocity which is equivalent to 4.8 m/s at the gap. A velocity at the upstream end of only 0.21 m/s (5.15 mm gap) is needed to have negative damping. When the gap is 2.2 mm, the Reynolds

number for the negative damping goes up to 61,060 or 7.7 m/s upstream of the support, which is equivalent to 21 m/s at the gap. Figure 3. 10 shows the total damping forces as functions of the upstream flow velocity. All flow velocities are believed to be within the practical engineering range in terms of orders of magnitude. This is especially to be contrasted with the case of unconfined axial flows which result in instability velocities far above any prototypical flow velocities.

For the support having a 0.29 mm gap, the entrance and exit effects on the negative damping can be seen in Figures 3.11 and 3.12. As seen in thes, the effect of δ on damping is obvious. The total damping force for δ=0.5 is approximately 10 times lower than the total damping force for δ=0.1. Furthermore, the exit effect is more dominant on the damping force than the entrance effect or the mid-way effect. These figures possibly explain why the expansion channel of the downstream end is primarily responsible for negative damping as many previous studies have shown.

3.5.2 Experimental cases

Pressure recovery and dimensionless performance coefficient

The pressure recovery efficiency η_s of the support is obtained by experiments based on the static pressures measured upstream and downstream of the diffuser. As expected, all of the measurements show that the pressure recovery efficiency η_s is not constant but varies with Reynolds number, which is seen in Figures 3.13 and 3.14. The efficiency

seems peak at some value of Reynolds number. The Reynolds number range from 1,000 to 5,000 is very important since it is within this range that instabilities with small gap supports are observed in experiments. With the largest gap, the Reynolds number range from 8,000 to 20,000 is also important. Unfortunately, however, we do not have measurements in this higher range of Reynolds number.

The resolution of our pressure gages is 10^{-2} *psi* (approximately 68.9 *Pascal*). Thus a difference less than the resolution cannot be measured at present. This is the reason why the η_s at low Reynolds numbers is not shown in the two figures for any of the supports. Based on Figures 3.13 and 3.14, one may use 0.2 as η_s for the 0.29 mm – 0.67 mm gap supports, and 0.45 for the 2.2 mm gap support. On the other hand, from Figure 3. 14, for 20 degree diffusers, we take 0.1 as η_s for the 0.29 mm – 0.67 mm gap supports, and 0.3 for the 2.2 mm gap support.

To determine a dimensionless diffuser performance coefficient δ based on the experiments, equation (3-21) may be expressed as

$$\delta = \frac{\Delta\eta}{\Delta h / H} = \frac{\eta_{peak} - \eta_{inital}}{\left(h_{peak} - h_{inital}\right)/H} \tag{3-63}$$

Assuming η_{peak} to be the value at the maximum vibration amplitude, and Δh to be at 70 percent of the gap, one may calculate δ. The *dynamic gap closure* Δh is assumed to be 70 percent of the gap based on the argument that since the *rms* vibration amplitude is measured, the maximum amplitude before impacting could be assumed to be the 70 percent of the gap. The peak δ is obtained when the vibration reaches the maximum amplitude. Based on this, one may calculate δ; for instance, in the case of the 0.29 *mm*/10° support, $\delta = 0.43$ (= (0.5-0.2)/0.7).

The calculated η_s and δ are summarized in Table 3.3.

Calculations for the experiments

For the calculations, the contraction loss factor K_a is set to 0.3, which is believed to be realistic for normal engineering piping. When the short-lossless entrance and the free-discharge exit are considered, the loss factor K_a and the performance coefficient $\boldsymbol{\delta}$ should be set to zero with the diffuser efficiency $\boldsymbol{\eta}$ =1. With these values, no loss entrance and full conversion of the dynamic pressure into static pressure are obtained.

As seen in Figure 3. 15, the trend of the stiffness force ratio as function of Reynolds number is very similar trend to that of Figure 3. 8. Since $\boldsymbol{\delta}$ has a strong effect on the fluidelastic forces, the difference between Figure 3. 8 and Figure 3. 15 comes from the different results of $\boldsymbol{\delta}$. For the case of the 0.67 mm gap support, the stiffnesses for the two different diffuser angles show almost the same behavior with increasing Reynolds

number. For the gaps smaller than 0.67 mm, the 10° diffuser loses fluidelastic stiffness at lower Reynolds number than the 20° diffuser.

Figure 3. 16 shows the total damping force ratio as a function of Reynolds number at the support gap. For the two small gap sizes, 0.29 mm and 0.42 mm, the damping of the 10° diffuser becomes negative at a lower Reynolds number than the 20° diffuser. On the other hand, for the largest gap, 2.2 mm, the damping of the 20° diffuser becomes negative at a lower Reynolds number than 10° diffuser.

The 0.29 mm/10° support is expected to have negative damping at a Reynolds number of 1,800 or 5.5 m/s at the gap, which is equivalent to 0.24 m/s upstream of the support. Before the 0.29 mm/20° support becomes negatively damped, the 0.42 mm/10° support loses positive damping at a Reynolds number of 2,800 or 6 m/s at the gap, which is equivalent to 0.38 m/s upstream of the support. A Reynolds number of 6,800 results in negative damping for the 0.67 mm gap supports. For the largest gap, 2.2 mm, negative damping occurs at Reynolds numbers of 23,500 and 24,700. These Reynolds numbers are equivalent to 9.5 m/s and 10 m/s respectively at the gap, or 3.48 m/s and 3.66 m/s upstream of the support.

Figure 3.17 shows the total damping ratio as a function of the upstream flow velocity corresponding to the Reynolds number in Figure 3. 16. As may be seen in the figure, all of the critical flow velocities are below 4 m/s which are believed to be well below

practical engineering flow velocities. All the calculated and measured critical flow velocities are summarized in Table 3.4. Although the calculated critical flow velocities for the 0.67 mm gap supports do not agree well with the experiment results, the calculated results are, overall, in reasonable agreement with the experiments.

It is worth noting that the Shimoyama and Yamada friction model (1957) shows some scatter in the Reynolds number range of 1,300 ~ 2,000. In addition, the friction loss with vibration may be different from the friction loss without vibration. The Shimoyama and Yamada model does not consider vibration. Applying the laminar friction model, equation (3-24), with very high η and δ (for instance, $\eta = \delta = 0.8$) for the 0.67 *mm* gap support, the critical flow velocity for the negative damping decreases down to a Reynolds number of 1,518 or 2 m/s at the gap which is equivalent to 0.20 m/s at the upstream instead of 0.85 m/s. This is the same value as the experimental value.

3.6 Conclusions

The stability behavior of a pinned-pinned flexible rod subjected to narrow annular flow over a finite-length gap support has been experimentally and analytically investigated. By the experimental approach, the critical flow velocities were measured for varying gap size and diffuser angles for a finite-length support. Analytically a solution was obtained for the perturbation pressure acting on a pinned-pinned cylinder subjected to a leakage flow at a finite-length gap support. For the analytical solution, two-dimensional

flow with two fluid boundary conditions was considered. The two sets of boundary conditions are, a lossless entrance and a full conversion exit for the ideal conditions, and a contraction-loss entrance and diffuser exit for practical boundary conditions.

In experiments with a 2.2 m long steel tube, and 3.8 cm long support, and significantly low air flow, flutter instability is observed for all supports; independently of the gap size and diffuser angle. With annular flow, the simply supported cylinder is known to lose stability by divergence at very high flow velocity beyond practical engineering applications. Interestingly, a small support plays a significant role to change the dynamic behavior of the pinned-pinned rod, decreasing the critical flow velocities down to engineering flow velocities. Generally speaking, the smaller gaps and the smaller diffuser angles lower the critical flow velocity for negative damping. On the other hand, for the largest gap (2.20 mm), the critical flow velocity of the larger diffuser angle (20^{o}) is lower than that of the smaller diffuser angle (10^{o}).

In the theory, the negative damping force is shown to be very dependent on the dimensionless diffuser performance efficiency ($\boldsymbol{\delta}$), which is the ratio of diffuser efficiency to dynamic gap closure. The other important result is that the negative damping force is mostly generated at the exit. From these two results, it may be concluded that expansion channels at the downstream end cause flutter instability. This is in agreement with previous research findings.

A semi-analytical model for the fluidelastic damping force is proposed based on the analytical pressure solution. In the case where no losses are assumed at the entrance and the exit of the support, fluidelastic damping remains positive at all Reynolds numbers. For the experimental cases, numerical calculation by the semi-analytical model yields results that are comparable with experiments. The smaller gap size and diffuser angle are shown to be more destabilizing. However, in the case of the largest gap (2.2 mm), the bigger diffuser angle (20^{o}) generates negative damping at a lower flow velocity.

For the pinned-pinned cylinder subjected to leakage flow in a finite-length gap support at its mid length, the critical flow velocity with compressed air ($\rho \approx 8.5\ Kg/m^3$) turns out to be less than 3 *m/s,* which is within the range of most engineering applications.

Table 3.1 Major dimensions of test apparatus

Item	Dimension
Inner Cylinder	Inner diameter: 14.15 *mm* Outer diameter: 15.93 *mm* Length: 2.2 *m* Young's modulus *(E)*: 266.1 N/ m^2
Outer glass tube	Inner diameter: 26.24 *mm* Gap: 5.16 *mm*
Support	Length: 38.1 *mm* Inner diameter (gap): (a) 16.51 *mm* (0.29 *mm*) (b) 16.76 *mm* (0.42 *mm*) (c) 17.27 *mm* (0.67 *mm*) (d) 20.32 *mm* (2.2 *mm*) Diffuser angle: 10° and 20°

Table 3.2 Fluid parameters and vibration characteristics of the inside cylinder

Item	**Dimension**
Fluid	(a) compressed air : ~ 100 *psig* (b) density: ~8.5 kg/m^3
Hydraulic diameter at support and L/D_h	(a) 16.51 support: 0.58 *mm*, L/D_h=50 (b) 16.76 support: 0.84 *mm*, L/D_h=34.8 (c) 17.27 support: 1.35 *mm*, L/D_h=21.7 (d) 20.32 support : 4.39 *mm*, L/D_h=6.6
Hydraulic diameter at glass tube and L/D_h	10.31 mm, L/D_h =203.6
Natural frequency (Hz) of the inner cylinder without flow: experiment (theory)	1st natural frequency: 12.5 (9.1) 2nd natural frequency: 40.2 (36.6) 3rd natural frequency: 89.2 (82.3) 4th natural frequency: 150.2 (146.3)
Damping factor of the inner cylinder	ζ_{1st} = 0.2 % for the 1st natural frequency

Table 3.3 Steady diffuser efficiency η_s and dimensionless diffuser performance coefficient δ for finite-length narrow-gap supports

Support	η_s	δ
1. 0.29 mm gap with 10° diffuser angle	0.2	0.43
2. 0.29 mm gap with 20° diffuser angle	0.07	0.1
3. 0.42 mm gap with 10° diffuser angle	0.3	0.43
4. 0.42 mm gap with 20° diffuser angle	0.07	0.1
5. 0.67 mm gap with 10° diffuser angle	0.2	0.285
6. 0.67 mm gap with 20° diffuser angle	0.1	0.285
7. 2.2 mm gap with 10° diffuser angle	0.4	0.357
8. 2.2 mm gap with 20° diffuser angle	0.3	0.43

Table 3.4 Comparison of the measured and the calculated critical flow velocity for negative damping

Support	η_s / δ	**Critical flow velocity at the upstream (m/s)**	
		Experiment	**Calculation**
1. 0.29 mm gap with 10°	0.2 / 0.43	0.10	0.23
2. 0.29 mm gap with 20°	0.07 / 0.1	0.19	0.54
3. 0.42 mm gap with 10°	0.2 / 0.43	0.22	0.36
4. 0.42 mm gap with 20°	0.07 / 0.1	0.45	0.85
5. 0.67 mm gap with 10°	0.2 / 0.285	0.12	0.84
6. 0.67 mm gap with 20°	0.07 / 0.285	0.20	0.85
7. 2.2 mm gap with 10°	0.4 / 0.357	2.82	3.49
8. 2.2 mm gap with 20°	0.3 / 0.43	1.21	3.38

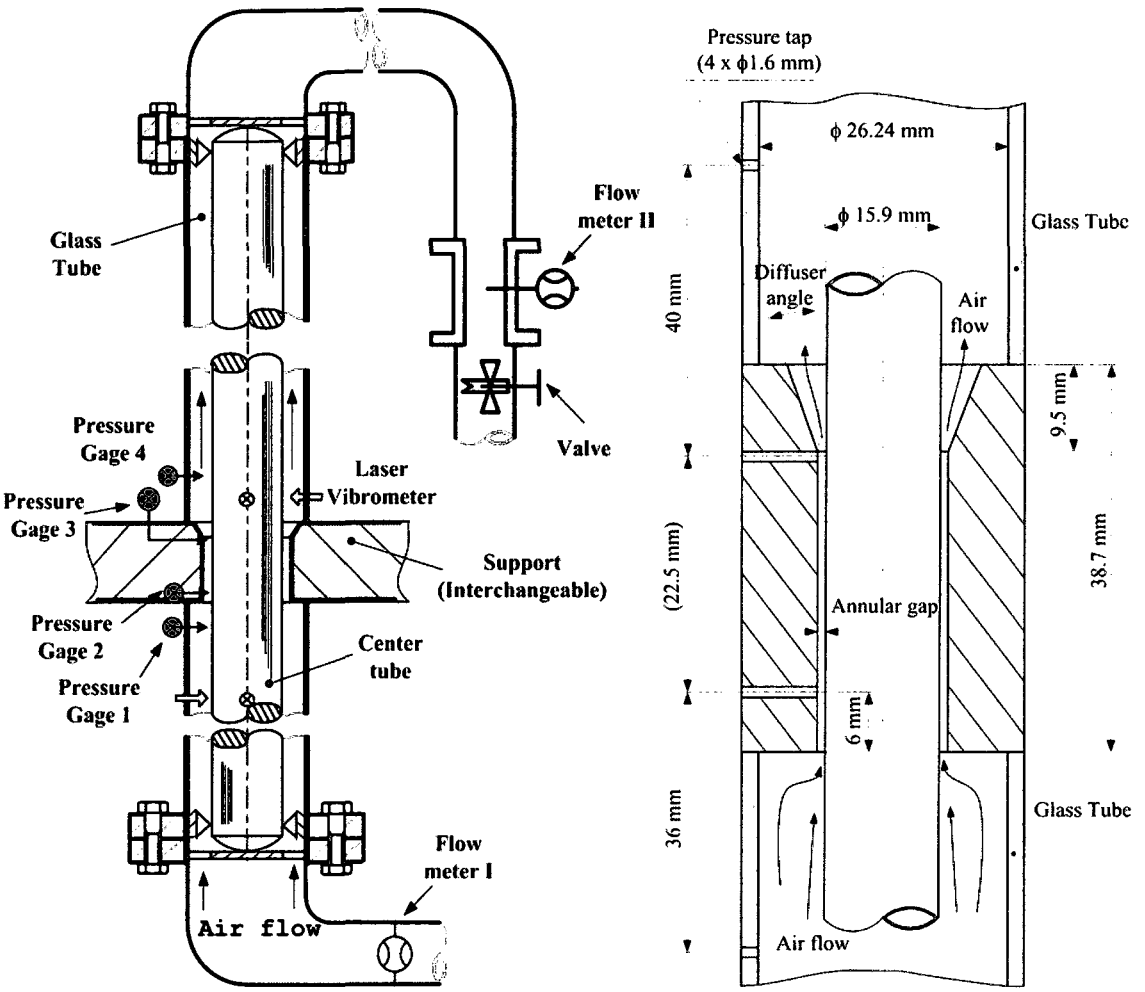

Figure 3.1 Schematic drawing of the test section. (a) Inner tube and instrument setup (b) Dimensions near the support

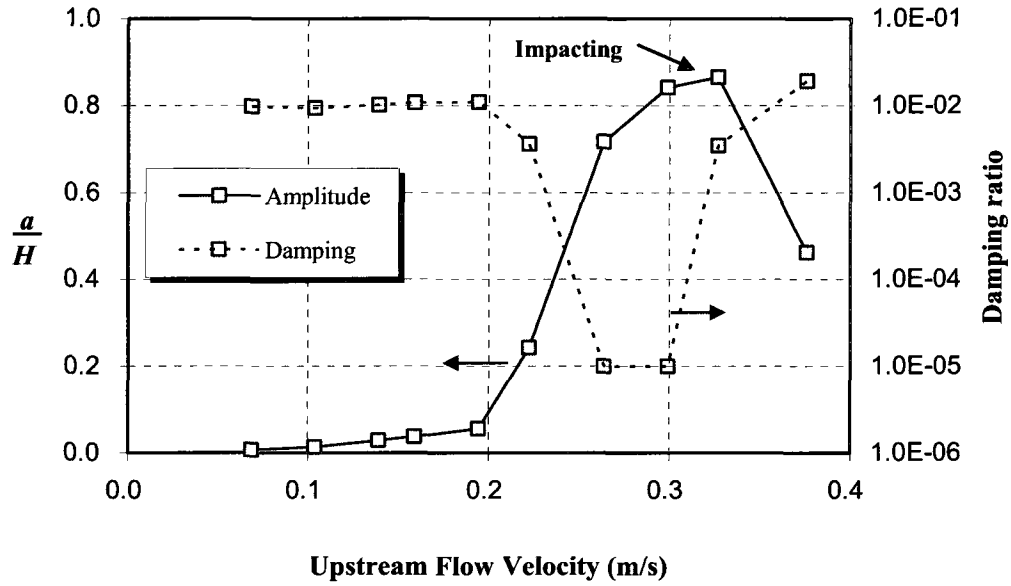

Figure 3.2 Vibration amplitude and damping ratio as a function of upstream flow velocity for the inside cylinder in the support with 0.29 mm gap and 20° diffuser angle

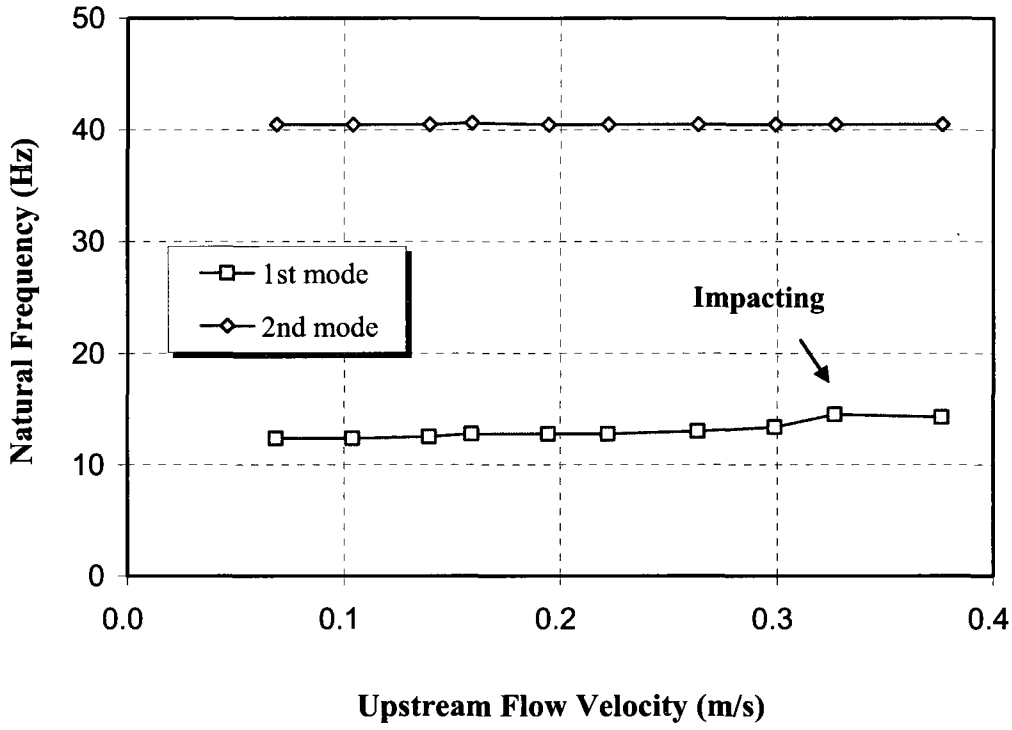

Figure 3.3 The first and the second natural frequencies as a function of upstream flow velocity for the inside cylinder in the support with 0.29 mm gap and 20° diffuser angle

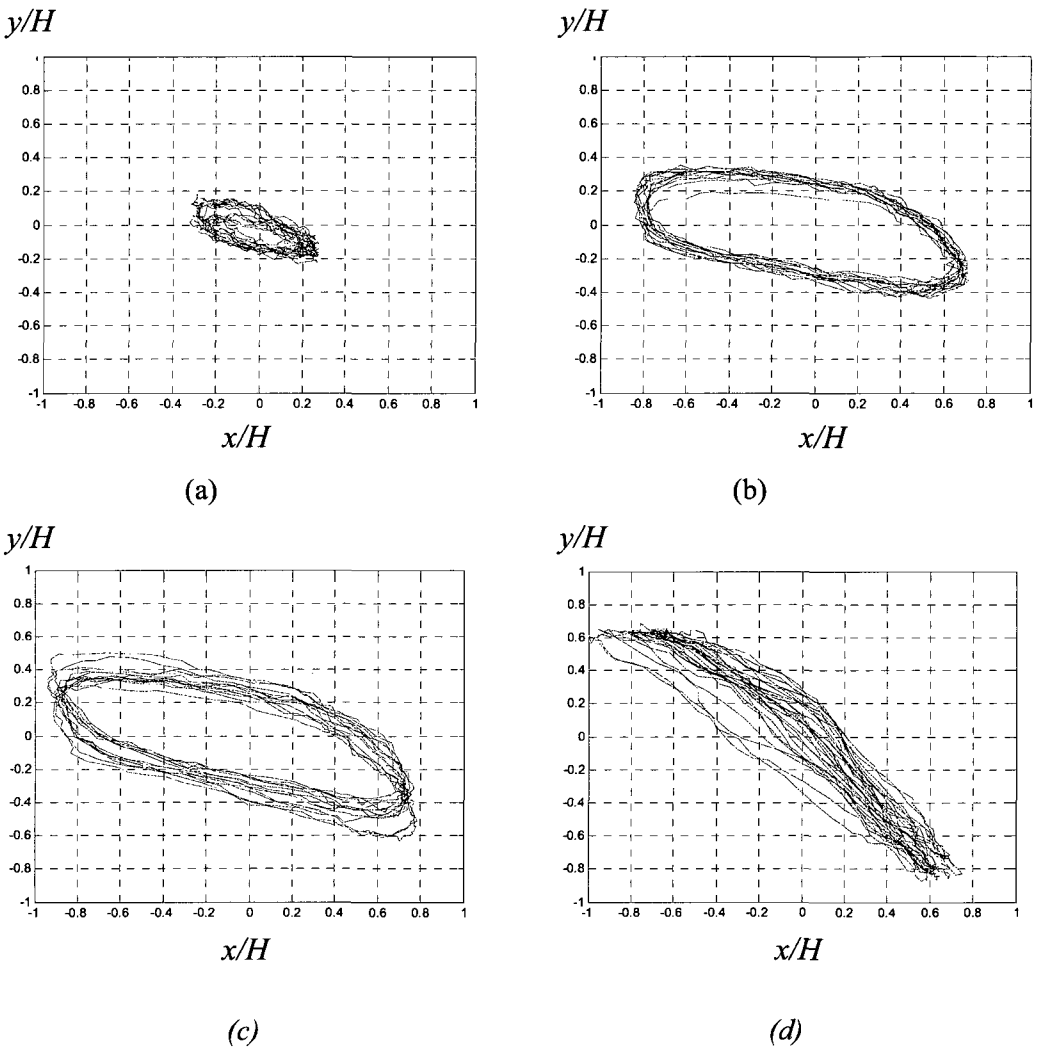

Figure 3.4 X-Y plots for the vibration of the inner cylinder in the support with 0.29 mm gap and 20° diffuser angle. Reynolds numbers (upstream velocity): (a) 1,682 (0.22 m/s), (b) 1,994 (0.26 m/s), (c) 2,262 (0.30 m/s), (d) 2,843 (0.38 m/s)

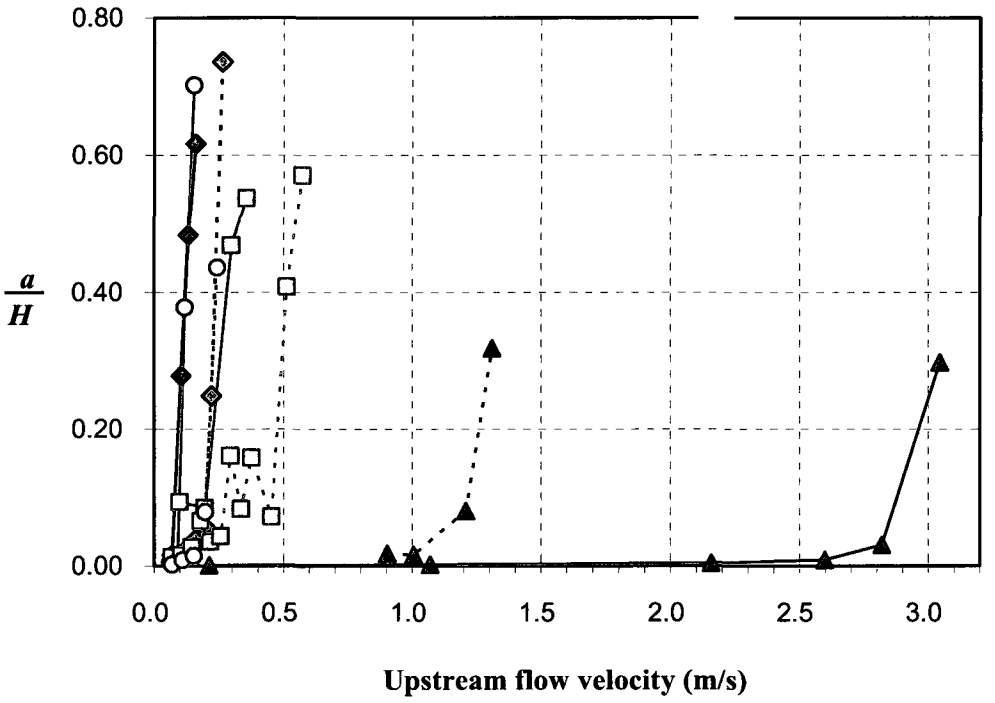

Figure 3.5 RMS amplitude of the inner cylinder as a function of flow velocity upstream of the support for different support gaps

: 0.29 mm /10° : 0.29 mm /20°

: 0.42 mm /10° : 0.42 mm /20°

: 0.67 mm /10° : 0.67 mm /20°

: 2.20 mm /10° : 2.20 mm /20°

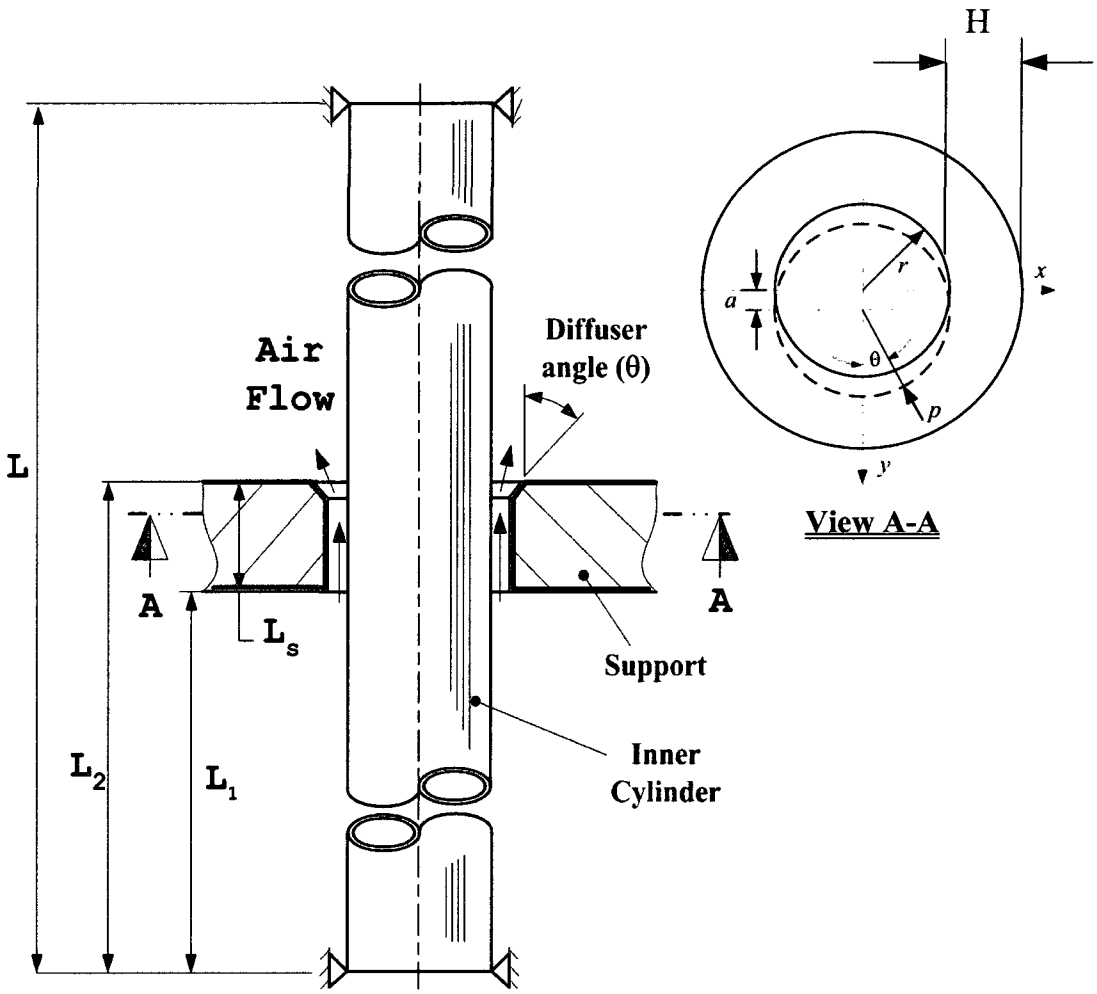

Figure 3.6 Analytical model for the inner cylinder with a finite-length gap support

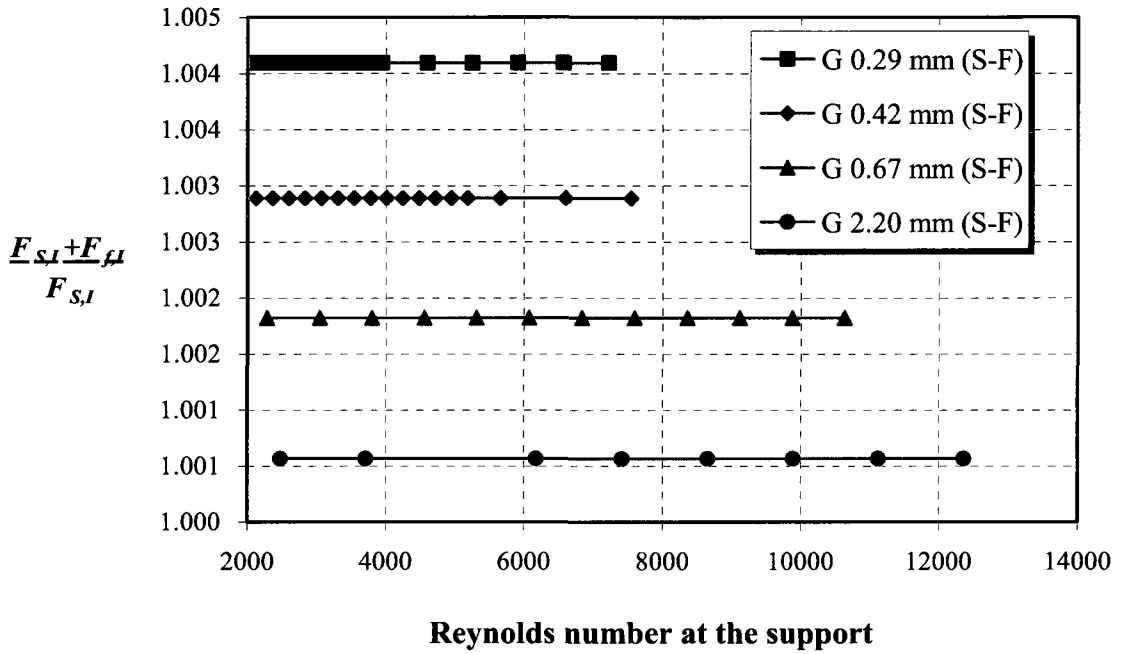

Figure 3.7 Ratio of total inertia force to structural inertia force as a function of Reynolds number at the gap. S-F: a short-lossless entrance and a free-discharge exit for the gap support. A vibration amplitude of 0.3 mm is assumed.

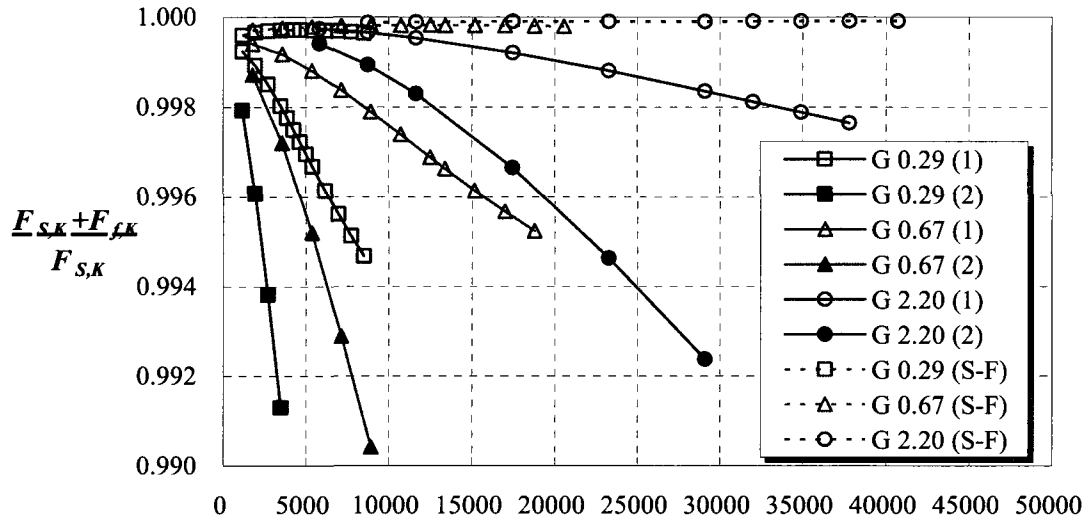

Figure 3.8 Ratio of total stiffness force to structural stiffness force as a function of Reynolds number at the gap for an amplitude of 0.3 mm at the 1st mode.

G 0.29 (1): Annular gap=0.29 mm, Ka=0.1, η=0.1, δ=0.1,

G 0.29 (2): Annular gap=0.29 mm, Ka=0.1, η=0.1, δ=0.5,

G 0.67 (1): Annular gap=0.67 mm, Ka=0.1, η=0.1, δ=0.1,

G 0.67 (2): Annular gap=0.67 mm, Ka=0.1, η=0.1, δ=0.5,

G 2.20 (1): Annular gap=2.20 mm, Ka=0.1, η=0.1, δ=0.1,

G 2.20 (2): Annular gap=2.20 mm, Ka=0.1, η=0.1, δ=0.5,

G 0.29 (S-F): Annular gap=0.29 mm, Short-lossless and free-discharge,

G 0.67 (S-F): Annular gap=0.67 mm, Short-lossless and free-discharge,

G 2.20 (S-F): Annular gap=2.20 mm, Short-lossless and free-discharge

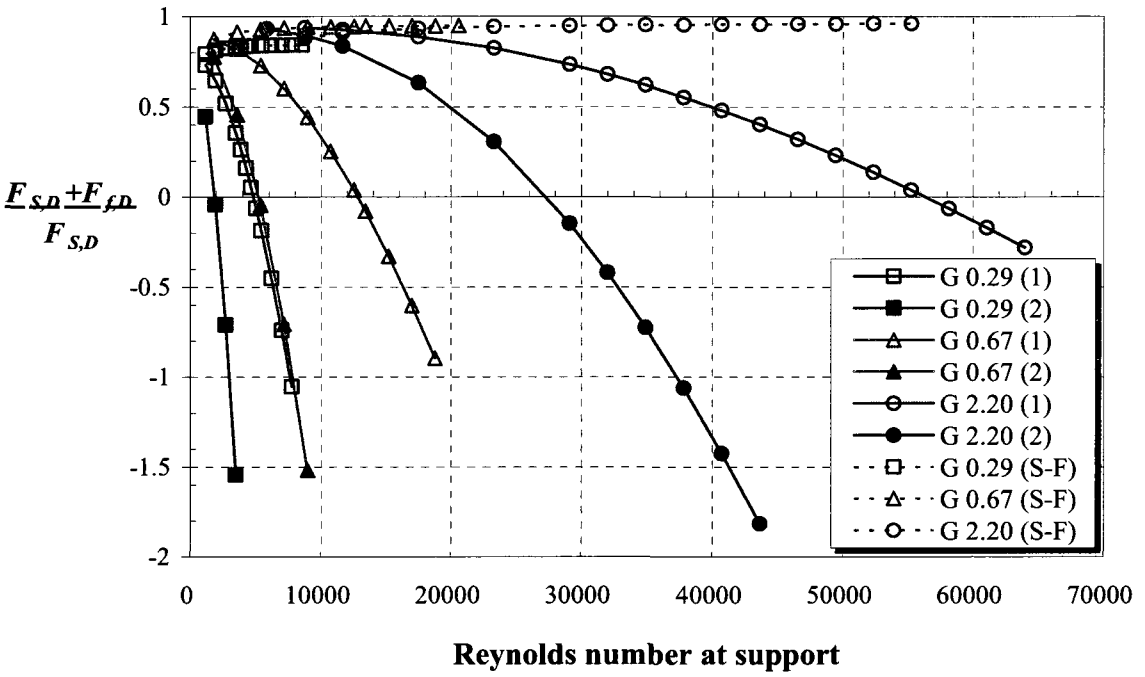

Figure 3.9 Ratio of total damping force to structural damping force as a function of Reynolds number at the gap for a structural damping factor of 0.2% and a max. amplitude of 0.3 mm in the 1st mode.

G 0.29 (1): Annular gap=0.29 mm, Ka=0.1, η=0.1, δ=0.1,

G 0.29 (2): Annular gap=0.29 mm, Ka=0.1, η=0.1, δ=0.5,

G 0.67 (1): Annular gap=0.67 mm, Ka=0.1, η=0.1, δ=0.1,

G 0.67 (2): Annular gap=0.67 mm, Ka=0.1, η=0.1, δ=0.5,

G 2.20 (1): Annular gap=2.20 mm, Ka=0.1, η=0.1, δ=0.1,

G 2.20 (2): Annular gap=2.20 mm, Ka=0.1, η=0.1, δ=0.5,

G 0.29 (S-F): Annular gap=0.29 mm, Short-lossless and free-discharge,

G 0.67 (S-F): Annular gap=0.67 mm, Short-lossless and free-discharge,

G 2.20 (S-F): Annular gap=2.20 mm, Short-lossless and free-discharge

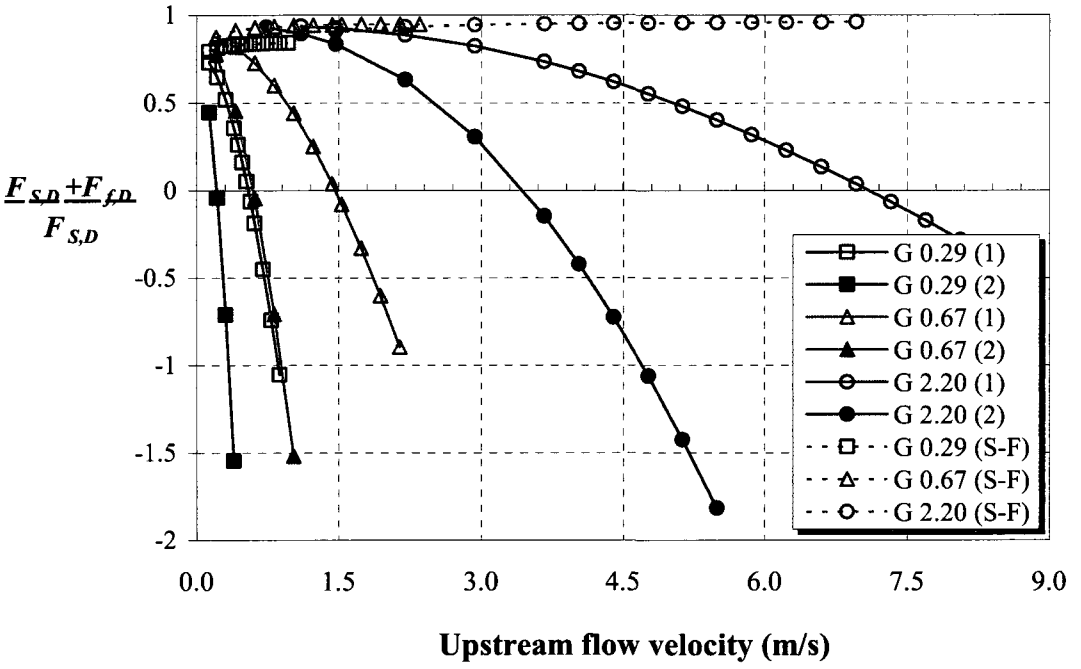

Figure 3.10 Ratio of total damping force to structural damping force as a function of upstream flow velocity for a structural damping factor of 0.2% and a max. amplitude of 0.3 mm in the 1st mode.

G 0.29 (1): Annular gap=0.29 mm, Ka=0.1, η=0.1, δ=0.1,

G 0.29 (2): Annular gap=0.29 mm, Ka=0.1, η=0.1, δ=0.5,

G 0.67 (1): Annular gap=0.67 mm, Ka=0.1, η=0.1, δ=0.1,

G 0.67 (2): Annular gap=0.67 mm, Ka=0.1, η=0.1, δ=0.5,

G 2.20 (2): Annular gap=2.20 mm, Ka=0.1, η=0.1, δ=0.5,

G 0.29 (S-F): Annular gap=0.29 mm, Short-lossless and free-discharge,

G 0.67 (S-F): Annular gap=0.67 mm, Short-lossless and free-discharge,

G 2.20 (S-F): Annular gap=2.20 mm, Short-lossless and free-discharge

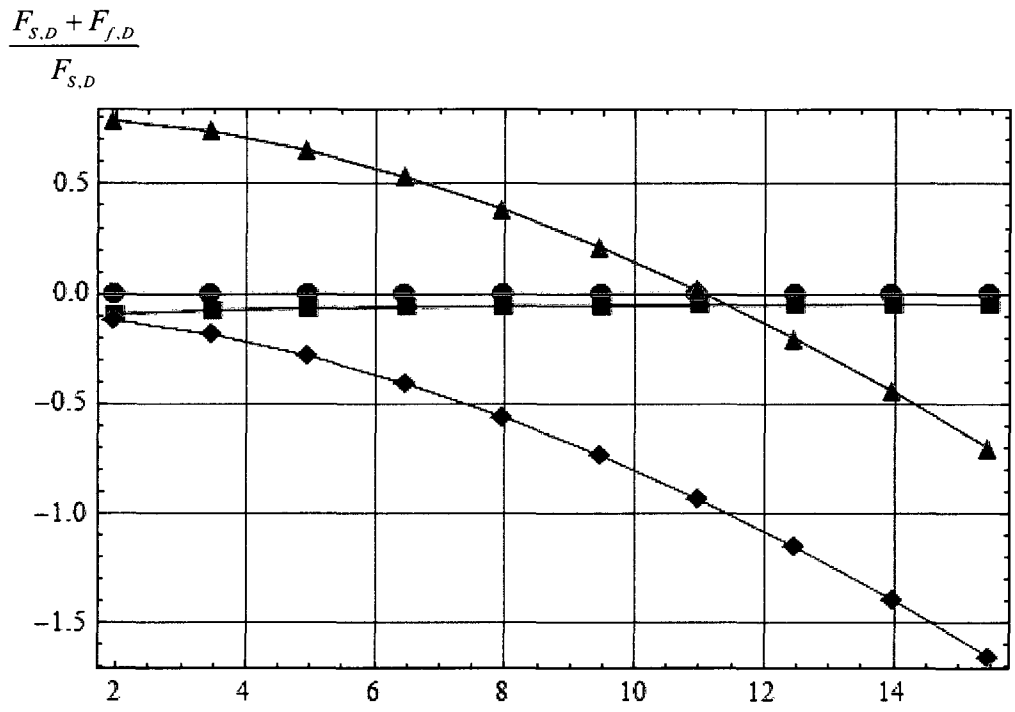

Figure 3.11 Ratio of total damping force to structural damping force with a finite-length support of 0.29 mm gap with Ka=0.1, η=0.1, δ=0.1.

- : Damping force at the entrance of the support
- : Damping force at the exit of the support
- : Damping force at mid-way along the support
- : Total damping force including the structural damping

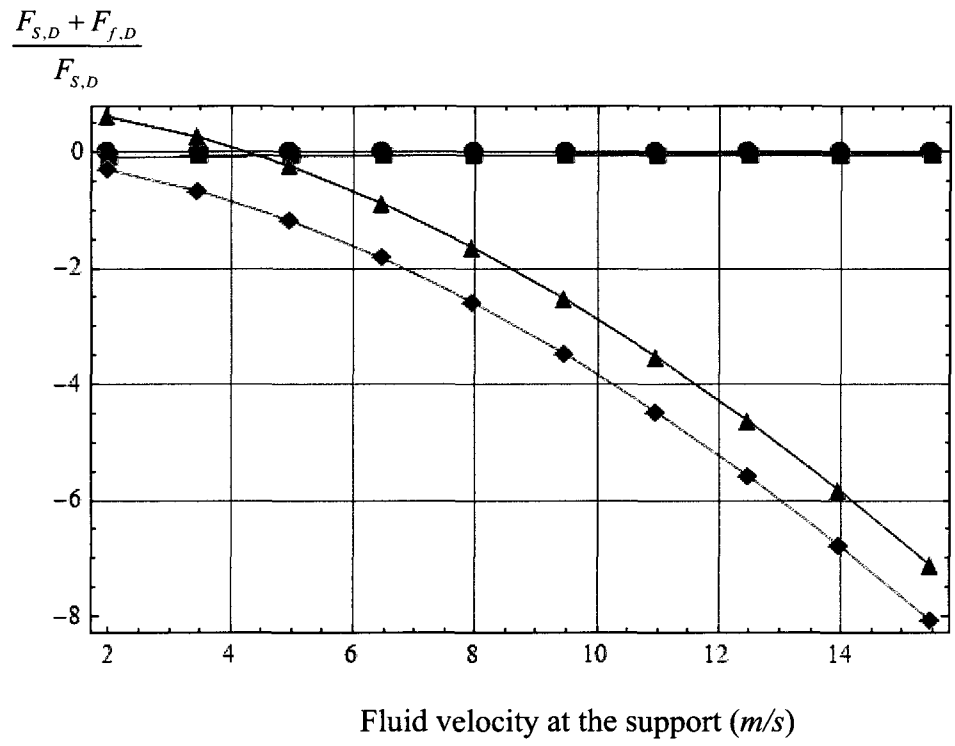

Figure 3.12 Ratio of total damping force to structural damping force with a finite-length support of 0.29 mm gap with Ka=0.1, η=0.1, δ=0.5

—■— : Damping force at the entrance of the support

—◆— : Damping force at the exit of the support

—●— : Damping force at mid-way along the support

—▲— : Total damping force including the structural damping

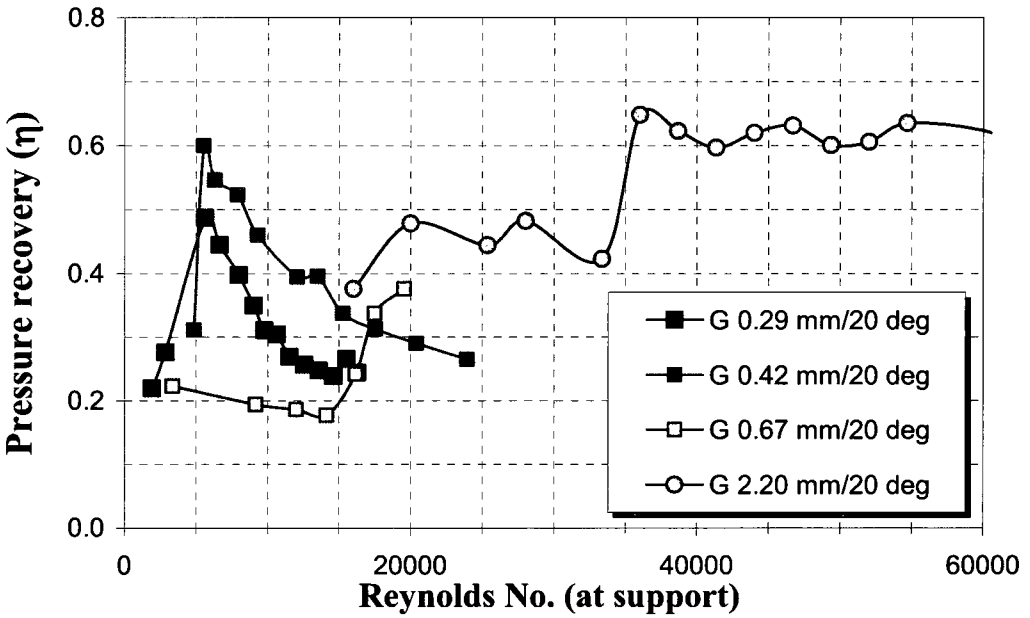

Figure 3.13 Pressure recovery measurements as functions of Reynolds number at the supports with 10 degree diffuser angle

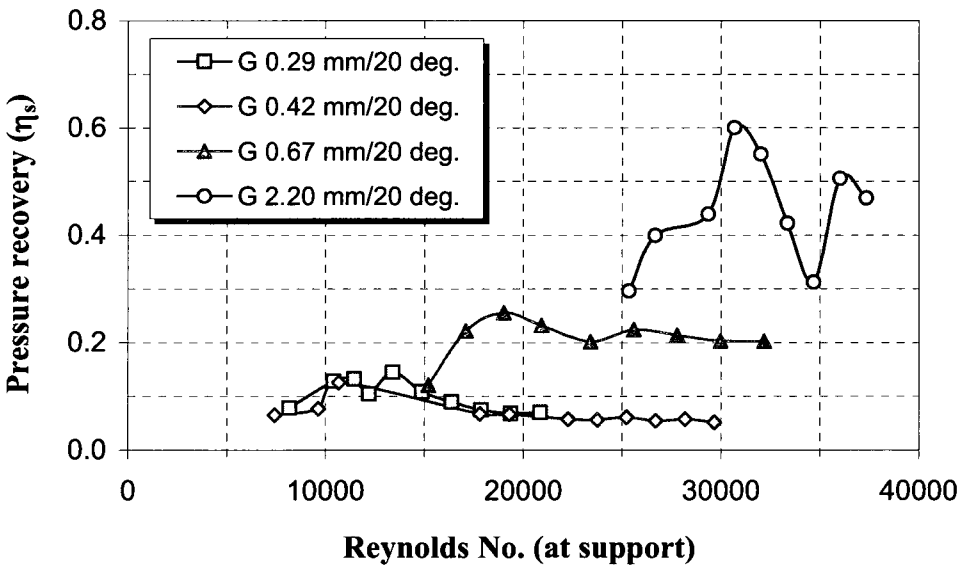

Figure 3.14 Pressure recovery measurements as functions of Reynolds number at the supports with 20 degree diffuser angle

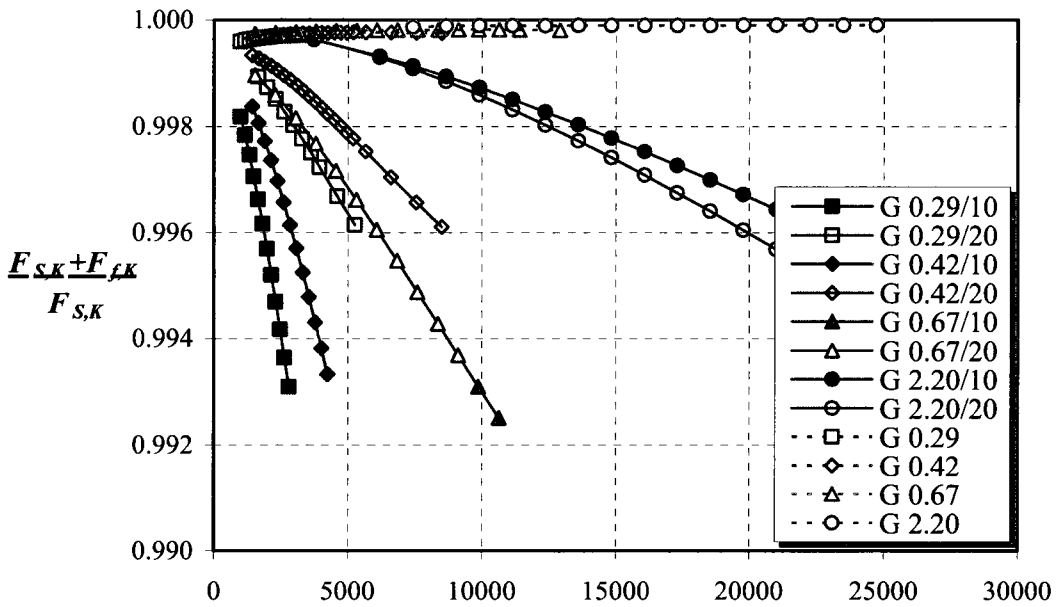

Figure 3.15 Ratio of total stiffness force to structural stiffness force as a function of Reynolds number at the gap. Dotted line and solid line correspond to a short-lossless entrance and a free-discharge exit, and a contraction-loss entrance and a diffuser exit, respectively. In the legend, G x.xx/yy represents a gap size of x.xx mm and a diffuser angle of yy deg.

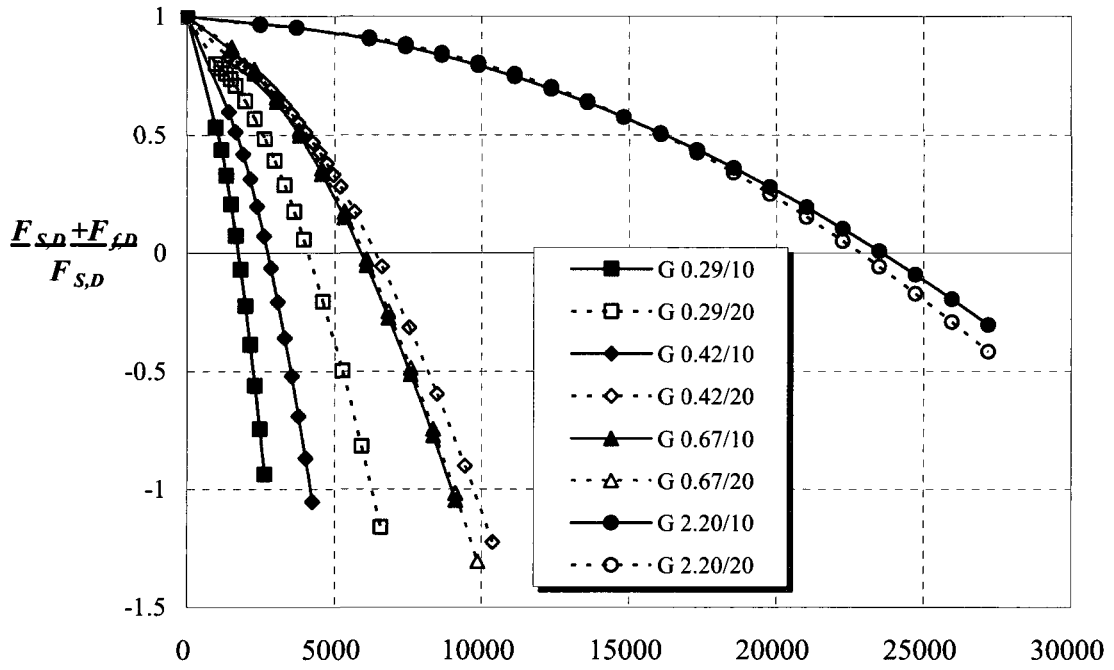

Figure 3.16 Ratio of total damping force to structural damping force as a function of Reynolds number at the gap for the contraction-loss entrance and the diffuser exit of the support. In the legend, G x.xx/yy represents for gap size of x.xx mm and a diffuser angle of yy deg.

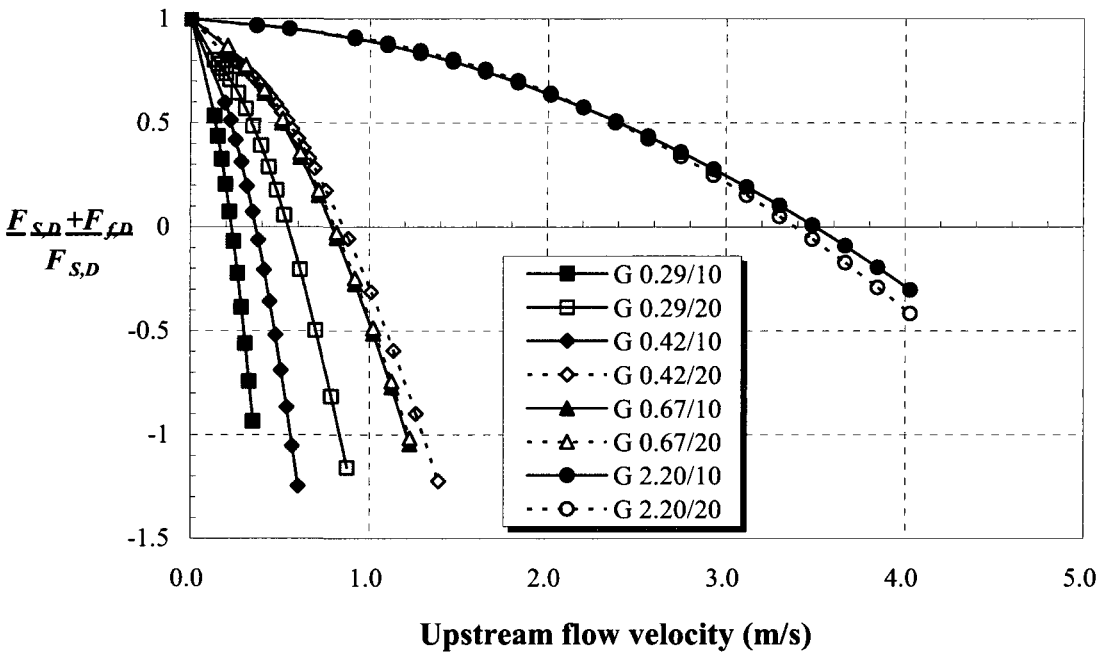

Figure 3.17 Ratio of total damping force to structural damping force as a function of upstream flow velocity for a contraction-loss entrance and a diffuser exit of the support. In the legend, G x.xx/yy represents a gap size of x.xx mm and diffuser angle of yy deg.

3.7 References

Blevins, R. D., 1990. Flow-Induced Vibration, Chapter 2.2, Van Nostrand Reinhold.

Childs, D., 1993. Turbomachinery rotodynamics, Chapter 4, John Wiley & Sons, Inc.

Fujita, K and Ito, T., 1992. Study of leakage-flow-induced vibration of an axisymmetric cylindrical rod due to axial flow, *Symposium on Flow-Induced Vibration and Noise*, ASME. PVP **244**, 33-43.

Fujita, K, Ito, T. Kawata, Y and Izumi, H., 1994. Axial leakage-flow-induced vibration of a long flexible rod with small gaps, Flow-Induced Vibration, ASME, PVP-Vol. 273, pp.133-143.

Kang, H.S, Mureithi, N.W. and Pettigrew, M, J., 2009. Analytical solution for a vibrating simply-supported cylinder subjected to 2-D concentric annular flow considering friction, (Submitted).

Hobson, D.E., 1982, Fluid-elastic instabilities caused by flow in an annulus, *Proceeding of BNES, 3rd international conference on vibration in nuclear plant*, 440-460. Keswick, U.K.

Langthjem, M. A., Morita, H. Nakamura, T. and Nakano, M., 2006, A flexible rod in annular leakage flow: Influence of turbulence and equilibrium offset, and analysis of instability mechanism, *J. of Fluids and Structures*, **22** 617-645.

Mateescu, D. and Paidoussis, M.P, 1985, The unsteady potential flow in axially variable annulus and its effect on the dynamics of oscillating rigid centre-body, *J. of Fluid Engineering*, **107**, 421-427.

Mateescu, D. and Paidoussis, M.P, 1987, Unsteady viscous effects on the annular-flow-induced instabilities of rigid cylindrical body in narrow duct, *J. of Fluids and Structures*, **1**, 197-215.

Mateescu, D., Paidoussis, M.P and Sim, W. G., 1988, Dynamics and Stability of a flexible cylinder in a narrow coaxial cylindrical duct, subjected to annular flow, *International Symposium on Flow-Induced Vibration and Noise*, ASME, Nov. 27-Dec. 2. 125-145 Chicago, Illinois.

Mulcahy, T.M., 1980, Fluid forces on rods vibrating in finite length annular regions, *J. of applied mechanics,* **47**, 234-240.

Spurr, A. and Hobson, D.E., 1984, Forces on the vibrating centerbody of an annular diffuser, *Symposium on Flow-induced Vibration*, ASME, **4**, 41-52.

Fujita, K and Ito, T., 1992, Study of leakage-flow-induced vibration of an axisymmetric cylindrical rod due to axial flow, S*ymposium on Flow-Induced Vibration and Noise*, ASME. PVP **244**, 33-43.

Yasuo, A. and Paidoussis, M. P., 1989, Flow-Induced Instability of Heat-Exchanger Tubes due to Axial flow in a Diffuser-shaped, Loose Intermediate Support, *J. of Pressure Vessel Technology*, **111**, 428-434.

CHAPTER 4

GENERAL DISCUSSION

4.1 Review of objectives

The primary purpose of this study was to obtain an analytical solution for the perturbation pressure inside of the annulus when a pinned-pinned inner cylinder is subjected to 2-D annular flow.

Comparing 1-D and 2-D annular flow models, the secondary purpose was to describe the limitations of the 1-D flow model for annular-flow-induced vibration of a continuous beam.

Thirdly, based on the analytical solution, the purpose was to investigate experimentally the finite-length diffuser-induced vibration of a cylinder in axial leakage flow, and to develop an analytical model to explain the experimental results.

Fourthly, the final goal of this study was to propose a semi-analytical model to predict the critical flow velocity for the pinned-pinned cylinder in terms of annular gap and diffuser angle of the finite-length gap support.

4.2 Contributions

Hobson's model has been extended to analyze a continuous beam subjected to a 2-D annular flow considering friction loss. The proposed friction model in Chapter 2 is capable of giving solutions for different support conditions. This study showed that the

dynamics of annular-flow-induced vibrations obtained by the pressure loss theory is almost the same as the dynamics by potential flow theory; the tube loses stability consecutively by divergence in the 1st and 2nd mode, then by the coupled-mode flutter. However, the critical flow velocity was predicted to be considerably lower.

It is shown that the one-dimensional model is limited to one-dimensional vibrations such as 1-d.o.f translational or rotational (rocking) motions which were studied by Hobson (1982), Fujita and Ito (1992 and 1994) and Porcher and de Langre (1997).

Experiments show that a pinned-pinned tube subjected to annular flow in a finite length narrow gap support first loses stability by flutter. With annular flow, the simply supported cylinder is known to lose stability by divergence at very high flow velocity. A small support at the mid length of the tube plays a significant role not only to change the dynamic behavior of the pinned-pinned rod but also to decrease the critical flow velocities down to engineering flow velocities. Generally speaking, the smaller the gap and the smaller the diffuser angle the lower the critical flow velocity.

In the theory, the negative damping force is shown to be strongly dependent on the dimensionless diffuser performance efficiency (δ), which is the ratio of diffuser efficiency to dynamic gap closure. The other important result is that the negative damping force is mostly generated at the exit of the support. From these two results, it may be concluded that expansion channels at the downstream end of the support cause flutter instability. This is in agreement with previous research findings.

A semi-analytical model for the fluidelastic damping force is proposed based on the analytical pressure solution. In the case where no losses are assumed at the entrance and the exit of the support, fluidelastic damping remains positive at all Reynolds numbers. The semi-analytical model yields results that are comparable with experiments. The smaller gap size and diffuser angle are shown to be more destabilizing.

For the pinned-pinned cylinder subjected to leakage flow in a finite-length gap support at its mid-span, the critical flow velocity with compressed air ($\rho \approx 8.5$ Kg/m^3) turns out to be less than 3 *m/s,* which is within the range of most engineering applications.

CHAPTER 5

CONCLUSION AND RECOMMENDATIONS

5.1 Conclusion

In this study, Hobson's work has been further extended to annular-flow-induced vibration of a pinned-pinned cylinder based on a two-dimensional flow model with friction. For the friction consideration, a new concept of a perturbation friction factor is introduced, which consists of a real and imaginary part. By using the proposed friction model, friction effects can be analyzed and applied for all the vibration modes. It is shown that not only the friction factor but also the perturbation pressure is strongly coupled with the mode shapes of the simply-supported cylinder.

With the proposed new friction factor, the theoretical solutions for unsteady pressure and flow velocities are easily obtained. In addition, the perturbation pressure can reasonably be represented using three terms; ω^2 related terms, ω related terms and ω independent terms. The ω independent term, the fluidelastic stiffness force, is the most dominant among the three terms, so that static-type instability may be expected.

The proposed two-dimensional flow model shows that the predicted fluid forces are significantly different from those of a one-dimensional fluid model for a pinned-pinned cylinder subjected to annular flow. It is believed that the large difference is attributable to the cylinder radius-to-length ratio and to whether or not circumferential flow is allowed. Considering that the one-dimensional flow model does not allow for fluid to be squeezed in the circumferential direction, utilization of the one-dimensional flow model is probably limited to radius-to-length ratios larger than 0.8, or to one-dimensional vibrations such as 1-d.o.f translational or rotational (rocking) motion (Hobson 1982, Fujita and Ito, 1992 and 1994, Porcher and de Langre, 1997).

The flow perturbation theory does lead to significant changes in the dynamics of the annular-flow-induced vibrations of a cylinder when compared to the confined mean flow velocity theory which does not consider perturbations. It turns out that small perturbations decrease the first dimensionless critical flow velocity down to 2.36 from 3.14 when only the mean flow is considered.

The proposed friction-based model is capable of giving solutions for different support conditions of a cylinder such as cantilevered and fixed-fixed cylinders. Also, it may further be extended to give an analytical solution to the problem of a finite-length annular gap support.

The stability behavior of a pinned-pinned flexible rod subjected to narrow annular flow over a finite-length gap support has been experimentally and analytically investigated. With the experimental approach, the critical flow velocities were measured for varying gap size and diffuser angles for a finite-length support. With the analytical approach, an analytical solution was obtained for the perturbation pressure acting on the pinned-pinned cylinder subjected to a leakage flow at a finite-length gap support. For the analytical solution, two-dimensional flow with two fluid boundary conditions was considered. The two sets of boundary conditions are, a lossless entrance and a full conversion exit for the ideal conditions, and a contraction-loss entrance and diffuser exit for practical boundary conditions.

In experiments with a 2.2 m long steel tube, a 3.8 cm long support, and a significantly small air flow, flutter instability is observed for all supports; independently of the gap size and diffuser angle. With annular flow, the simply supported cylinder is known to lose stability by divergence at very high flow velocity beyond practical engineering applications. Interestingly, a small support plays a significant role to change the dynamic behavior of the pinned-pinned rod, decreasing the critical flow velocities down

to engineering flow velocities. The critical flow velocity obtained experimentally is much lower than practical flow velocities generally encountered in power generation plants. Generally speaking, the smaller the gap and the smaller the diffuser angle the lower the critical flow velocity for negative damping. However, for the largest gap (2.20 mm), the critical flow velocity of the larger diffuser angle (20^{o}) is lower than that of the smaller diffuser angle (10^{o}).

In the theory, the negative damping force is strongly dependent on the dimensionless diffuser performance efficiency (δ), which is the ratio of diffuser efficiency to dynamic gap closure. It is also found that the negative damping force is mostly generated at the exit. From these two results, it is concluded that an expansion channel at the downstream end causes flutter instability, in agreement with previous research findings.

A semi-analytical model for the fluidelastic damping force is proposed based on the analytical pressure solution. In the case where no losses are assumed at the entrance and the exit of the support, fluidelastic damping remains positive at all times. For the experimental cases, numerical calculation by the semi-analytical model yields results that are comparable with experiments. The smaller gap size and diffuser angle are more destabilizing. However, in the case of the largest gap (2.2 mm), the bigger diffuser angle (20^{o}) generates negative damping at a lower flow velocity.

For the pinned-pinned cylinder subjected to leakage flow in a finite-length gap support at its mid length, the critical flow velocity of the compressed air ($\rho \approx 8.5$ Kg/m^3) turns out to be below 3 m/s. This falls within the range of engineering flow velocity.

5.2 Recommendations

For the annular flow problem, using the perturbation flow model, a critical flow velocity of 2.36 in dimensionless form is predicted. By the unperturbed confined axial flow

theory, a critical flow velocity of 3.14 in dimensionless form is predicted for a pinned-pinned tube. The perturbation theory developed in the thesis, therefore, needs to be verified experimentally.

The thesis has covered only a simply-supported tube. Basically, the pinned-pinned tube is a conservative system excluding friction effects, so that one may assume that dynamics of the fixed-fixed tube may not be different from the pinned-pinned tube. What about a cantilevered tube? It is known that the cantilevered tube has interesting dynamic behavior. To obtain analytically the single mode flutter, the perturbation assumption is unnecessary. If the critical flow velocity is reduced, however, the dynamics of the cantilevered tube become possibly more complex and more interesting.

The thesis used the experimental model of Shimoyama and Yamada (1937) for the friction model. However, Shimoyama and Yamada obtained the experimental data from a fixed annulus. No vibration of the inner tube was considered. When the inner tube is vibrating, friction loss in a finite-length support could be different. The following graph, Figure 4.1, was recently obtained by the author for friction loss as functions of Reynolds numbers. The same notations as in Figure 3.15 are used. As shown in Figure 4.1, the measured friction loss is not exactly coincident with Shimoyama and Yamada's model prediction. Annular-flow-induced vibration, therefore, still needs many clarifications by flow measurements.

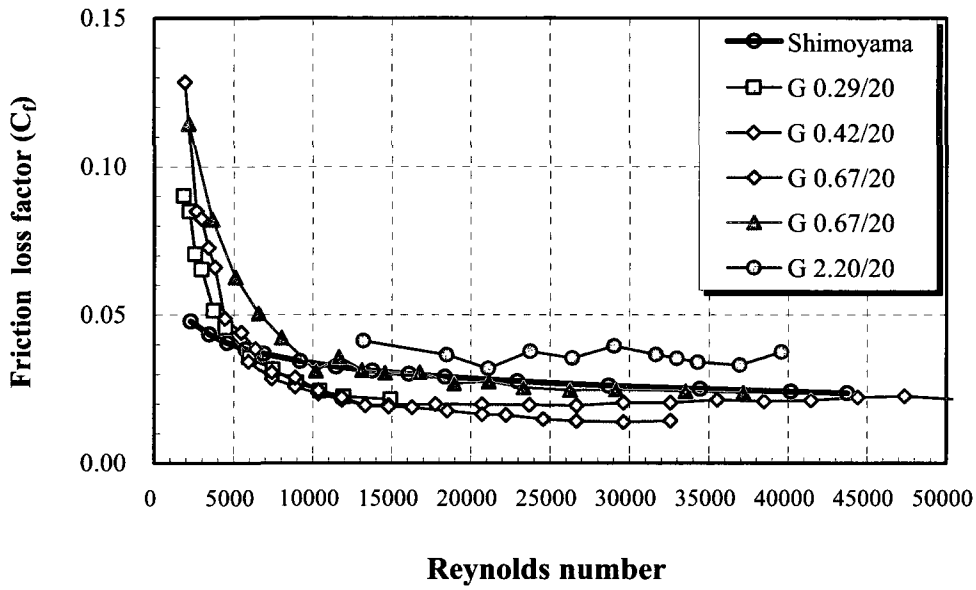

Figure 5.1 Friction loss factor for annular gap as a function of Reynolds number
(The notation of Figure 3.15 is used here)

REFERENCES

Fujita, K and Ito, T., 1992. Study of leakage-flow-induced vibration of an axisymmetric cylindrical rod due to axial flow, Symposium on Flow-Induced Vibration and Noise, ASME. PVP-Vol. 244, pp.33-43.

Fujita, K, Ito, T. Kawata, Y and Izumi, H., 1994. Axial leakage-flow-induced vibration of a long flexible rod with small gaps, Flow-Induced Vibration, ASME, PVP-Vol. 273, pp.133-143.

Fujita, K and Shintani, A, 2001. Axial leakage-flow-induced vibration of the elastic rod as the axisymmetric continuous flexible beam. Journal of Pressure Vessel Technology 123, 421-428.

Fujita, K., Morikazu, H. and Shintani, A., 2004. Dynamic behavior of pre- and post instability of an axisymmetric elastic beam subjected to axial leakage flow, International conference on Flow-induced vibration, Ecole Polytechnique, Paris, July 6-9.

Gorman, D. J., Goden, J.L. and Planchard, J., 1987. Analytical and Experimental Study of the Vibratory Response of a Flexible Tube Subjected External Annular Flow, Part way along its Length, Proceedings of International Conference on Flow-Induced Vibrations, ed., R. King, Bowness-on-Windermere, U.K., 1987, pp. 339-347.

Hobson, D.E., 1982. Fluid-elastic instabilities caused by flow in an annulus, pp. 440-460, Proceeding of BNES, 3rd international conference on vibration in nuclear plant, Keswick, U.K , pp. 440-460.

Hobson, D.E. and Jedwab, M., 1988. Investigation of the effect of eccentricity on the unsteady fluid forces on the centerbody of an annular diffuser, J. of Fluid and Structures 4, pp. 155-169.

Inada,F and Hayama,S, 1988. A study on leakage-flow-induced vibrations (fluid dynamic force acting on the walls of a one dimensional, narrow passage), JSME International Journal, Series III,31, pp.39-47.

Inada,F and Hayama,S, 1990. A study on leakage-flow-induced vibrations. Part 1. Fluid dynamic forces and moments acting on the walls of a narrow tapered passage, J. of Fluids and Structures 4, pp. 395-412.

Inada,F and Hayama,S, 1990. A study on leakage-flow-induced vibrations. Part 2. Stability analysis and experiments for two-degree-of-freedom systems combining translational and rotational motions, J. of Fluids and Structures 4, pp. 413-428.

Inada,F and Hayama,S,, 2000. Mechanisms of leakage-flow-induced vibrations-Single-degree-of -freedom and continuous systems, In Flow Induced Vibration (eds S. Ziada & T. Staubli), Rotterdam, pp.837-844.

Inada, F., 2004. Mechanism of leakage-flow-induced vibrations of continuous system, International conference on Flow-induced vibration, Ecole Polytechnique, Paris, July 6-9 2004.

Langthjem, M. A., Morita, H. Nakamura, T. and Nakano, M., 2006. A flexible rod in annular leakage flow: Influence of turbulence and equilibrium offset, and analysis of instability mechanism, J. of Fluids and Structures, 22 617-645.

Li,D.-W., Kaneko, S., Hayama, S., 2002. A study on annular leakage-flow-induced vibrations. Journal of Fluids and Structures 16, 909 – 930.

Mateescu, D. and Paidoussis, M.P, 1985. The unsteady potential flow in axially variable annulus and its effect on the dynamics of oscillating rigid centre-body, J. of Fluid Engineering, Vol. 107, pp 421-427.

Mateescu, D. and Paidoussis, M.P, 1987. Unsteady viscous effects on the annular-flow-induced instabilities of rigid cylindrical body in narrow duct, J. of Fluids and Structures, Vol. 1, pp. 197-215.

Mateescu, D., Paidoussis, M.P and Sim, W. G., 1988. Dynamics and Stability if a flexible cylinder in a narrow coaxial cylindrical duct, subjected to annular flow, International Symposium on Flow-Induced Vibration and Noise, ASME, Chicago, Illinois, Nov. 27-Dec. 2. pp.125-145.

Mateescu, D., Paidoussis, M.P and Sim, W. G., 1994, Spectral solutions for unsteady annular flows between eccentric cylinders induced by transverse oscillations, J. Sound and Vibration, 177(5), pp. 635-649.

Mulcahy, T.M., 1980. Fluid forces on rods vibrating in finite length annular regions, J. of Applied Mechanics vol.47, pp.234-240.

Mulcahy, T.M., 1984. Leakage-flow-induced vibrations of a tube -in-tube slip joint, Symposium on the flow-induced vibrations, ASME Winter Annual Meeting, New Orleans, Louisiana, pp. 15-24.

Mulcahy, T.M., 1988. One-dimensional leakage-flow vibration instabilities, J. of Fluids and Structures, 2, pp.383-403.

Nagakura, H and Kaneko, S, 1993. Stability of a cantilever beam subjected to one-dimensional leakage flow, Proceedings Asian-Pacific Conference, Kitakyushu, Japan, Vol. 1, pp. 248-253.

Paidoussis, M. P., 1966. Vibrations of cylinders with supported ends, induced by axial flow, Proceedings Institution of Mechanical Engineers,180, pp. 268-278.

Paidoussis, M. P., 1973. Dynamics of cylindrical structures subjected to axial flow, J. of Sound and Vibration, 29, pp. 365-385.

Paidoussis and Issid, N.T., 1974. Dynamic stability of pipes conveying fluid, J. of Sound and Vibration, 33, pp.267-269.

Paidoussis, M. P., 1974. The Dynamical Behavior of Cylindrical Structure in Axial Flow, Annals of Nuclear Science and Engineering, Vol. 1, pp. 83-106.

Paidoussis, M. P., 1974. Vibration of Cylindrical Structures Induced by Axial Flow, Trans. of the ASME J. of Engineering for Industry, Vol. 96, pp. 547-552.

Paidoussis, M.P and Pettigrew, M.J., 1979. Dynamics of flexible cylinders in axisymmetrically confined axial flow, J. of Applied Mechanics vol.46, pp.37-44.

Paidoussis, M .P., 2004. Fluid-structure interactions: Slender structures and axial flow, Elsevier Academic Press, Vol.2, pp.787.

Parkin, M.W. and P.C. Watson, 1984. Reduction of Vibration caused by flow in an annular diffuser, Symposium on the flow-induced vibrations, ASME Winter Annual Meeting, New Orleans, Louisiana, pp. 1-14.

Porcher, G., de Langre, E., 1997. A friction-based model for fluidelastic forces induced by axial flow. In: M.P. Païdoussis, et al. (Eds.), Proceedings 4th Int'l Symposium on Fluid–Structure Interactions, Aeroelasticity, Flow-Induced Vibration and Noise, Vol. II, AD-Vol. 53-2. ASME, New York, pp. 67–74.

Sakuma, Y., Paidoussis, M.P. and Price, S.J. 2008a. Dynamics of trains and train-like articulated systems travelling in confined fluid-Part1: Modeling and basic dynamics, 24, pp. 932-953.

Sakuma, Y., Paidoussis, M.P. and Price, S.J. 2008b. Dynamics of trains and train-like articulated systems travelling in confined fluid-Part1: Wave propagation and flow-excited vibration, 24, pp. 954-976.

Shimoyama, Y, Yamada, Y., 1957. Experiments on the labyrinth packing (1st report). Transactions of Japan Society of Mechanical Engineers, Part 3 23, 44-49 (in Japanese).

Sim, W. G., 1987, Stability of a flexible cylinder in axisymmetrically confined flow, Master Thesis of Master of Engineering, McGill University.

Spur, A. and Hobson, D.E., 1984. Forces on the vibrating centerbody of an annular diffuser, Symposium on Flow-induced Vibration, ASME, Vol. 4, pp. 41-52.

Tanaka, S., Hirata, T., Kaneko, S. and Watanabe, T., 2001. Aerodynamic vibration of combined rigid bodies due to leakage-flow, In Flow-Induced Vibration-2001 (ed. Pettigrew, M.J.), PVP-Vol. 420-2, pp.45-52.

White, Frank M., 2003. Fluid Mechanics, 5th Ed. Chapter 6, McGraw-Hill.

Wu, X., Kaneko. S., 2005. linear and nonlinear analyses of sheet flutter induced by leakage flow, Journal of Fluids and Structures, 20, 927-948.

Yasuo, A. and Paidoussis, M. P., 1989. Flow-Induced Instability of Heat-Exchanger Tubes due to Axial flow in a Diffuser-shaped, Loose Intermediate Support, J. of Pressure Vessel Technology, 111, pp.428-434.

APPENDICES

APPENDIX I: Linearization of fluid equations

The non-linear fluid equations in the (x, θ) plane may be written as follows (Hobson, 1982):

Continuity equation:

$$\frac{\partial}{\partial x}\left(\overline{h}\,\overline{u}\right)+\frac{1}{r}\frac{\partial}{\partial \theta}\left(\overline{h}\,\overline{v}\right)+\frac{\partial \overline{h}}{\partial t}=0 \tag{I-1}$$

x-Momentum:

$$\rho\frac{\partial}{\partial t}\left(\overline{h}\,\overline{u}\right)+\frac{\partial}{\partial x}\left[\overline{h}\left(\overline{p}+\rho\overline{u}^{2}\right)\right]+\frac{\rho}{r}\frac{\partial}{\partial \theta}\left(\overline{h}\,\overline{u}\,\overline{v}\right)-\overline{p}\frac{\partial \overline{h}}{\partial x}+\tau_{x}=0 \tag{I-2}$$

θ-Momentum:

$$\rho\frac{\partial}{\partial t}\left(\overline{h}\,\overline{v}\right)+\rho\frac{\partial}{\partial x}\left(\overline{h}\,\overline{u}\,\overline{v}\right)+\frac{1}{r}\frac{\partial}{\partial \theta}\left[\overline{h}\left(\overline{p}+\rho\overline{v}^{2}\right)\right]-\frac{\overline{p}}{r}\frac{\partial \overline{h}}{\partial \theta}+\tau_{\theta}=0 \tag{I-3}$$

These equations can be linearized by assuming that $\overline{h}$, $\overline{p}$, $\overline{u}$ and $\overline{v}$ may be expressed as the sum of a steady component and a small perturbation component as follows:

$$\overline{h}=H+h(x,\theta,t) \tag{I-4}$$

$$\overline{p}=P+p(x,\theta,t) \tag{I-5}$$

$$\overline{u}=U+u(x,\theta,t) \tag{I-6}$$

$$\overline{v} = \quad + \mathrm{v}(x,\theta,t) \tag{I-7}$$

Equation (I-7) reflects the fact that there is no mean circumferential flow velocity.

Substituting equations (I-4) ~ (I-7) into equation (I-1) and retaining only the first order terms gives

$$\frac{\partial}{\partial x}(Uh+Hu)+\frac{1}{r}\frac{\partial}{\partial\theta}(Hv)+\frac{\partial}{\partial t}(h)=0 \tag{I-8}$$

Since the steady components are independent of x and θ, equation (I-8) simplifies to

$$\frac{\partial u}{\partial x}+\frac{1}{r}\frac{\partial v}{\partial\theta}=-\frac{U}{H}\frac{\partial h}{\partial x}-\frac{1}{H}\frac{\partial h}{\partial t} \tag{I-9}$$

Similarly, substituting equations (I-4) ~ (I-7) into equations (I-2) and (I-3) and keeping only the first order terms gives

$$\rho\frac{\partial}{\partial t}(Hu+Uh)+\frac{\partial}{\partial x}\left(Hp+\rho U^2h+2U\rho Hu\right)+\frac{\rho}{r}\frac{\partial}{\partial\theta}(HUv)=0 \tag{I-10}$$

$$\rho\frac{\partial}{\partial t}(H\,v)+\rho\frac{\partial}{\partial x}(HU\overline{v})+\frac{1}{r}\frac{\partial}{\partial\theta}(Hp+Ph+..)-\frac{P}{r}\frac{\partial h}{\partial\theta}+\tau_\theta=0 \tag{I-11}$$

Simplifying and rearranging, the following form of the first order x-momentum and θ-momentum equations is obtained.

$$\frac{\partial p}{\partial x}+\rho\frac{\partial u}{\partial t}+\frac{\rho}{r}U\frac{\partial v}{\partial\theta}+2U\rho\frac{\partial u}{\partial x}+\frac{\tau_x}{H}=-\frac{\rho U}{H}\frac{\partial h}{\partial t}-\frac{\rho U^2}{H}\frac{\partial h}{\partial x} \tag{I-12}$$

$$\frac{1}{r}\frac{\partial p}{\partial \theta}+\rho\frac{\partial v}{\partial t}+\rho U\frac{\partial v}{\partial x}+\frac{\tau_\theta}{H}=0 \qquad \text{(I-13)}$$

Equations (I-9), (I-12) and (I-13) correspond to equations (2-2), (2-3) and (2-4), respectively, in Chapter 2.

APPENDIX II: The first order fluid boundary conditions for a diffuser exit

Considering diffuser efficiency $\bar{\eta}$ at the exit, Bernoulli's equation relating the pressure at locations just before and after the exit is

$$\frac{\bar{p}_{out} - \bar{p}_{in}}{\rho \bar{u}^2 / 2} = \bar{\eta} \tag{II-1}$$

Expressing the pressure, velocity and diffuser efficiency in terms of steady and perturbation components (with $\bar{\eta} = \eta_s + \eta_p(x, \theta, t)$), one obtains

$$(P_{in} + p_{in}) + (\eta_s + \eta_p) \cdot \frac{\rho}{2}(U^2 + 2Uu) = P_{out} \tag{II-2}$$

$P_{out} = \bar{p}_{out}$ is based on the reasonable assumption that there is no perturbation past the exit. Equation (II-2) can be separated into the following equations: one for the steady terms, and the other for the perturbation terms

$$\frac{P_{out} - P_{in}}{\rho U^2 / 2} = \eta_s \tag{II-3}$$

$$p_{in} + \eta_s \rho U u + \eta_p \frac{\rho}{2} U^2 = 0 \tag{II-4}$$

Assuming that the perturbation recovery coefficient η_p is a function of $h(x)$, one can write (Hobson, 1982)

$$\eta_p = \frac{\Delta\eta_s}{\Delta h} \cdot h \tag{II-5}$$

Defining the dimensionless diffuser performance coefficient δ as follows:

$$\delta = \frac{\Delta\eta_s}{\Delta h / H} \tag{II-6a}$$

the following convenient expression for η_p is obtained:

$$\eta_p = \frac{h}{H} \cdot \delta \tag{II-6b}$$

Then, substituting into equation (II-4), considering the exit location, one obtains

$$p(L) + \eta_s \rho U u(L) + \delta \frac{\rho}{2H} U^2 h(L) = 0 \tag{II-7}$$

Similarly, when the diffuser exists at the entrance, *x=0,* the following equation can be obtained:

$$p(0) + \eta_s \rho U u(0) + \delta \frac{\rho}{2H} U^2 h(0) = 0 \tag{II-8}$$

Appendix III: Childs' procedures (Childs, 1993)

We start with equations (2-11) ~ (2-12c) without friction consideration.

$$h(x,\theta,t) = Y(x,t)cos\theta + Z(x,t)sin\theta \tag{2-11}$$

$$u(x,\theta,t) = u_{1c}(x,t)cos\theta + u_{1s}(x,t)sin\theta \tag{2-12a}$$

$$v(x,\theta,t) = v_{1c}(x,t)cos\theta + v_{1s}(x,t)sin\theta \tag{2-12b}$$

$$p(x,\theta,t) = p_{1c}(x,t)cos\theta + p_{1s}(x,t)sin\theta \tag{2-12c}$$

Substituting the five equations into equation (2-2) gives

$$\begin{aligned}&\frac{\partial u_{1c}}{\partial x}\cos\theta + \frac{\partial u_{1s}}{\partial x}\sin\theta + \frac{1}{r}\frac{\partial}{\partial\theta}\left(v_{1c}cos\theta + v_{1s}\sin\theta\right)\\ &= -\frac{U}{H}\frac{\partial Y}{\partial x}\cos\theta - \frac{U}{H}\frac{\partial Z}{\partial x}\sin\theta - \frac{1}{H}\frac{\partial Y}{\partial t}\cos\theta - \frac{1}{H}\frac{\partial Y}{\partial t}\sin\theta\end{aligned} \tag{III-1}$$

Similarly, equation (2-3) and (2-4) yield

$$\begin{aligned}&\rho\frac{\partial u_{1c}}{\partial t}\cos\theta + \rho\frac{\partial u_{1s}}{\partial t}\sin\theta + \frac{\partial p_{1c}}{\partial x}\cos\theta + \frac{\partial p_{1s}}{\partial x}\sin\theta + 2U\rho\frac{\partial u_{1c}}{\partial x}\cos\theta\\ &+2U\rho\frac{\partial u_{1s}}{\partial x}\sin\theta + \frac{\rho}{r}U\frac{\partial}{\partial\theta}\left(v_{1c}cos\theta + v_{1s}\sin\theta\right)\\ &= -\frac{\rho U}{H}\frac{\partial Y}{\partial t}\cos\theta - \frac{\rho U}{H}\frac{\partial Y}{\partial t}\sin\theta - \frac{\rho U^2}{H}\frac{\partial Z}{\partial x}\cos\theta - \frac{\rho U^2}{H} - \frac{U}{H}\frac{\partial Z}{\partial x}\sin\theta\end{aligned} \tag{III-2}$$

$$\rho\frac{\partial}{\partial t}\left(v_{1c}\cos\theta+v_{1s}\sin\theta\right)+\rho U\frac{\partial}{\partial x}\left(v_{1c}\cos\theta+v_{1s}\sin\theta\right)$$
$$+\frac{1}{r}\frac{\partial}{\partial\theta}\left(p_{1c}\cos\theta+p_{1s}\sin\theta\right)=0 \qquad \text{(III-3)}$$

Equation (III-1) can be separated into two equations.

$$\frac{\partial u_{1c}}{\partial x}\cos\theta+\frac{1}{r}\frac{\partial}{\partial\theta}\left(v_{1s}cos\theta\right)=-\frac{U}{H}\frac{\partial Y}{\partial x}\cos\theta-\frac{1}{H}\frac{\partial Y}{\partial t}\cos\theta \qquad \text{(III-4)}$$

$$\frac{\partial u_{1s}}{\partial x}\sin\theta-\frac{1}{r}\frac{\partial}{\partial\theta}\left(v_{1c}\sin\theta\right)=-\frac{U}{H}\frac{\partial Z}{\partial x}\sin\theta-\frac{1}{H}\frac{\partial Y}{\partial t}\sin\theta \qquad \text{(III-5)}$$

Eliminating $\cos\theta$ and $\sin\theta$ from these equations, multiplying (III-5) by 'i' and adding the result to (III-4) yields

$$\frac{\partial}{\partial x}\left(u_{1c}+iu_{1s}\right)+\frac{1}{r}\frac{\partial}{\partial\theta}\left(v_{1s}-iv_{1c}\right)=-\frac{U}{H}\frac{\partial}{\partial x}\left(Y+iZ\right)-\frac{1}{H}\frac{\partial}{\partial t}\left(Y+iZ\right) \qquad \text{(III-6)}$$

Next we define the following four complex variables

$$h=Y+iZ \qquad \text{(III-7)}$$
$$u=u_{1c}+iu_{1s} \qquad \text{(III-8)}$$
$$v=v_{1c}+iv_{1s} \qquad \text{(III-9)}$$
$$p=p_{1c}+ip_{1s} \qquad \text{(III-10)}$$

Using equations (III-7) ~ (III-9) and employing complex variable properties, equation (III-6) reduces to the form

$$\frac{\partial u}{\partial x} - i\frac{1}{r}v = -\frac{U}{H}\frac{\partial h}{\partial x} - \frac{1}{H}\frac{\partial h}{\partial t} \tag{III-11}$$

By using the same procedure, equations (III-2) and (III-3) become

$$\frac{\partial p}{\partial x} + \rho\frac{\partial u}{\partial t} - i\rho\frac{U}{r}v + 2\rho U\frac{\partial u}{\partial x} = -\rho\frac{U}{H}\frac{\partial h}{\partial t} - \rho\frac{U^2}{H}\frac{\partial h}{\partial x} \tag{III-12}$$

$$-i\frac{1}{r}p + \rho\frac{\partial v}{\partial t} + \rho U\frac{\partial v}{\partial x} = 0 \tag{III-13}$$

Appendix IV: Solution for a short-lossless entrance and a full-discharge exit fluid boundary conditions

Analytical solutions consist of homogeneous solutions, which can be obtained by setting the right hand side to zero, and adding the particular solutions. For the pinned-pinned cylinder, knowing that the eigenfunction is a sine function, the solutions may be expressed as

$$h(x,t) = a\,sin\left(\frac{m\pi}{L}x\right)e^{i\omega t} \tag{IV-1}$$

$$u(x,t) = \sum_{j=1}^{3}\overline{u}_j \cdot e^{\Lambda_j x}\cdot e^{i\omega t} + \left(u_s \cdot h + u_c \cdot \frac{dh}{dx}\right)\cdot e^{i\omega t} \tag{IV-2}$$

$$p(x,t) = \sum_{j=1}^{3}\overline{p}_j \cdot e^{\Lambda_j x}\cdot e^{i\omega t} + \left(p_s \cdot h + p_c \cdot \frac{dh}{dx}\right)\cdot e^{i\omega t} \tag{IV-3}$$

$$v(x,t) = \sum_{j=1}^{3}\overline{v}_j \cdot e^{\Lambda_j x}\cdot e^{i\omega t} + \left(v_s \cdot h + v_c \cdot \frac{dh}{dx}\right)\cdot e^{i\omega t} \tag{IV-4}$$

Substituting the assumed solutions above into the equations (III-11) ~ (III-13), in Appendix III, one obtains the following equations.

$$\begin{aligned}&\Lambda_j \cdot \sum_{j=1}^{3}\overline{u}_j \cdot e^{\Lambda_j x}\cdot e^{i\omega t} + \left(u_s \cdot \frac{dh}{dx} + u_c \cdot \frac{d^2h}{dx^2}\right)\cdot e^{i\omega t} \\ &-\frac{i}{r}\left[\sum_{j=1}^{3}\overline{v}_j \cdot e^{\Lambda_j x}\cdot e^{i\omega t} + \left(v_s \cdot h + v_c \cdot \frac{dh}{dx}\right)\cdot e^{i\omega t}\right] = -\frac{U}{H}\frac{dh}{dx}\cdot e^{i\omega t} - \frac{i\omega}{H}h\cdot e^{i\omega t}\end{aligned} \tag{IV-5}$$

$$\Lambda_j \cdot \sum_{j=1}^{3} \overline{p}_j \cdot e^{\Lambda_j x} \cdot e^{i\omega t} + \left(p_s \cdot \frac{dh}{dx} + p_c \cdot \frac{d^2 h}{dx^2} \right) \cdot e^{i\omega t}$$
$$+\rho \left[i\omega \cdot \sum_{j=1}^{3} \overline{u}_j \cdot e^{\Lambda_j x} \cdot e^{i\omega t} + i\omega \cdot \left(u_s \cdot h + u_c \cdot \frac{dh}{dx} \right) \cdot e^{i\omega t} \right]$$
$$-i\rho \frac{U}{r} \left[\sum_{j=1}^{3} \overline{v}_j \cdot e^{\Lambda_j x} \cdot e^{i\omega t} + \left(v_s \cdot h + v_c \cdot \frac{dh}{dx} \right) \cdot e^{i\omega t} \right]$$
$$+2\rho U \left[\Lambda_j \cdot \sum_{j=1}^{3} \overline{u}_j \cdot e^{\Lambda_j x} \cdot e^{i\omega t} + \left(u_s \cdot \frac{dh}{dx} + u_c \cdot \frac{d^2 h}{dx^2} \right) \cdot e^{i\omega t} \right] \qquad \text{(IV-6)}$$
$$+i\omega\rho \frac{U}{H} h \cdot e^{i\omega t} + \rho \frac{U^2}{H} \frac{\partial h}{\partial x} \cdot e^{i\omega t} = 0$$

$$-i\frac{1}{r} \left[\sum_{j=1}^{3} \overline{p}_j \cdot e^{\Lambda_j x} \cdot e^{i\omega t} + \left(p_s \cdot h + p_c \cdot \frac{dh}{dx} \right) \cdot e^{i\omega t} \right]$$
$$+i\omega\rho \left[\sum_{j=1}^{3} \overline{v}_j \cdot e^{\Lambda_j x} \cdot e^{i\omega t} + \left(v_s \cdot h + v_c \cdot \frac{dh}{dx} \right) \cdot e^{i\omega t} \right] \qquad \text{(IV-7)}$$
$$+\rho U \left[\Lambda_j \cdot \sum_{j=1}^{3} \overline{v}_j \cdot e^{\Lambda_j x} \cdot e^{i\omega t} + \left(v_s \cdot \frac{dh}{dx} + v_c \cdot \frac{d^2 h}{dx^2} \right) \cdot e^{i\omega t} \right] = 0$$

In equations (IV-5) ~ (IV-7), separating purely fluid-related terms (the homogeneous parts of each solution) and the terms in parenthesis (the particular solution components), setting each separately to zero and canceling out common terms, one can obtain the following equations,

$$\begin{bmatrix} \Lambda_j & 0 & -i\frac{1}{r} \\ \rho\left(i\omega + 2U\Lambda_j\right) & \Lambda_j & -i\frac{\rho U}{r} \\ 0 & -i\frac{1}{r} & \rho(i\omega + U\Lambda_j) \end{bmatrix} \begin{Bmatrix} \overline{u}_j \\ \overline{p}_j \\ \overline{v}_j \end{Bmatrix} = 0 \qquad \text{(IV-8)}$$

$$\frac{(Ur + Hru_s - iHv_c)}{Hr}\frac{dh}{dx} + \frac{\left(-iHv_s - Hr\lambda_m{}^2 u_c + ir\omega\right)}{Hr}h = 0 \tag{IV-9}$$

$$\frac{r\rho U^2 + H\left(p_s r + 2r\rho U u_s - i\rho U v_c + i r\rho\omega u_c\right)}{Hr}\frac{dh}{dx} - \frac{H\left[r\lambda_m{}^2\left(p_c + 2\rho U u_c\right) + i\rho\left(Uv_s - r\omega u_s\right)\right] - ir\rho\omega U}{Hr}h = 0 \tag{IV-10}$$

$$\frac{-ip_c + \rho r\left(i\omega v_c + Uv_s\right)}{r}\cdot\frac{dh}{dx} + \frac{-ip_s + \rho r\left(i\omega v_s - \lambda_m{}^2 U v_c\right)}{r}\cdot h = 0 \tag{IV-11}$$

In equation (IV-8), to have nontrivial solutions, the determinant of the matrix must be zero. From the non-triviality condition, the following three eigenvalues, $\Lambda_1 = -\frac{1}{r}$, $\Lambda_2 = \frac{1}{r}$ and $\Lambda_3 = -i\frac{\omega}{U}$ are obtained (Hobson, 1982). Knowing that $h = \sin\left(\lambda_m x\right)$ and $dh/dx = \lambda_m \cos\left(\lambda_m x\right)$, equations (IV-9) ~ (IV-11) yield six equations from which the six coefficients (u_s, u_c, p_s, p_c, v_s, and v_c) are determined. Equation (IV-9) yields

$$Ur + Hru_s - iHv_c = 0, \tag{IV-12}$$

$$-iHv_s - Hr\lambda_m{}^2 u_c + ir\omega = 0 \tag{IV-13}$$

Similarly, equations (IV-10) and (IV-11) give

$$r\rho U^2 + H\left(p_s r + 2r\rho U u_s - i\rho U v_c + i r\rho\omega u_c\right) = 0 \tag{IV-14}$$

$$H\left[r\lambda_m{}^2\left(p_c + 2\rho U u_c\right) + i\rho\left(Uv_s - r\omega u_s\right)\right] - ir\rho\omega U = 0 \tag{IV-15}$$

$$-ip_c + \rho r\left(i\omega v_c + Uv_s\right) = 0 \tag{IV-16}$$

$$-ip_s + \rho r\left(i\omega v_s - \lambda_m{}^2 Uv_c\right) = 0 \tag{IV-17}$$

Utilizing the six equations (IV-12) ~ (IV-17), the six unknown coefficients can be determined as follows:

$$u_s = -\frac{r^2\lambda_m{}^2}{H\left(1+r^2\lambda_m{}^2\right)}U \tag{IV-18}$$

$$u_c = i\frac{r^2\omega}{H\left(1+r^2\lambda_m{}^2\right)} \tag{IV-19}$$

$$p_s = \frac{\rho r^2\left(U^2\lambda_m{}^2+\omega^2\right)}{H\left(1+r^2\lambda_m{}^2\right)} \tag{IV-20}$$

$$p_c = -i\frac{2\rho r^2\omega U}{H\left(1+r^2\lambda_m{}^2\right)} \tag{IV-21}$$

$$v_s = \frac{r\omega}{H\left(1+r^2\lambda_m{}^2\right)} \tag{IV-22}$$

$$v_c = -i\frac{rU}{H\left(1+r^2\lambda_m{}^2\right)} \tag{IV-23}$$

Substituting equations (IV-18) ~ (IV-23) into (IV-2) ~ (IV-4), the final solutions are

$$u(x) = \sum_{j=1}^{3}\overline{u}_j \cdot e^{\Lambda_j x} - \left[\frac{r^2\lambda_m{}^2}{H\left(1+r^2\lambda_m{}^2\right)}U\cdot h - i\frac{r^2\omega}{H\left(1+r^2\lambda_m{}^2\right)}\cdot\frac{dh}{dx}\right] \tag{IV-24}$$

$$p(x)=\sum_{j=1}^{3}\overline{p}_j\cdot e^{\Lambda_j x}+\left[\frac{\rho r^2\left(U^2\lambda_m{}^2+\omega^2\right)}{H\left(1+r^2\lambda_m{}^2\right)}\cdot h-i\frac{2\rho r^2\omega U}{H\left(1+r^2\lambda_m{}^2\right)}\cdot\frac{dh}{dx}\right] \tag{IV-25}$$

$$v(x)=\sum_{j=1}^{3}\overline{v}_j\cdot e^{\Lambda_j x}+\left[\frac{r\omega}{H\left(1+r^2\lambda_m{}^2\right)}\cdot h-i\frac{rU}{H\left(1+r^2\lambda_m{}^2\right)}\cdot\frac{dh}{dx}\right] \tag{IV-26}$$

With the following eigenvalue dependence,

$$(1)\ \Lambda_1=-\frac{1}{r}:\ i\overline{u}_1-\overline{v}_1=0,\ \overline{p}_1+\rho\left(U-ir\omega\right)\cdot\overline{u}_1=0 \tag{IV-27}$$

$$(2)\ \Lambda_2=\frac{1}{r}:\ i\overline{u}_2+\overline{v}_2=0,\ \overline{p}_2+\rho\left(U+ir\omega\right)\cdot\overline{u}_2=0 \tag{IV-28}$$

$$(3)\ \Lambda_3=-i\frac{\omega}{U}:\ \overline{v}_3+\frac{r\omega}{U}\cdot\overline{u}_3=0,\ \overline{p}_3=0 \tag{IV-29}$$

For a short-lossless inlet, $p(0)$ and $u(0)$ are needed. Introducing $x=0$ into equations (IV-24) and (IV-25) gives

$$u(0)=\overline{u}_1+\overline{u}_2-\frac{r^2\lambda_m{}^2U}{H\left(1+r^2\lambda_m{}^2\right)}\cdot h\Big|_{x=0}+i\frac{r^2\omega}{H\left(1+r^2\lambda_m{}^2\right)}\cdot\frac{dh}{dx}\Big|_{x=0} \tag{IV-30}$$

$$p(0)=\overline{p}_1+\overline{p}_2+\frac{\rho r^2\left(U^2\lambda_m{}^2+\omega^2\right)}{H\left(1+r^2\lambda_m{}^2\right)}\cdot h\Big|_{x=0}-i\frac{2\rho r^2\omega U}{H\left(1+r^2\lambda_m{}^2\right)}\cdot\frac{dh}{dx}\Big|_{x=0} \tag{IV-31}$$

Substituting equations (IV-30) and (IV-31) into equation (2-5) gives

$$\overline{p}_1+\overline{p}_2-i\frac{2\rho r^2\omega U}{H\left(1+r^2\lambda_m{}^2\right)}\cdot\left.\frac{dh}{dx}\right|_{x=0}+\rho U\cdot\left(\overline{u}_1+\overline{u}_2+i\frac{r^2\omega}{H\left(1+r^2\lambda_m{}^2\right)}\cdot\left.\frac{dh}{dx}\right|_{x=0}\right)=0 \tag{IV-32}$$

$\overline{u}_3$ is zero because the inlet flow can be assumed to be irrotational so that the vortical velocity is zero. For a full-discharge exit, $p(L)$ is needed. Introducing $x=L$ into equation (IV-25) gives

$$p(L)=\overline{p}_1\cdot e^{-L/r}+\overline{p}_2\cdot e^{L/r}-i\frac{2\rho r^2\omega U}{H\left(1+r^2\lambda_m{}^2\right)}\cdot\left.\frac{dh}{dx}\right|_{x=L} \tag{IV-33}$$

Therefore, for a short-lossless entrance and a free-discharge exit, the following equation is obtained using equations (IV-27), (IV-28), (IV-32), (IV-33) with the irrotational assumption ($\overline{u}_3=0$)

$$\begin{bmatrix}-\rho(ir\omega-U) & 0 & 0 & 1 & 0\\ 0 & \rho(ir\omega+U) & 0 & 0 & 1\\ 0 & 0 & 1 & 0 & 0\\ \rho U & \rho U & 0 & 1 & 1\\ 0 & 0 & 0 & e^{-\frac{L}{r}} & e^{\frac{L}{r}}\end{bmatrix}\begin{Bmatrix}\overline{u}_1\\ \overline{u}_2\\ \overline{u}_3\\ \overline{p}_1\\ \overline{p}_2\end{Bmatrix}=\begin{bmatrix}0\\ 0\\ 0\\ ir^2\omega\dfrac{\rho U+1}{H\left(1+r^2\lambda_m{}^2\right)}\cdot\left.\dfrac{dh}{dx}\right|_{x=0}\\ i\dfrac{2\rho r^2\omega U}{H\left(1+r^2\lambda_m{}^2\right)}\cdot\left(\dfrac{dh}{dx}\right)_{x=L}\end{bmatrix} \tag{IV-33}$$